

**ALMA MATER STUDIORUM - UNIVERSITÀ DI BOLOGNA**

---

**FACOLTA' DI INGEGNERIA**

**CORSO DI LAUREA IN INGEGNERIA ENERGETICA**

*DIPARTIMENTO DI INGEGNERIA ENERGETICA, NUCLEARE E DEL CONTROLLO  
AMBIENTALE*

**TESI DI LAUREA**

in  
Radioprotezione

**MONTE CARLO SIMULATION OF THE WENDI-2 NEUTRON  
DOSIMETER**

**CANDIDATA:**

Silvia Tolo

**RELATORE:**

Prof. Ing. Domiziano Mostacci

**CORRELATORI:**

Prof.ssa Ing. Isabelle Gerardy

Dott. Frédéric Stichelbaut

Anno Accademico 2011/2012

Sessione I



# ABSTRACT

Il presente lavoro di tesi, sviluppato nell'arco di sei mesi presso l'Institut Supérieur Industriel de Bruxelles (ISIB) in collaborazione con Ion Beam Application Group (IBA, Louvain la Neuve), ha come principale soggetto lo studio della risposta del rem meter WENDI-2 commercializzato da Thermo Scientific. Lo studio si è basato principalmente sull'uso del codice Monte Carlo MCNPX 2.5.0, simulando la risposta del detector sia in caso di campi di radiazione neutronica monoenergetici sia in corrispondenza di spettri neutronici continui. La prima fase è stata dedicata alla modellizzazione MCNPX del rem counter, consentendo così la valutazione della sua funzione risposta. Questa è stata ricostruita interpolando 93 punti, ciascuno calcolato in corrispondenza di un singolo valore di energia di una sorgente puntiforme, compreso tra 1 meV e 5 GeV. In tal caso è stata rilevata un'ottima corrispondenza tra i risultati ottenuti e quelli riportati nella letteratura scientifica esistente. In una seconda fase, al fine di ottenere informazioni sulla risposta di WENDI II in corrispondenza di campi complessi di radiazione, simulazioni MCNPX sono state realizzate riproducendo un ambiente di lavoro esistente presso la sede IBA di Louvain la Neuve: la risposta del detector è stata valutata in corrispondenza di 9 diverse posizioni all'interno di un bunker contenente un ciclotrone PET (18 MeV H<sup>-</sup>), implicando la rilevazione di campi di radiazione neutronica continui ed estesi dalle energie termiche fino a 18 MeV. I risultati ottenuti sono stati infine comparati con i valori di dose ambiente equivalente calcolata nelle stesse condizioni di irraggiamento.



# TABLE OF CONTENTS

NOMENCLATURE	7
INTRODUCTION	9
CHAPTER I: Neutron Detection	11
1.1 DETECTOR CHARACTERISATION	11
1.2 NEUTRON SOURCES	13
1.2.1 Spontaneous Fission	14
1.2.2 Production of Neutrons through ( $\alpha$ ,n) Reaction	15
1.2.3 Photoneutron Sources	17
1.3 NEUTRON DETECTION TECHNIQUES	19
1.3.1 Slow Neutron Detection	20
1.3.2 Fast Neutron Detection	26
CHAPTER II: Radiation Protection	31
2.1 BIOLOGICAL ASPECTS	31
2.2 DOSIMETRIC QUANTITIES	33
2.3 OPERATIONAL QUANTITIES	38
2.3.1 External Exposure	39
2.3.2 Internal Exposure	42
2.4 RADIATION STANDARDS REGULATION	43
CHAPTER III: Rem Meters	47
3.1 DOSE EQUIVALENT EVALUATION	48
3.2 HISTORY AND STATE OF THE ART	49

3.3 WENDI-II	51
CHAPTER IV: IBA Group	59
4.1 HISTORICAL OVERVIEW	59
4.2 IBA APPLICATIONS	62
4.2.1 Sterilization and Ionization	63
4.2.2 Radioisotopes	65
4.2.3 Advanced Radiotherapy	67
CHAPTER V: Modelling WENDI-2	71
5.1 MCNP and MCNPX	71
5.2 WENDI-2 RESPONSE FUNCTION	75
5.2.1 Input file WENDI	76
5.2.2 Input file TUBE	80
5.2.3 Simulations Results	81
5.3 COMPARISON WITH FORMER STUDIES	86
5.4 COMPARISON WITH FLUENCE-TO-DOSE CONVERSION FUNCTION	88
CHAPTER VI: WENDI-2 Response	91
6.1 INPUT FILE	91
6.2 RESULT ANALYSIS	95
6.3 COMPARISON WITH $H^*(10)$ CALCULATION	98
CONCLUSIONS	103
REFERENCES	105
RINGRAZIAMENTI	109

# NOMENCLATURE

CEA	Commissariat à l'énergie atomique et aux énergies alternatives
ENDF	Evaluated Nuclear Data File
GEANT	Geometry and Tracking
IBA	Ion Beam Applications
ICRP	International Commission on Radiological Protection
LET	Linear Energy Transfer
MCNP	Monte Carlo N-Particle Transport Code
MCNPX	Monte Carlo N- Particle (eXtended) Code
PET	Positron Emission Tomography
VISED	Visual Editor
WENDI	Wide Energy Neutron Detection Instrument



# INTRODUCTION

The large use of radiations in a wide variety of industrial fields, as well as their applications in medicine, entail the increasing need for efficient systems of monitoring and therefore requires the availability of reliable measuring instruments. In this context, neutron metrology plays a prominent role, thanks to the current developments in nuclear medicine, in particular with regards to proton therapy applications in which the production of secondary high-energy neutrons is a technological problem of great significance. In spite of the large variety of neutron detection instruments present on the market, in the majority of cases the response functions of these devices are poorly characterised and the existing scientific literature proves insufficient to gain an adequate knowledge of their behaviour.

The subject of the present thesis is the study of the response of the extended-range rem meter WENDI-2, produced by Thermo Scientific. Any measurement is inevitably influenced by the nature of the detector itself, and a detector cannot be characterised by same detection effectiveness for every energy value of the incoming radiation; hence, the measurement will be more or less precise according to the characteristics of both detector and radiation measured. The response function of Rem meters is designed to match approximately, in a specified energy range, a suitable fluence-to-dose conversion function to yield real-time measurements of neutron equivalent dose. Among these detectors, WENDI-2 appears extremely promising, showing a good response in terms of ambient dose equivalent on a range of energies larger than that considered by other rem meters. The objective of this work has been to provide information on the reliability of the detector dose estimation in monoenergetic as well as continuous neutron radiation fields. The main instrument used in this investigation has been a Monte Carlo code: by means of MCNPX simulations the response function of the device has been reproduced and comparisons with equivalent ambient dose estimation have been made.

This work has been carried out as a result of collaboration among the Alma Mater Studiorum (University of Bologna), the Institut Supérieur Industriel de Bruxelles (ISIB)

and the Ion Beam Application Group (IBA, Louvain la Neuve), a worldwide leader company in ionizing radiation applications and undisputed number one in the field of proton therapy.

The present thesis is structured in six chapters. In the first a theoretical background regarding neutron metrology is presented, involving the description of neutron source and of the most common neutron detection techniques. The risk linked to ionizing radiation as well as the main principles and quantities used in radiation protection are analysed in the second chapter. The third chapter concerns itself with the description of rem meters, evaluating their operating principle and the general structure and characteristics of these instruments. A brief survey of the IBA group history and application is provided in the fourth chapter. In the last part the results of the investigation are shown together with their analysis and their comparison with suitable existing data: the fifth chapter treats the reproduction by means of MCNPX simulations of the WENDI-2 response function to monoenergetic neutron point sources while the sixth is dedicated to a specific case-study involving a continuous neutron radiation field.

# CHAPTER I

## Neutron Detection

Nowadays, according to the develop of scientific research and implementations – from the design of nuclear reactor instrumentation to the particle physics and material science – and of radiation use associated to health physics applications, as the hadron therapy or other technics related to the fight against cancer, improvements in radiation protection field are constantly requested. In order to realize this purpose, it is necessary to assure the development, in terms of reliability, of the primary instrument related to the scientific research in radiation field, which is the radiation detection. In light of these considerations, the present chapter focuses on the detection of neutrons: before analysing all the main available neutron sources, the operation and the main properties of a general radiation detector are outlined. Then, the properties associated to a general radiation detector are briefly described; finally, different neutron detection techniques and the related interaction with matter are analysed in order to build the background necessary to deal with the following steps of this work.

### 1.1 DETECTOR CHARACTERISATION

The detection of any kind of radiation is based on the knowledge of the interaction process that occurs between the radiation specie taken into account and a suitable target chosen for the purpose. In a wide variety of detectors, the result of the radiation interaction is the production of a given amount of electric charge in the active volume of the device. The collection of these charges, realised generally by means of the imposition of electric fields, allows forming the basic electric signal. The latter, that is the output given by the device, can be built in different ways, according to the mode of operation of the analysed detector. In particular, three different modes can be defined: the *pulse mode*,

the *current mode* and the *mean square voltage mode* [Knoll,2000]. In the first case, the detector instrumentation is designed to record each quantum of radiation that interacts in the active volume: this approach allows preserving information on the amplitude and timing of individual events, making this mode of operation extremely attractive for a wide range of applications. Operating in this way, each amplitude pulse carries essential information about the charges produced by a particular radiation interaction in the active volume. Therefore, different amplitudes will reveal differences in the incoming radiation energy. In spite of this, the different magnitude of the pulse can be due to intrinsic fluctuations in the detector response to monoenergetic radiation: the pulse amplitude distribution is a property associated to each detector and it gives information about the device itself as well as about incoming energy. The most common way of visualise the output information is the *differential pulse height distribution*: it involves on the abscissa a linear scale of pulse amplitude, from zero to a value exceeding the amplitude of any pulse measured, while the ordinate is the ratio of the differential number,  $dN$ , of the pulses observed within the differential amplitude increment  $dH$ , and the increment itself. For those applications in which event rates are very large, using the pulse mode is not possible because of the overlap of the pulses and consequently the impossibility of distinguishing different events. In these cases, it is possible to have recourse to the *current mode*: considering a fixed response time of the detector, the signal collected is an average current, obtained including many of the fluctuations in the intervals between different interactions. This value, averaged on the response time, is then related to the interaction rate as well as to the amount of charges produced per interaction. The relative response to large-amplitude events can be improved by means of the *Mean Square Voltage Mode*. In particular, the latter is most useful in applications that involve the presence of different types of radiations, where the amount of charges produced is very different according to the type of interactions. Indeed, while in the current mode the signal reflects the charges contributed by each type of radiation, in the MSV mode the derived output is proportional to the square of the charge per event. In this light, with regard to the detector response, the radiation that gives the larger contribution in terms of average electric charge per event will have a larger importance.

The response function given by the detector, can be evaluated in terms of *energy resolution*: this property is related to the ability of a given measurement to resolve fine detail of incident radiation energy. In general, with regards to the response associated to a

monoenergetic source, the resolution will be as much better as the width of the corresponding distribution, centred on the incident energy value, appears narrower. Finally, evaluating the reliability of the measurements related to a particular detector, it is indispensable to estimate the efficiency of that device. The *absolute counting efficiency* can be define as the fraction of radiation emitted by the source and recorded by the detector:

$$\epsilon_{abs} = \frac{\text{number of pulses recorded}}{\text{number of radiation quanta emitted by the source}} \quad (1.1)$$

Clearly, the *absolute counting efficiency* is not only a detector property but it depends also on the detection geometry and on the setup of the measurement. On the contrary, it is possible to calculate the *intrinsic counting efficiency* as a fundamental property of the device:

$$\epsilon_{int} = \frac{\text{number of pulses recorded}}{\text{number of radiation quanta incident on detector}} \quad (1.2)$$

The intrinsic efficiency of a general detector is influenced by different factors, as the detector material, the radiation energy, the thickness offered by the device to the incoming radiation and the nature of the event recorded.

## 1.2 NEUTRON SOURCES

Comparing the different types of neutron sources with those related to other kinds of radiations, as gamma rays, the scant variety of the former, appears clearly. Actually, there does not exist a practical isotope source of neutrons: although a nucleus excited with an energy value greater than the neutron bidding energy can emit subatomic uncharged particles during the decay, this phenomenon does not represent a real mechanism of continuous neutron production. These excited states of the nuclei are not the result of a convenient radioactive decay process, useful as neutron source: for this reason, the

choices of neutron sources is restricted to those based on spontaneous fission or on nuclear reactions in which the incident particle is the result of a conventional decay process. In what follows some details are presented on the main types of source.

## 1.2.1 Spontaneous Fission

Several fast neutrons can be promptly emitted, thanks to fission mechanism, together with others reaction results, such as heavy particles and prompt gamma rays – as well as gamma and beta activity associated to the fission products accumulated in the sample. The main advantage related to this neutron production mechanism is that a sample of a radionuclide, characterised by an appreciable spontaneous fission decay probability (such as some transuranic nuclides), can be considered a simple and convenient isotopic neutron source.

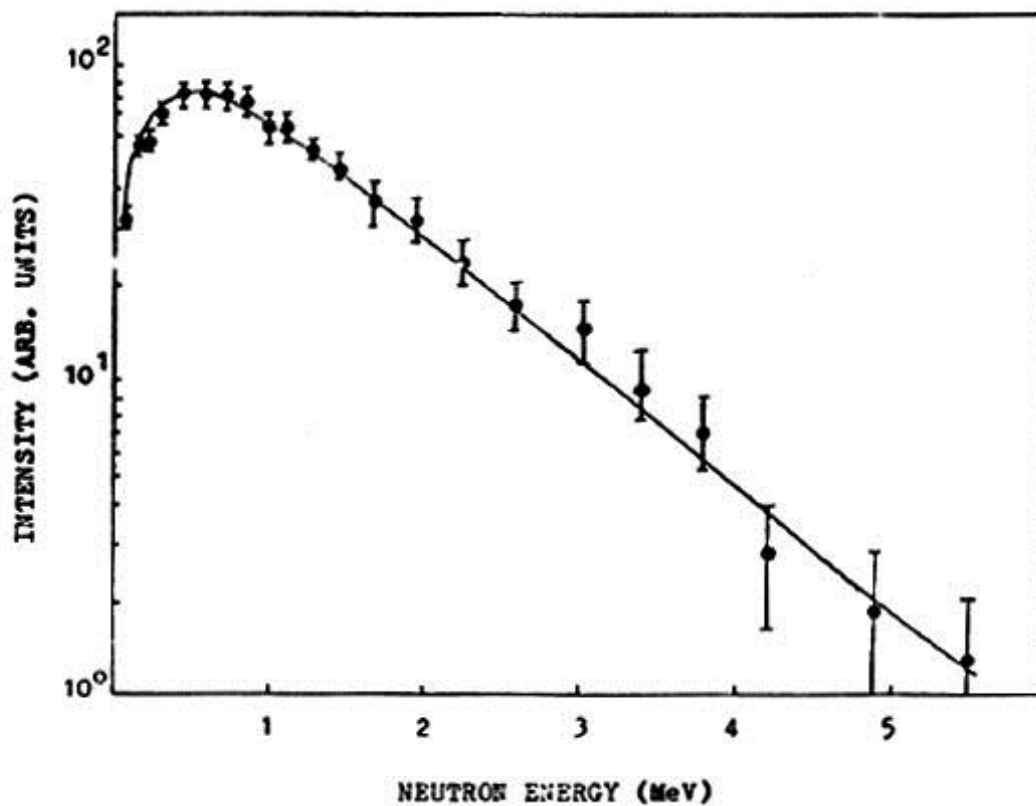


Figure 1.1 Measured neutron energy spectrum from the spontaneous fission of  $^{252}\text{Cf}$

On the other hand, the important activity related to this type of nuclear reaction, required an efficient shielding of the sample: the latter is generally encapsulated in a sufficient thick container, in order to release only the fast neutrons and the gamma rays. Clearly, these types of source are far from being monoenergetic, on the contrary they are characterised by the neutron energy spectrum of the decaying nuclide. Producing 3.8 neutrons on average per fission, the most common among the spontaneous fission sources is  $^{252}\text{Cf}$  nuclide: the large use of this isotope is due to its convenient half-life – equal to 2.56 years and then long enough to represent an available source – and to its easy availability, being the most widely produced element among all the transuranic nuclides. Although the dominant decay mechanism is type alpha, with an emission rate equal to 32 times that for spontaneous fission,  $2.30 \times 10^6$  neutrons are produced per unit of time by each microgram of the sample. Indeed, compared with the other isotopic neutron sources,  $^{252}\text{Cf}$  sources involve a small quantity of active material, generally equal to some micrograms, and consequently they occupy a small volume of space, surrounded by the encapsulation requirements. As it is possible to see in the energy spectrum plotted in Figure 1.1, the yield of the emitted neutrons is particularly high for the energy values from 0.2 and 1.5 MeV, although the neutron production remains significant also for the higher energies.

## **1.2.2 Production of Neutrons through ( $\alpha$ ,n) Reaction**

This kind of source consents the production of neutrons thanks to the interaction with matter of  $\alpha$  particles. The main attraction of this mechanism involves the availability of this specie of radiation: alpha particles can be obtained from the direct decay of a large number of accessible radionuclides. In order to obtain a consistent number of emitted neutrons, a target must be associated to the  $\alpha$  emitter; in other words, a self-contained neutron source can be easily achieved by the union of an alpha-emitter and a suitable target material. Among the different materials that can lead to a convenient rate of ( $\alpha$ ,n) reactions, the maximum production of neutrons is reached using beryllium: the interaction of an alpha particle - characterised by an incident energy at least higher than 5.71 MeV, Q-value of the reaction - with a beryllium atom, leads to the emission of a neutron with a

kinetic energy equal to the difference between the incident energy and the reaction Q-value. Most of the sources of this kind consist of a stable alloy formed by beryllium and different actinide elements, which are the alpha emitters of practical interest. In Table 1.1 the characteristic of the most common Be( $\alpha$ ,n) sources are listed.

SOURCE	HALF-LIFE	$E_{\alpha}$ [MeV]	NEUTRON YIELD PER $10^6$ PRIMARY $\alpha$ PARTICLES
$^{239}\text{Pu}/\text{Be}$	24000 y	5.14	65
$^{210}\text{Po}/\text{Be}$	138 d	5.3	73
$^{238}\text{Pu}/\text{Be}$	87.4 y	5.48	79
$^{241}\text{Am}/\text{Be}$	433 y	5.48	82
$^{244}\text{Cm}/\text{Be}$	18 y	5.79	100
$^{242}\text{Cm}/\text{Be}$ + daughters	162	6.1	118
$^{226}\text{Ra}/\text{Be}$ + daughters	1602 y	Multiple	502
$^{227}\text{Ac}/\text{Be}$ + daughters	21.6 y	Multiple	702

**Table 1.1** Characteristics of Be( $\alpha$ ,n) Neutron Sources

Because of the long chains of daughter products associated to Ra/Be and Ac/Be sources, these alloys are not appropriate for those applications in which the intense gamma emission can invalidate the measurements. Excluding these two compounds, the remaining radioisotopes listed in the table involve simpler alpha decays, with a much lower gamma background. In spite of this, because of the involved activities of the actinide elements, special precautions must be taken to ensure the safety of the material encapsulation. Indeed, the active material – consisting in the described alloys – is usually sealed within two stainless steel cylinders, individually welded. An additional space is required within the inner cylinder in order to allow the location of the helium gas, produced when the alpha particles are stopped and neutralized in the active volume.

The choice of a particular ( $\alpha$ ,n) neutron source, among those presented, is made primarily on the basis of the availability and cost of the associated alloy and with regards to the half-life of the isotope.

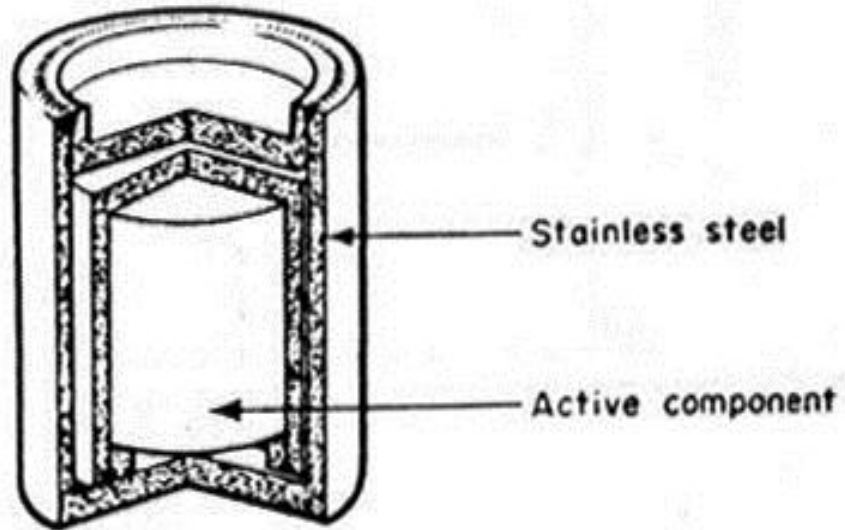


**Figure 1.2** Typically double-walled construction for Be ( $\alpha,n$ ) sources

Other charged particles can be involved in neutron production by means of their reaction with target nuclei. Since the alpha particles represent the only radiation species conveniently available from radioisotopes, reactions involving protons, deuterons and so on, must rely on the use of accelerators. In particular, the emission of neutrons as a result of the interaction of accelerated protons with matter is of great interest with regard to the task of this work.

### 1.2.3 Photoneutron Sources

The production of neutrons, as a result of the interaction of radiation with matter, is not only related to the use of charged particles: it can be realised also having recourse to gamma rays irradiation of an appropriate target. To be more precise, the photoneutron source consists in supplying to a target nucleus the necessary excitation energy – required to allow the emission of a free neutron – by means of photon absorption. Taking into account this neutron production mechanism, to realise a photoneutron source, it is necessary to associate a gamma emitter, encapsulated in an aluminium container, to a

surrounding appropriate target. Only two are the reactions of any practical interest with respect to this type of neutron production:



In order to realize the reactions, the incident photon is supposed to have energy at least equal to the  $Q_{\text{value}}$  associated to the respective process. For gamma-rays energies higher than this minimum, the corresponding neutron energy can be calculated taking into account the incident power, the mass of the neutron, the weight of the recoil nucleus and the direction of flight of the produced particle. In light of this, it is easy to realize that the main advantage of this neutron production mechanism consists in the possibility to obtain an almost monoenergetic neutron source: if the incident radiation is nearly monoenergetic also the particles emitted will be characterised by a narrow energy range, thanks to the little influence on the latter of the emission angle. In spite of this, for large source, the emission spectrum is influenced by the neutron scattering occurring within the source before the emission.

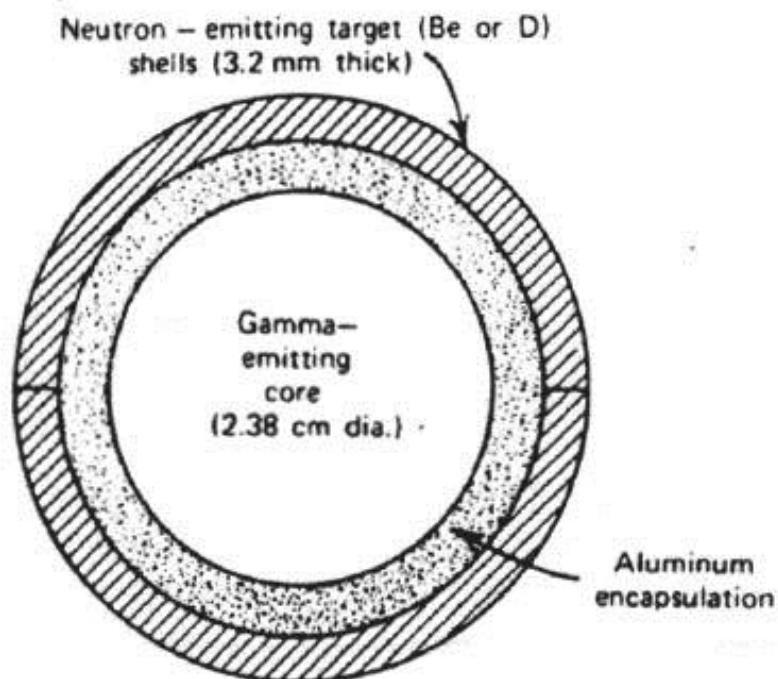


**Figure 1.3** Structure of a spherical photoneutron source

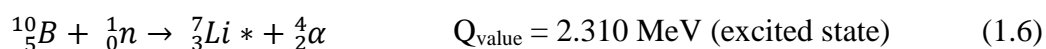
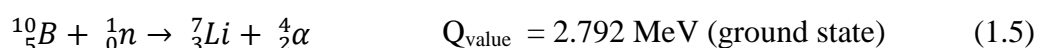
On the other hand, the main disadvantage associated to the use of photonuclear sources is the involvement of a large gamma activity to realise a consistent neutron yield. In addition, many gamma emitters used for these sources are characterised by a half-life short enough to require a reactivation process between different applications.

### **1.3 NEUTRON DETECTION TECHNIQUES**

Because of the absence of electrical charge, neutrons cannot be detected directly as it is possible to do with other kinds of particles such as protons or ions and so forth. For this reason, in order to detect neutrons, it is necessary to rely on a conversion process, where the interaction of the uncharged particles with matter produces charged particles that is possible “to see” with conventional means. In this way the direct detection of the charged particles allows deducing the presence of neutrons. In order to choose a nuclear reaction that might be useful in neutron detection, several factors must be considered: first of all, the relative cross section must be as large as possible, so that small detector sizes are permitted. Moreover, the target isotope taken into account for the conversion reaction must be easily available – as a nuclide characterised by a high isotopic abundance in nature or as the result of an inexpensive artificial process of enrichment. Finally, an important factor is the  $Q_{\text{value}}$  associated to the neutron capture reaction. This value, indeed, determines the quantity of energy released after the exothermic reaction: in other words a high  $Q_{\text{value}}$  corresponds to a high energy of the reaction products, allowing a good discrimination against gamma-ray events in the detection process. The latter has an important role related to the reliability of the measurements, because of the large gamma activity associated to the neutron emission in many applications. Since the cross sections for neutrons, regardless of the type of reactions and taking into account a large variety of materials, are a strong function of the incident energy of the particles, the detection strategies are different, according to the range of values associated with the neutron energy. Below, the treatment of the techniques developed for neutron revelation will be divided in two parts, consistent with the region of the energy domain considered.

### 1.3.1 Slow Neutron Detection

The neutrons characterised by energies below the cadmium cutoff, that is equal to 0.5 eV, are conventionally defined “slow neutrons”. In what follows, the main conversion reactions related to this part of the energy domain will be analysed. A great part of the detectors for slow neutron revelation involves the use of boron-10 as target material, to produce an (n, $\alpha$ ) conversion reaction. This process can evolve in two different results: although in both cases the emission of an alpha particle occurs, when thermal neutrons are involved, only the 6% of the events has, as a result, the emission of a lithium-7 recoil nucleus in its ground state. The remaining 94% of reactions leads to an excited state of the product, as per the schemes 1.5 and 1.6.



The success of this reaction in neutron detection is related primarily to the large associated cross section in this region of the energy domain, as shown in Figure 1.4. In addition, the natural isotopic abundance of boron-10 is 19.8% and supplies of this element enriched in its  ${}^{10}\text{B}$  concentration are easily available. On the other hand, the  $Q_{\text{value}}$  of both the reactions is much higher than the incident energy and it is completely distributed between the reaction products. Thus the initial neutron energy is completely submerged by that released by the reaction, consequently it is not possible to extract information about the energy of the incident neutron from calculation of the energy of the products.

The most common boron compounds, used in slow neutron detection is the boron trifluoride,  $\text{BF}_3$ : this gas serves as a target for the incident particles as well as counter operating gas. Because of the high performance as proportional gas and because of the associated high boron concentration, the use of this compound is largely preferable over other combinations for devices based on boron reaction. These latter are universally designed using an external cylindrical cathode and a central wire, characterised by a small diameter of 0.1 mm or less, as anode. As cathode a low neutron cross section material,

generally aluminium, is used. In the planning stage of a  $\text{BF}_3$  counter tube, as well as in the measuring phase, three aspects are particularly significant: the wall effect, the gamma discrimination and, finally, the effects of aging.

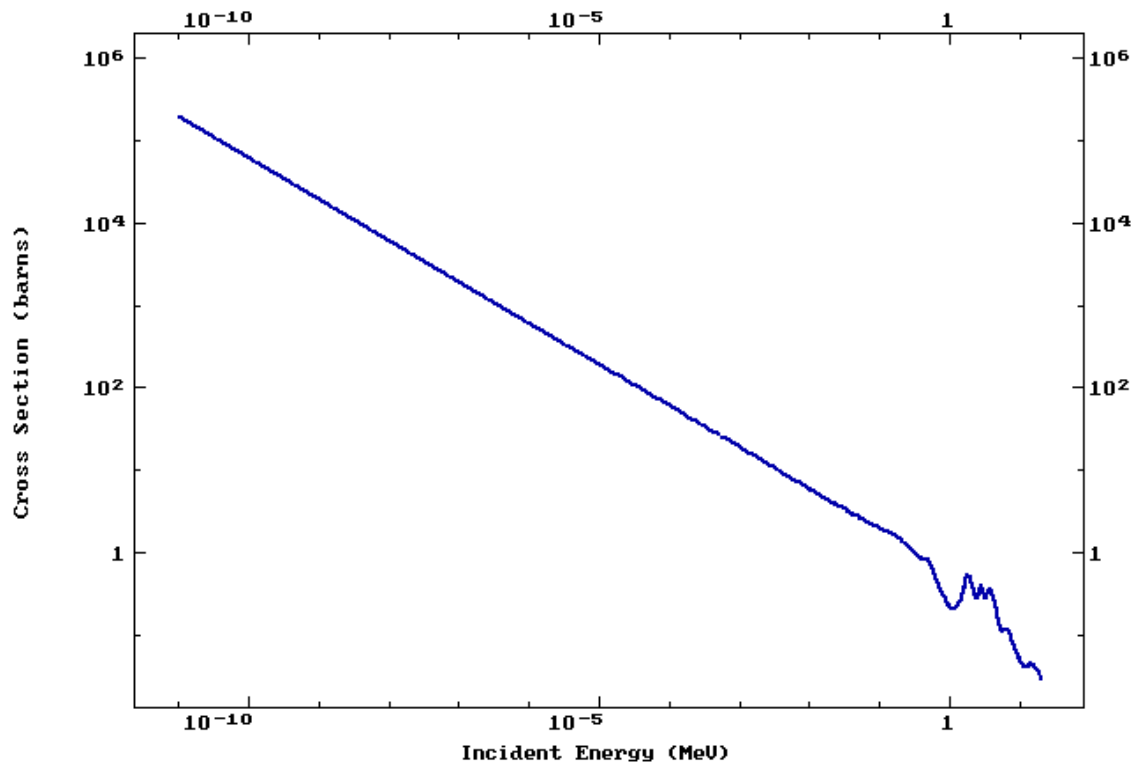


**Figure 1.4** Cross section of (n, $\alpha$ ) reaction in  $^{10}\text{B}$  [ENDF, 2012]

The revelation of neutrons is based on the collection of the charges produced that deposit their energy in the counter volume. But not all the reactions occur sufficiently far from the walls of the counter tube to deposit the whole energy of the products within the gas volume: if the size of the tube is not large compared to the range of the alpha particles and the lithium recoil nuclei produced, some of the reaction products will escape from the detector. Therefore, because of the leakage of part of the resulting reaction energy, a smaller pulse is produced: the main result of this process is a cumulative effect known as wall effect, the main consequences of which are the modification of the expected height pulse spectra and the loss of detector efficiency. In order to reduce this effect and increase the detector resolution, without modifying the size of the device, it is possible to increase the pressure of the filling  $\text{BF}_3$  gas – generally the values used in counter tubes of this type is between 13 and 80 kPa. The spectrum obtained is also influenced by the production of

electrons, due to the interaction of photons with the detector walls. A peak is introduced in the lower part of the energy range, because of the deposition in the active volume of a part of the energy of the electrons produced. Generally, a simple amplitude discrimination can easily eliminate the gamma rays contribution to the count rate, thanks to the lower deposition energy related to this kind of radiation; in spite of this, when the photons flux is important, complications occur, reducing the effectiveness of the amplitude discrimination. In particular, higher values of gamma rays flux can induce chemical changes in the BF<sub>3</sub> gas, leading to the impossibility of separating gamma interaction results from those related to the neutron-induced events. Finally, as for other proportional counters, the performance of the BF<sub>3</sub> tubes is affected by a degradation effect related to aging. This behaviour can be ascribed to the contamination of the anode wire and cathode walls, due to the presence of molecular dissociation products. To reduce the contaminations by means of absorbing agents, use of charcoal within the tube was evaluated by different studies with good results. In addition to the BF<sub>3</sub> proportional tubes, other solutions for neutron detection are available based on the use of boron. The introduction of a solid boron coating on the interior walls of a conventional counter tube allows the use of different, and more appropriate, proportional gases. This configuration has the advantage of being more resistant to the effects of contamination and, in addition, because the reaction of interest occurs on the detector walls, precautions for wall effect are not necessary. In fact, according to the conservation of the momentum, the two reaction products are emitted in opposite directions and consequently only one of these deposits its energy in the proportional gas volume. Nevertheless, the boron-lined proportional counters are not very common compare to BF<sub>3</sub> tubes, because of the lower performance in terms of counting stability and gamma discrimination ability.

Another element used to obtain an (n,α) conversion reaction for neutron detection is lithium. The interaction of neutrons with <sup>6</sup>Li isotope leads to the production of an alpha particle and a triton, according to the reaction 1.7:



Since the neutron incident energy is negligible compared to the Q<sub>value</sub> of the reaction, and the lithium reaction goes exclusively to the ground state of the product nucleus, it is possible to calculate the emission energy of the products – equal to 2.73 MeV for the

triton and 2.05 MeV for the alpha particle. In addition, the resultant particles are emitted in opposite directions when the incoming neutron energy is low, as in the thermal region.

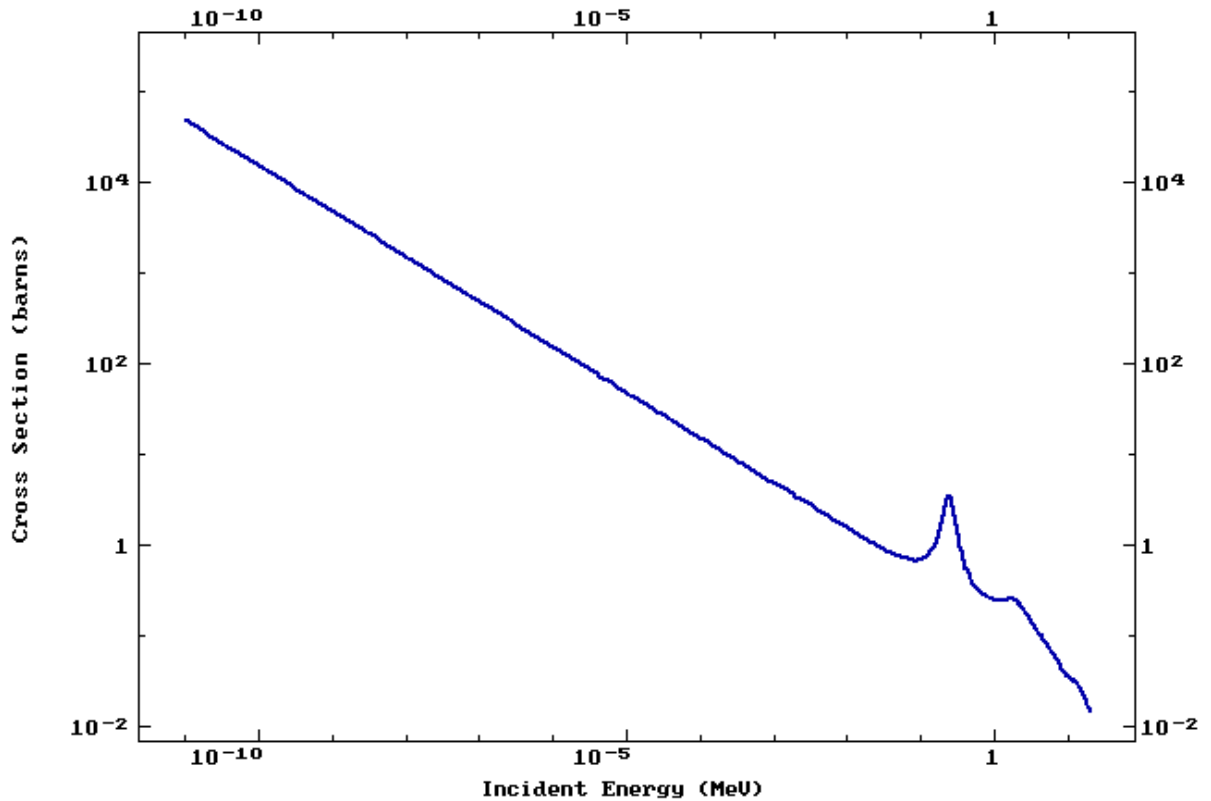


**Figure 1.5** Cross section of (n,α) reaction in  ${}^6\text{Li}$  [ENDF, 2012]

The thermal neutron cross section for  ${}^6\text{Li}$  is lower than that for the  ${}^{10}\text{B}$  but, because of the high  $Q_{\text{value}}$  and large availability of the isotope, this reaction remains a good alternative. Counter tubes based on lithium are not available because a stable lithium-containing gas does not exist. For this reason the use of this isotope in neutron detection is reduced to scintillators containing crystalline lithium iodide. This hygroscopic compound is available in crystals hermetically sealed in a thin material, provided with an optical window; because of its high density, a little dimension of the sample is sufficient to obtain efficient slow neutron detection. In the devices of this kind, since the ranges of reaction products are smaller compared with the size of the scintillator, the resultant spectrum is free of wall effects and consists of a single peak for each neutron interaction. It is important to consider that the scintillation efficiency associated to the lithium iodide is quite the same for electrons and alpha particles: in light of this, a single interaction of a gamma ray

produces a pulse height proportional to the incident energy of the photon. Therefore the ability to discriminate against gamma rays is dramatically reduced.

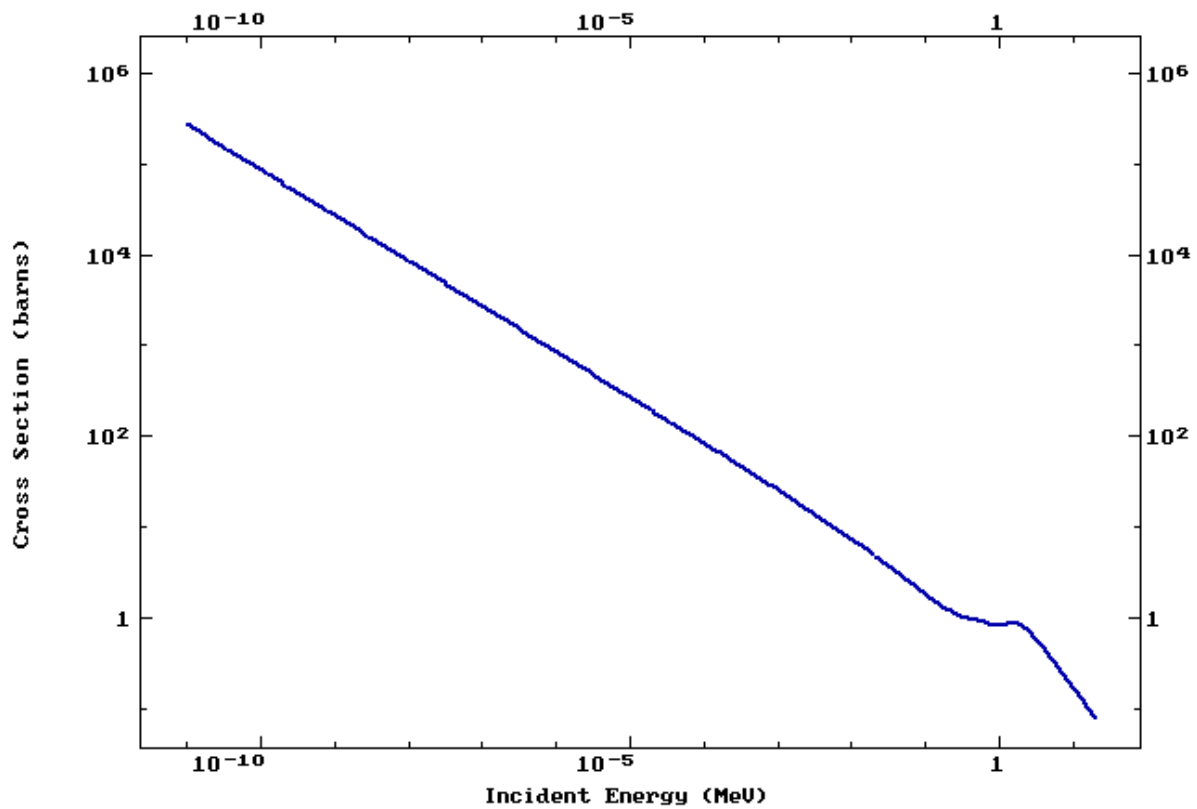


Figure 1.6 Cross section of (n,p) reaction in  $^3\text{He}$  [ENDF, 2012]

The largest cross section of interest in terms of slow neutron detection is that related to the reaction 1.8.



The products of the neutron interaction with  $^3\text{He}$  isotope are a triton recoil nucleus, emitted with energy equal to 0.191 MeV, and a proton, characterised by an energy of 0.573 MeV.

Although the cross section, as can be seen in the graph, is significantly higher than that for the boron reaction, the use of the  $^3\text{He}$  nuclide for neutron detection is hampered by the high cost of this isotope. In spite of this, the trend of the cross section allows using this conversion reaction for a neutron energy range much larger than that associated to the slow neutrons. The (n,p) reaction described is realised in  $^3\text{He}$  proportional counter, in

which helium-3 gas of sufficient purity serves as target nuclide and as proportional gas. As mentioned for the boron case, the ranges of the reaction products are not always small with respect to the tube size, therefore the wall effect is important, especially in light of the low atomic mass of  $^3\text{He}$ . To reduce the impact of this problem, in the revelation process, different strategies can be used: a first approach consists in increasing the tube size, so that most of the reactions occur far from the detector walls; another step is to increase the gas pressure in the tube to reduce the range of the reaction products. The same result can be obtained also through the introduction of a small quantity of a heavier gas in the active volume, enhancing the stopping power of the medium. Compared with the  $\text{BF}_3$  tubes, the counters based on helium reaction show a better performance also at much higher gas pressure; for this reason they are widely preferred for applications in which high detector efficiency is required. In addition, these devices are more resistant to the aging effect. On the other hand, the low  $Q_{\text{value}}$  of the conversion reaction leads to more difficult gamma discrimination. This disadvantage can be partially offset by the introduction of gas additives, such as  $\text{CO}_2$  or Ar, that, accelerating the electron drift, allow ignoring the gamma contribution to the count rate, thanks to the use of a shorter shaping time. Other aspects influence the gamma interaction and contribution, such as the choice of wall material and the use of an activate carbon coating as an impurities absorber. The latter can be introduced in order to obviate the production of electronegative poisons with use, extending significantly the useful life of the device.

Devices containing Gadolinium take advantage of the highest nuclear cross section, equal approximately to 255 000 barns in the thermal region, associated with neutron capture by this element. The useful reaction products for detection applications are fast electrons, produced together with gamma-rays. In light of this the discrimination against gamma interactions in count rate is much more complicate than in the cases analysed previously, constituting the main disadvantage of this detection technique. This process is more frequently employed in neutron imaging, where the revelation of conversion electrons gives information about the location of the neutron interaction.

Also neutron-induced fission events can be used as conversion reactions in slow neutron detection. In particular, the large amount of energy released by the fission event assures a simple discrimination against both gamma rays and alpha particles. Almost all the fissionable nuclides are alpha emitters: for this reason the devices based on this type of reaction are characterised by a spontaneous output signal that, as mentioned before, can

be easily identified on the basis of pulse amplitude discrimination. The most popular type of fission detector is an ionization chamber internally lined with fissile material.

### **1.3.2 Fast Neutron Detection**

In principle, all the conversion reactions previously described are suitable for the revelation of fast neutrons. However, in the higher energies region, the strong decrease of the cross section associated to those reactions causes the fall of the probability of neutron interaction in this part of the domain. In light of this, devices for the revelation of fast neutron must have a different detection strategy to reach an acceptable efficiency. Before delving into the features of this kind of detectors, it is essential to introduce an attractive aspect of the fast neutron detection, which is far from being available in the lower region of the energetic domain, i.e. the possibility to evaluate the energy of the incident particles. When this energy becomes comparable to the  $Q_{\text{value}}$  of the interaction, the contribution of the incoming particles is no longer negligible; therefore if the kinetic energy of the reaction products is measurable, it is equally possible to estimate the initial spectrum of the incident neutrons. In spite of this opportunity, the purpose of a wide variety of detectors, including that on which this study focuses, consists in recording the presence of neutrons, regardless of their kinetic peculiarities. To realise this goal, counters based on neutron moderation are widely used: on the one hand the moderating process eliminates all the information on the original energy of the incoming particles, on the other hand this mechanism allows increasing the detector efficiency, moving the neutrons to the energy region of higher cross section values. The devices based on this strategy consist of any slow neutron detector, like those described before, surrounded by a moderating material containing hydrogen – the choice of this element is ascribable to the high neutron scattering cross section, to the deep knowledge of its energy dependence and finally to the possibility to transfer up to the entire incident neutron energy in a single collision with a hydrogen nucleus. Particular attention must be paid, in the planning phase, to the thickness of the moderator material. Increasing the latter, the number of neutron collisions proportionally raises, ensuring that lower energy neutrons reach the active volume of the counter tube. Therefore, this enlargement of the moderating region seems to lead to a development of detection efficiency, thanks to the decrease of the most probable energy

value of the neutrons reaching the inner cell. In spite of this first consideration, other factors, associated to the moderator thickness, tend to offset this efficiency growth: the increasing of the neutron capture probability in the moderating phase and of the likelihood of neutron escape before reaching the detector. Considering this, the efficiency of a fast neutron counter based on moderation shows a maximum in correspondence of a specific value of the moderator thickness, according to the incident neutron energy. A model of this kind of device, in its most common spherical assembly, is more deeply investigated in the following sections of this work.

Detectors based on fast neutron-induced reactions are also available, allowing, as introduced before, the knowledge of the energy spectrum of the incoming particles. This is not the only advantage linked to the use of these devices: the absence of the moderation step permits to obtain a fast detector signal, which, on the contrary, is not assured in the designs described previously. Since in counters that have recourse to moderating material, the production of the output signal can require tens or hundreds of microseconds, because of the thermal diffusion of the neutrons.

In particular two reactions are of interest for fast neutron spectroscopy:  ${}^3\text{He}(n,p)$  and  ${}^6\text{Li}(n,\alpha)$ . Although both these reactions were described previously, additional considerations must be made regarding the fast neutron region. First of all, concerning the lithium reaction, the large  $Q_{\text{value}}$  of 4.78 MeV, that is an advantage in thermal neutron detection, is instead a limitation for spectrometry: it reduces the possible applications of this technique to neutrons with energies above several hundred keV. Moreover, as shown before, the cross section associated to this interaction drops off with increasing incident energy, excepted for a resonance peak at 250 MeV. A different reaction becomes dominant at these incoming neutron energies, leading to the production of three products, as shown for the reaction 1.9.



The neutron produced by the interaction, normally escapes from the system: as a consequence of this, a continuum of deposited energy is present also for monoenergetic neutrons. Therefore, this reaction is undesirable and influences the response of the detector, introducing an additional difficulty in the measurement of incident neutron

energy. In addition to this continuous contribution, considering a monoenergetic neutron source, the response function is characterised by the presence of two different peaks: one located at an energy value equal to the incident energy plus the  $Q_{\text{value}}$  of the reaction and a second maximum in correspondence of a value of 4.78 MeV. The latter is related to the interaction of thermal neutrons, that can be the results of a moderation process occurred in the ambient walls or in any other material in the vicinity of the detector. Because of the large value of the associated cross section, this contribution cannot be eliminated and is usually termed *epithermal peak*. It can provide a convenient energy point for the detector calibration. Scintillators, containing lithium iodide or glass matrices in which the isotope is encapsulated, are available for fast neutron spectroscopy. Also in the use of  $^3\text{H}$  as target nucleus, the influence of competitive reactions becomes important for fast neutron energies. In particular the elastic scattering, the cross section of which is almost equal to that of the (n,p) reaction at 150 keV, is three times more probable than the interaction of interest at 2 MeV. Furthermore, at neutron energies above 4.3 MeV the production of deuterium after a neutron capture event becomes possible. In light of these interaction mechanisms, neglecting the wall effect and considering a monoenergetic source, the pulse height spectrum will be characterised by three main peculiarities. First of all, there is present a peak centred at an energy value equal to that of the monoenergetic source summed to the (n,p) reaction Q value: this maximum is related to the occurrence of (n,p) interactions of undisturbed neutrons incoming directly from the source. The elastic scattering and the consequent transfer of a fraction of the incoming energy to the recoil  $^3\text{He}$  nucleus, influence the spectrum too. In fact, below an energy value equal to 75% of the incoming neutron energy, the spectrum is characterised by the presence of a continuum, due to the detection of incident neutrons decelerated by collisions with the target nuclide. Finally, the last contribution is the epithermal peak, associated to the revelation of those neutrons that undergo (n,p) reactions in the  $^3\text{He}$  after being moderated in external materials. Several are the detector designs based on the helium conversion reaction. The performance of  $^3\text{He}$  counter tube can be improved at the price of added complexity, such as in the case of slow neutron detection. Devices based on different techniques are also available, such as scintillators and ionization chambers or sandwich spectrometers. In particular these latter, available also for the lithium reaction, consist in two semiconductor diode detectors bounding a thin layer of active material – for example lithium fluoride or pure elemental  $^3\text{He}$ . When a neutron, coming from the source, interacts with the target nuclide in the medium, the reaction products are emitted in

opposite direction. Therefore a coincident signal is recorded by the two adjacent detectors, while any background event that occurs only in one detector is automatically eliminated.

An additional conversion reaction is actually suitable for the fast neutrons: the elastic neutron scattering. As discussed before, in the slow neutrons region the incident energy of the particles is so low that the kinetic contribution, transferred to the target nucleus in an elastic scattering event, is no longer significant or measurable. On the contrary, with regard to more energetic neutrons, a scattering event gives rise to a recoil nucleus, characterised by a portion of the kinetic energy of the incoming neutron. Generally, since the targets are always light nuclei, the resultant recoil nucleus, such as alpha particle or proton, loses all its energy in the detector medium. Several species of target nuclide are available for these applications, such as deuterium, helium and hydrogen, but the latter is by far the most popular. In particular the recoil nuclei related to the use of hydrogen as target element, are named *recoil protons*, and consequently the devices based on this process are known as *proton recoil detectors*. For all practical applications, the target nuclei are considered at rest, consequently the total kinetic energy, before and after the scattering event, is equal to that of the original particles. The amount of energy transferred for a single event in hydrogen, can go from zero to all the neutron energy: for this reason, the average energy of the recoil protons is about half that of the incident particles. This aspect of the process entails, for neutrons energies above few hundreds keV, the possibility of detecting preferentially fast neutrons, assuring a satisfying discrimination against low-energy event as background gamma rays. In addition, the presence of thermal neutrons is not recorded by means of elastic scattering, but it might at most lead to the occurrence of competitive reactions in the target material. The most common way to use proton recoil mechanism in fast neutrons detection is through the use of hydrogen-containing scintillators, characterised by a pulse height distribution approximately rectangular.



# **CHAPTER II**

## **Radiation Protection**

Only four months after the discovery of X-rays by the physicist W.C. Roentgen in 1895, the existence of skin effects in radiation researchers was noticed and linked to the radioactive nature of their studies. But the consequences of radiation exposition, in terms of biological damage, are not only restricted to the “deterministic effects”, i.e. adverse tissue reactions due to the death or malfunction of cells as a result of exposure to high doses. On the contrary, the adverse health effects of radiation exposure can be classified in two main categories: in addition to the above mentioned deterministic effects, stochastic consequences were observed in the individuals exposed, like cancer and neoplasia. The main goal of radiation protection is protecting people from the harmful effects of ionizing radiations, thus permitting their beneficial use in medicine, science and industry. For this purpose, it was necessary – and it is still essential – to study and to improve material and theoretical instruments to measure the strength of the radiation fields, as well as to impose accurate exposure limits. Therefore, since the discovery of radiation and radioactivity, protection standards have been imposed and they have evolved driven mainly by two factors: new information on the radiation effects on biological systems and changing attitude towards acceptable risk. In this chapter the effects of ionizing radiation on biological structures are briefly described and the main dosimetric and operational quantities are introduced. Finally, the present protection standards will be discussed in short.

### **2.1 BIOLOGICAL ASPECTS**

To address the need for an international system of radiological protection – to be used world-wide as the common basis for radiological protection standards and legislation –

the International Commission on Radiation Protection (ICRP) was established in 1928. Since that date, all the aspects of radiological protection have been studied publishing more than one hundred reports and developing reliable guidelines based on the current scientific knowledge of radiation exposures and effects. In the following pages, the two main categories of radiation exposure effects are described, according to the definitions presented in the ICRP publication 103. As said before, the radiological damages are classified in two categories: deterministic and stochastic effects. The occurrence of the first kind of injury, which consists in a tissue reaction, is associated to a dose threshold value. Radiation damage must produce the death or serious malfunction of a significant number of cells in the tissue to be clinically relevant. Above the threshold value, the seriousness of the lesion increases proportionally with the dose, entailing the decrease of the tissue-regenerative capacity. Tissue damages can be divided into two types: the precocious reactions, consisting in inflammations or losses of cells occurring within days or weeks after the exposure moment, and the delayed events, subsequent to a precocious reaction. However, for an absorbed dose value lower than 100mGy, no relevant functional damages have been recorded. The induction of stochastic effects is much more difficult to observe because of the random nature of the related events. The main instruments for analysing this category of biological damages are epidemiologic studies. Notwithstanding the inevitable presence of uncertainty, experimental studies show evidence of a relationship between risk of neoplasia and exposure to dose values equal to 100 mSv or lower. On the contrary, there is no direct proof of any link between the risk of hereditary diseases and radiation exposure, but experimental observations lead to advocate the introduction of this risk in the protection system. During the last two decades, data concerning the increase of the frequency of different non-tumoral-diseases in irradiated populations were collected. Although these studies reinforced the statistic evidence concerning the association of cardiac diseases, ictus, digestive malfunctions, respiratory diseases and so forth with dose, the ICRP has not recognised the available data as suitable for a complete evaluation of the detriment subsequent to low dose exposition. More generally, no proof of additional risk was found with regard to dose values below 1 Gy. Because of the incomplete knowledge of the interaction, at low doses, between the irradiation and other agents, a modification of the previous risk estimations was evaluated by the United Nations Scientific Committee on the Effects of Atomic Radiation [*UNSCEAR, 2000*]. In light of these considerations, the model chosen for radiation protection practice is the Linear Non-Threshold. The latter is based on the

assumption that, below a dose value of about 100 mSv, the increment of the probability of developing cancer or hereditary diseases is directly proportional to the increase of the dose. In other words, this model asserts that there is no threshold value for exposure, below or above which the response is non-linear: in spite of conflicting experimental results, in light of the limited knowledge on the mechanisms of development of the radiation consequences, this kind of prudent approach is largely preferable.

## 2.2 DOSIMETRIC QUANTITIES

To satisfy adequately the need to evaluate the importance, in terms of biological effects, of radiation exposure, dosimetric quantities were developed. In general, radiation protection quantities are based on the estimation of energy deposition, through the irradiation, in the organs and tissues of the human body. However, to evaluate the risk related to exposure it is necessary to take into account the biological effectiveness of radiation received; this effectiveness is associated to both the different quality of the irradiating species and the intrinsic sensitivity associated to the target tissues or organs. In *Publication 60 [ICRP, 1991]*, the concepts of *dose equivalent* and *effective dose* were defined, providing the possibility to evaluate the total amount of dose as the sum of different contributions – such as different radiation types or irradiation modalities. An additional source of complication lies in the impossibility of a direct measurement of the quantities mentioned so far: operational measurable quantities have been defined to allow the evaluation of H and E. The procedure concerning the estimation of the effective dose, primary instrument in the field of radiation protection, consists of different steps. The *absorbed dose*  $D$  is used as the basic dosimetric physical quantity: it is averaged on volumes, organs or tissues of interest, while the differences regarding the biological effectiveness of the radiations and targets sensibility are taken into account by means of weighting factors. This quantity is used for every kind of ionizing radiation as well as for every irradiation geometry. It is defined as the ratio of the average energy ( $d\mathcal{E}$ ), that the ionizing radiation deposits in an infinitesimal element of target material, to the mass of the infinitesimal element itself ( $dm$ ), as shown in formula 2.1.

$$D = \frac{d\epsilon}{dm} \quad (2.1)$$

The unit of measurement of the absorbed dose in the International System (SI) is the gray (Gy), defined as the absorption of one joule of ionizing radiation by one kilogram of matter. Since this quantity is calculated on the average value of the absorbed energy, it is not affected by the random fluctuations related to the single interactions occurred in the tissue. Moreover, it is a measurable quantity, characterised by standards defined in order to estimate its value: on this basis, it is possible to assert that the absorbed dose has all the requirements of a physical basic quantity.

To calculate the *effective dose*, an average of the values of equivalent dose, thus obtained, weighted over the interested organs and tissues is taken. Hence, the effective dose is found on the basis of the exposition related to different external radiation fields and radionuclides introduced in the body – in addition to considerations concerning physical interactions and biological reactions. The reliability of the calculated average value in terms of representation of the real absorbed dose, depends on the homogeneity of the irradiation and on the incident radiation nature. In particular, in case of partial exposure or heterogeneous irradiation, tissue damages can occur even if the averaged absorbed dose, or the effective dose, is lower than the threshold value. On the other hand, the *equivalent dose* for the target considered,  $H_T$ , gives direct information on the contribution of a particular organ or tissue to the total detriment caused by uniform irradiation of the organism, and it is calculated by means of radiation weighting factors,  $w_R$ . These latter multiply the average absorbed dose  $D_{T,R}$ , calculated with regard to the radiation R hitting the target of interest T, obtaining the equivalent dose as shown in the equation 2.2:

$$H_T = \sum_R w_R D_{T,R} \quad (2.2)$$

The equivalent dose is expressed in sievert (Sv), equal to  $J \cdot kg^{-1}$ , like the gray used to measure the absorbed dose, since the weighting factors are dimensionless. The values of this multiplier elicit a distinction between high- and low-LET (Linear Energy Transfer) radiations. The average amount of energy released by a radiation over the length of its

track, expressed through the LET value, represents an important indicator in the evaluation of biological damage produced by charged particle radiation. High LET radiations have the high values of radiation weighting factor because of the larger ionizing power, or rather, because of the capacity of depositing a large amount of energy in a very short distance.

TYPE OF RADIATION	RADIATION WEIGHTING FACTOR ( $w_R$ )
Photons	1
Electrons and muons	1
Protons and charged pions	2
Alpha particles, fission fragments, heavy ions	20
Neutrons	Continuous function of energy

**Table 2.1** Radiation weighting factor values for different types of radiations [ICRP, 2008]

The  $w_R$  values were defined on the basis of the Relative Biological Effectiveness (RBE) associated to the different radiation types. The latter can be described as a measure of the capacity of a specific ionizing radiation to produce a specific biological effect, expressed with respect to a reference radiation. In the case of the neutrons, the biological effectiveness of the radiation hitting living tissue is a function of the energy of the incident particle, as shown in Figure 2.1. As can be seen, the most important incident neutron energies, in terms of biological effects, are those between 0.001 and 1000 MeV. On a quality level, the main effects to take into account in the evaluation of neutron radiation exposure are:

- Production of secondary photons, due to the absorption of the neutron in the tissue, the probability of which increases with the decrease of the incident energy;
- Increasing of the recoil proton energies with increasing of incident energy;
- Emission of heavy charged particles associated to high energy neutrons;
- Spallation processes for very high energies

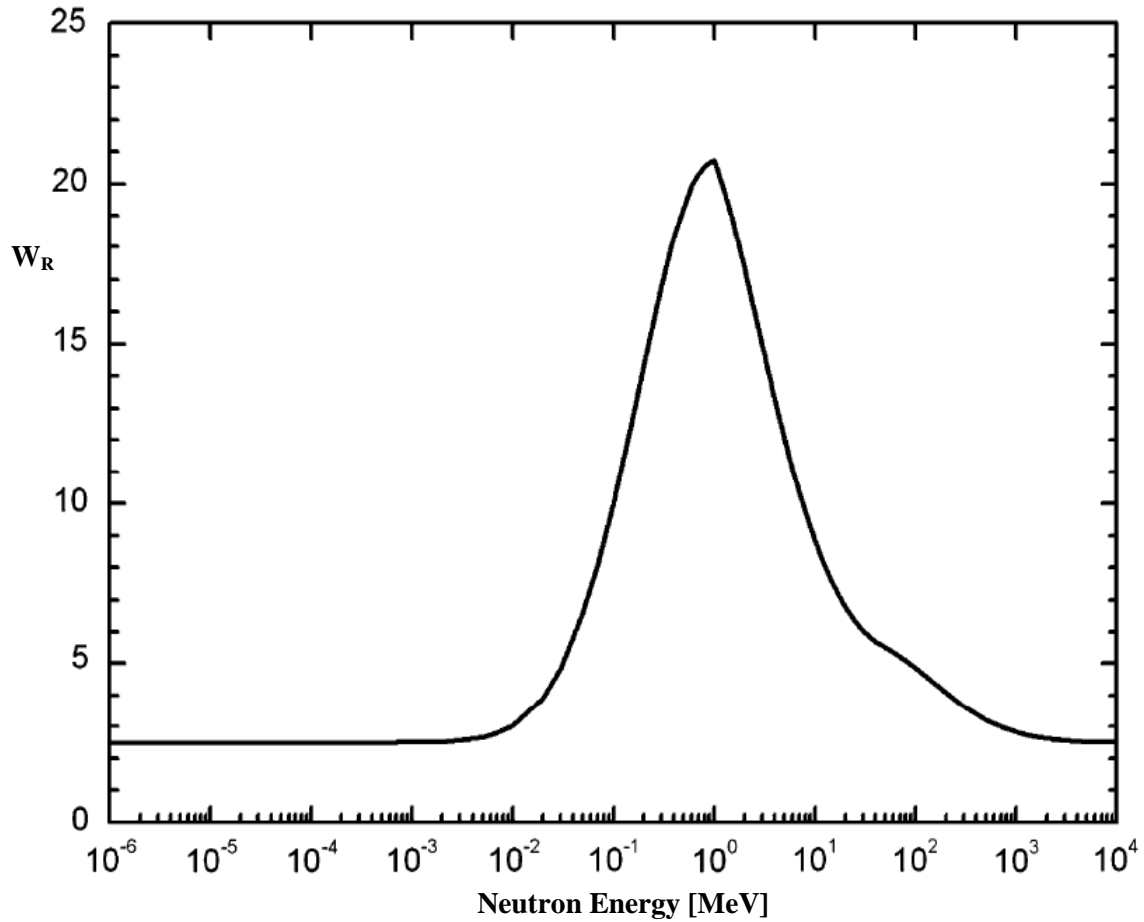


Fig. 2.1 Radiation weighting factor function for neutrons [ICRP, 2008]

Moreover, the use of a continuous function for the neutron weighting factors, is related also to the consideration that most part of neutron expositions involve energy spectra extending continuously over some width.

To calculate the effective dose, all the contributions in terms of equivalent dose must be summed. Furthermore, it is necessary to take into account the different importance, in terms of occurrence of stochastic effects, related to the various organs and tissues: each contribution is associated to a tissue weighting factor  $w_T$ , characterising the target of interest. The effective dose is calculated as a weighted sum of equivalent doses to the different tissues, as shown in formula 2.3.

$$E = \sum_T w_T H_T = \sum_T w_T \sum_R w_R D_{T,R} \quad (2.3)$$

The weighting factors associated to the different tissues, like those related to the radiation nature mentioned before, are normalised to one:

$$\sum_T w_T = 1 \qquad \sum_R w_R = 1 \qquad (2.4)$$

The unit of measurement of the effective dose is the same as for the equivalent dose, the sievert ( $1\text{Sv} = 1 \text{ J}\cdot\text{kg}^{-1}$ ).

TISSUE	$w_T$	$\sum w_T$
Bone marrow (red), colon, lung, stomach, breast, remainder tissues	0.12	0.72
Breast, remaining tissues (adrenal glands, lungs, pancreas, heart, lymph nodes etc.)	0.08	0.08
Bladder, liver, thyroid, oesophagus	0.04	0.16
Bone surface, brain, salivary glands, skin	0.01	0.04
	TOTAL	1.00

**Table 2.2** Tissue weighting factor for different organs [ICRP, 2008]

The tissue weighting factor values, shown in Table 2.2, are defined on the basis of epidemiological studies concerning the induction of cancer and the risk of hereditary effects among exposed populations. These values are obtained averaging over all ages and both sexes, to obtain a result independent of single individual characteristics. The value of the factor for the remaining tissues involves average values associated to thirteen additional organs.

The effective dose, just as the equivalent dose, cannot be directly measured directly in practical applications: for this reason, to assign a reliable value to these quantities, it proved necessary to evaluate suitable conversion coefficients. These latter are different, according to the exposure condition: in the case of external irradiation, the conversion factor is estimated with computational human body models, taking into account different radiation fields. In the calculation of the conversion coefficients related to the radionuclides ingestion, biokinetic models and physiological reference values are used in addition to the human phantoms. These latter are produced from tomographic images and

consist of three-dimensional pixels (the so called voxels). In order to obtain the equivalent dose for the “Reference Person”, each of these volumetric elements is shaped as a combination of the values that approximate the mass of the organs attributed to the “Reference Man” and the “Reference Woman” – the human phantoms approximating the prototypes of men and women on which the standards of radiation protection rely. Concerning these phantoms, conversion coefficients are evaluated with regard to physical measurable quantities, such as particle fluence, air kerma (Kinetic Energy Released for unit of Mass) or activity incorporation for internal exposure. Table 2.3 shows the different quantities used in radiation protection.

<b>DOSE QUANTITIES</b>		
<b>Basic physical quantities</b>	<b>Operational quantities [Sv]</b>	<b>Protection quantities [Sv]</b>
Fluence ( $m^{-2}$ )	Ambient dose equivalent	Equivalent dose for organs and tissues
Kerma (Gy)	Directional dose equivalent	Effective dose for the whole body
Absorbed dose (Gy)	Personal dose equivalent	

**Table 2.3** Summary of the different type of dose quantities

With those conversion factors it is possible to relate the dosimetric quantities, and consequently the associated protection limits, to the operational quantities discussed in the following pages [ICRP,2008].

## **2.3 OPERATIONAL QUANTITIES**

As said in paragraph 2.1, the radiation protection quantities relating to the body (the dose equivalent and the effective dose) are not directly measurable and are consequently not available for monitoring. To evaluate them with respect to the irradiated tissues or organs, it is necessary to use practical and measurable quantities. These latter, then, are introduced with the aim of giving an estimate or an upper limit, related to the dosimetric quantities analysed, in most exposure conditions. In the table 2.4, the different dose

quantities are presented. The operational quantities are generally used in practical guidelines and in control standards. To satisfy adequately this purpose, two primary categories of irradiation nature are taken into account: the external and the internal exposures.

### **2.3.1 External Exposure**

In the individual or environmental monitoring of external irradiation, specific practical quantities for the equivalent dose are defined. The associated values are considered an accurate approximation of those related to the main dosimetric quantities. The unavoidable need of dosimetric operational quantities is primarily due to:

- the necessity of quantities related to a single point of measurement in ambient monitoring;
- the need in ambient dosimetry to have values independent of the angular directional distribution of radiation;
- the need to define reference standards for the physical quantities, in order to calibrate instruments of measure;

The radiation protection field covers a wide variety of applications and consequently different operative quantities are required. In particular, with regards to the work monitoring of spaces or to the definition of controlled and supervised areas, free-in-air-measurements are preferable, while, in terms of limitation of individual exposition, personal dosimeters are used. Because of the more complex radiation field registered by the dosimeters, due to the influence of back-diffusion or radiation absorption in the body, the values resulting from the two different types of measurements can differ significantly. For this reason, different operative quantities are used in the two kinds of measurement, as shown in Table 2.4.

These operational quantities are defined and constantly revised by the International Commission of Radiation Units (ICRU). In the ICRU 1993b, it is specified that both  $H^*(10)$  and  $H_p(10)$  are related to highly penetrating radiation, as photons with energy

above 12 keV or neutrons, while  $H'(0.07, \Omega)$  and  $H_p(0.07)$  refer to low penetrating radiation, as  $\beta$ -rays.

TASK	DOSIMETRIC OPERATIVE QUANTITIES	
	Ambient monitoring	Individual monitoring
Evaluation of effective dose	Ambient dose equivalent $H^*(10)$	Personal dose equivalent $H_p(10)$
Evaluation of skin, hands, feet and eye lens doses	Directional equivalent dose $H'(0.07, \Omega)$	Personal dose equivalent $H_p(0.07)$

**Table 2.4** Dosimetric operational quantities introduced in ICRP publications

It must be noted that in some cases the estimate of personal dose is obtained by means of ambient equivalent dose, as in monitoring of doses to aircraft crew. All these operational quantities, in the case of external irradiation, are defined on the basis of an equivalent dose value evaluated at one point within a simple phantom, the ICRU sphere. It consists of a sphere of tissue-equivalent material, with a diameter of 30 cm and a density of  $1 \text{ g}\cdot\text{cm}^{-3}$ . The tissue contains oxygen (mass fraction 76.2%), carbon (11.1%), hydrogen (10.1%) and nitrogen (2.6%), to approximate adequately the human body in terms of radiation field diffusion and attenuation.

As mentioned, in environmental monitoring, the operational quantity of reference is the ambient dose equivalent  $H^*(10)$ . This is defined as the dose equivalent which would be generated in the associated oriented and expanded radiation field at a depth of 10 mm on the radius of the ICRU sphere which is oriented opposite to the direction of incident radiation. An oriented and expanded radiation field is an idealized radiation field in which the particle flux density and the energy and direction distribution of the radiation show the same values at all points of a sufficient volume as the actual radiation field at the point of interest. as schematically represented in the Figure 2.2.

In most external exposure applications in practice, the ambient dose equivalent provides a prudent estimate or an upper limit value associated to the quantities of interest. However, this consideration is not always true for individuals subject to high energy irradiation, as in proximity of high energy accelerators or in cosmic radiation fields. Actually, in these cases, the depth of 10 mm, considered through the ambient equivalent dose  $H^*(10)$ , is not

sufficient to obtain the build-up of the incident charged particles in that point. In other words, if the incident radiation is characterised by a very high energy, the charged particle will not reach equilibrium in the distance considered and therefore the operational quantity will be an underestimation of the actual dose imparted.

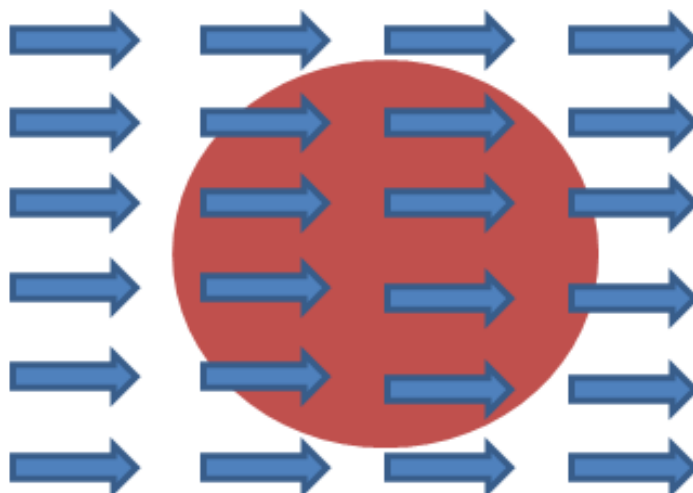


**Fig. 2.2** Schematic representation of an oriented and expanded radiation field

In ambient monitoring of low-penetration radiations, the operational quantities used are the directional equivalent dose  $H'(0.07, \Omega)$  and  $H'(3, \Omega)$ . The first is defined as the dose equivalent produced in the ICRU sphere at a depth of 0.07 mm on the radius characterised by a direction  $\Omega$ , and represents the skin dose. In the case of strongly penetrating radiation, skin dose will not significantly contribute to the effective dose. Therefore, the directional dose equivalent is only important for low penetrating radiation, such as alphas, betas with energies lower than 2 MeV and photons with energies lower than 15 KeV. In the evaluation of doses to the eye lens the ICRU recommends instead the use of a depth value equal to 3 mm, and consequently of the quantity  $H'(3, \Omega)$ . In spite of this, the  $H'(3, \Omega)$ , as well as the personal equivalent dose  $H_p(3)$ , have been rarely used and few instruments are available for these types of measurement. For the eye lens dose monitoring the use of the personal equivalent dose  $H_p(0.07)$  is more commonplace. Summarizing, the only quantity really used in ambient monitoring of low-penetration-radiations is the  $H'(0.07, \Omega)$ . Regarding the one-directional radiation, chiefly in case of calibration procedures, the operational quantity can be written as  $H'(0.07, \alpha)$ , where  $\alpha$  is the angle included between the direction  $\Omega$  and that of the incident radiation track. Often,

in practical applications, the  $\Omega$  value is not specified because the interest is focused on the maximum value of the operational quantity in the point considered. This estimate is usually obtained rotating the dosimeter during the measurement process, until the highest value is reached.

The individual monitoring of external exposure is effected by personal dosimeters. Therefore, the associated operational quantity has to take into account the particular configuration of the problem due to the wearing of the measurement device – the value obtained depends on the irradiation conditions around the device. The individual exposure is monitored through the personal equivalent dose  $H_p(d)$ . This one is defined as the dose equivalent in soft tissue, at an appropriate depth,  $d$ , below a specified point on the body, corresponding to the position of the personal dosimeter. In estimating the effective dose, a depth of 10 mm is recommended, while to evaluate the equivalent dose for the skin, hands or feet, it is preferable to use  $d=0.07$  mm, and  $d=3$ mm for eye lens dose evaluation. Anyway, the aim of an operational quantity for individual monitoring is to provide the evaluation of the effective dose in each irradiation condition. Consequently the personal dosimeter must be worn in a position that is representative of body exposure. If the dosimeter is positioned in correspondence of the fore part of the trunk, the  $H_p(10)$  provides a conservative estimate of  $E$ , even in case of lateral or isotropic incidence of radiation on the body. On the contrary, if the exposition is essentially coming from the posterior direction, a dosimeter placed at the front cannot provide an adequate measure of the effective dose. In addition, in case of partial exposition of the body, the personal dosimeter can provide an inexact value of the effective dose.

### **2.3.2 Internal Exposure**

The determination of the dose due to nuclides incorporated in the body, generally through inhalation or ingestion, is based on the calculation of the radiation activity introduced. The latter can be estimated by direct measurements on the body, or by measuring the activity present in environmental and biological samples. In general, biokinetic models must be used: the incorporated dose is evaluated combining the incorporated activities measured with suitable coefficients of reference (in terms of  $Sv \cdot Bq^{-1}$ ), provided by the

Commission and mentioned also in the UE guideline (UE, 199) as well as in the international Basic Safety Standards (IAEA, 1996). These factors, given for a large number of radionuclides, are determined both for the general population and for exposed workers. On the other hand, studies have demonstrated that a different procedure can be, in some cases, more suitable [Berkovski *et al.*, 2003]. In particular, advantages were found in calculating the effective dose directly from the measurements, by means of suitable functions. These functions are used to evaluate the activity incorporated at  $t=0$  from the activity at the moment of the measurement. However, to interpret correctly the values obtained this method requires additional tables, supposed to be provided by the Commission, concerning the “dose per unit content” and its time dependence. This method could simplify the analysis of the monitoring data and a development of the procedure in this direction is greatly desirable.

## **2.4 RADIATION STANDARDS REGULATION**

The wide variety of exposure situations is categorised by three main types that cover the entire range of irradiation circumstances: the planned, existing and emergency exposure situations. The first of these categories encompasses sources and situations appropriately managed within the system of radiological protection – for example protection during medical applications of radiation is included in this class. The naturally occurring exposures, as well as exposures due to past events and accidents or practices unrelated to the radiological protection system, are comprised in the second category, i.e. the existing exposure situations. These are defined as exposure situations that already exist when a decision on control has to be taken, such as those caused by natural background radiation. The most common case of this category is related to the presence of indoor radon in dwellings and workplaces. Finally, the emergency exposure situations involve unexpected circumstances such as those that may occur during the operation of a planned situation, or from a malicious act, requiring urgent attention and rapid interventions.

At this point, it is necessary to specify the three key principles, introduced in ICRP publications, which are the basis of radiological protection. The first two of these criteria, the principles of *justification* and *optimisation*, are related to all the different exposure situations described; on the contrary, the assumption of application of dose limits applies exclusively for doses expected to be incurred with certainty as a result of planned exposure situations. More precisely, the principles mentioned are defined as follows:

- *The principle of Justification* declares that “any decision that alters the radiation exposure situation should do more good than harm”.
- *The principle of Optimisation of Protection* (or *ALARA principle*) asserts that “the likelihood of incurring exposure, the number of people exposed, and the magnitude of their individual doses should all be kept as low as reasonably achievable, taking into account economic and societal factors”.
- *The principle of Application of Dose Limits* asseverates that “the total dose to any individual from regulated sources in planned exposure situations other than medical exposure of patients should not exceed the appropriate limits specified by the Commission.

In addition to exposure situations, classifications are provided with respect to the role of the exposed individuals. Three categories of exposure are specified in these terms: occupational exposures, public exposures and medical exposures (of patients, carers, volunteers etc.). Special attention is required in the face of pregnancy of a female worker, to attain the same level of protection for the embryo as for members of the public.

In light of these classifications of exposure conditions, the concepts of *dose constraint* and *reference level* were introduced to optimise the protection in terms of individual dose limitation. The dose constraint should not be confused with the *dose limit*, which is a person-related quantity having the statute of a legal limit to the dose that an individual can receive from the entirety of practices to which he/she can be exposed. The principle of limitation of individual doses is conceptually different from the establishment of constraints for optimisation of given sources. In selecting a constraint the existence of a source upper bound should be taken into account such that the numerical values of the constraints should be no larger than that of this upper bound. The objective of a dose

constraint is to constitute a ceiling to the values of individual doses from a source, practice or task that could be determined to be acceptable in the process of optimisation of protection for that source [OECD, 1996].

In the ICRP radiation protection recommendations, dose constraints are provided concerning planned situations, while reference levels are suggested for emergency and existing exposure situations. This terminological distinction concerning exposure situations, expresses the different applicable dose limitation strategy. In detail, in planned situations the restrictions of individual doses can be obtained in the design phase and it is possible to anticipate that the values will be lower than the constraints imposed. On the contrary, in the other situations a larger variety of exposures can exist and, consequently, the optimisation process can be applied to initial individual doses above the reference value.

	<b>OCCUPATIONAL EXPOSURE</b>	<b>PUBLIC EXPOSURE</b>	<b>MEDICAL EXPOSURE</b>
<b>PLANNED EXPOSURE</b>	Dose limit Dose constraint	Dose limit Dose constraint	Diagnostic reference level (Dose constraint <sup>b</sup> )
<b>EMERGENCY EXPOSURE</b>	Reference level	Reference level	n/a
<b>EXISTING EXPOSURE</b>	n/a <sup>a</sup>	Reference level	n/a

<sup>a</sup> Exposure resulting from long-term remediation operations or from protracted employment in affected areas should be treated as part of planned occupational exposure, even though the source of radiation is “existing”.

<sup>b</sup> Comforters, carers, and volunteers in research only.

**Table 2.5** Dose constraints and reference levels used in the system of radiological protection (ICRP 103)

The estimate of dose constraints and reference levels must take into account the circumstances of exposure; moreover, it is important to specify that these values do not represent a boundary between “dangerous” and “safe” level of dose: as discussed before, there does not exist a step change in the risk for human health related to irradiation. In the Table 2.5 the different types of dose restrictions are presented with reference to the exposure situations and categories.

The annual individual dose limits related to the planned exposures exposure situation, are presented in Table 2.6. In addition, in case of medical exposures a diagnostic reference level is estimated, to take into consideration potential additional exposures.

<b>LIMIT QUANTITY</b> (protection dose quantity)	<b>EXPOSED WORKERS</b> (aged over 18)	<b>APPRENTICES AND STUDENTS</b> (aged between 16 and 18)	<b>PUBLIC</b>
<b>Effective dose</b>	100 mSv/ 5 <sup>a</sup> 50 mSv on a single year	6 mSv	1 mSv
<b>Equivalent dose for the lens of the eye<sup>a</sup></b>	150 mSv	50 mSv	15 mSv
<b>Equivalent dose for the skin and extremities</b>	500 mSv	150 mSv	50 mSv

<sup>a</sup> New data on the radiosensitivity of the eye, which will lead to a reduction of the present dose limit values, are expected.

**Table 2.6** Dose limits recommended in planned exposure situations

# CHAPTER III

## Rem Meters

To evaluate the doses associated to a particular radiation field, it is necessary to know the exposure characteristics, to wit the species, the energy and direction distribution of the incoming radiation. Therefore, the monitoring of stray radiation at workplaces, like that associated to the shielding of high-energy proton accelerators, is a difficult task. In most applications dosimetric evaluations are required concerning complex radiation fields, which may be composed of neutrons, charged hadrons, muons, photons and electrons. The involvement of different radiation species, with spectra extending over a wide range of energies and complex direction distributions, introduces a large uncertainty into the analysis of the radiation field itself. In other words, it is not always possible to know exactly the exposure conditions, and consequently it is not always feasible to calculate the dosimetric quantities of interest on the basis of knowledge of the radiation field involved.

The need to have a valid instrument to evaluate the equivalent dose also in complex fields is posed, first of all, by neutron exposure: the strong penetrating power of these particles makes neutron radiation a particularly dangerous form of ionizing radiation. Actually, in the majority of cases, this kind of radiation is responsible for the larger fraction of an exposed worker's equivalent dose. For these reasons, throughout the world, neutron rem meters are used by health physicists for real-time measurement of neutron equivalent dose, becoming the instrument of choice in radiation fields in which the neutron spectrum is either unknown or poorly characterised. In this chapter, the main characteristics of this kind of devices and the associated state of the art are analysed. Finally the structure and features of the WENDI-2 rem meter, the study of which is the principal task of this work, is examined.

### 3.1 DOSE EQUIVALENT EVALUATION

Although nowadays the name of these devices sounds definitely obsolete – it refers to the unit of radiation dose introduced in 1962 and substituted, in the International System of Units, by the Sievert (1 rem = 0.01 sievert) – they are, possibly, the most common instrument for neutron monitoring in the workplace. Generally, a rem counter is comprised of a thermal neutron detector placed inside a moderator: the design of the device ensures a good correspondence between the response function of the instrument and the curve of the conversion coefficients from neutron fluence to  $H^*(10)$ , over a large range of energies. In other words, the response function of the detector is designed to match approximately, on a particular energy range, a suitable fluence-to-dose conversion function. According to the ICRP recommendations, the appropriate calibration function for this purpose is the Ambient Dose Equivalent, already mentioned in the former chapters. This quantity, for a known neutron spectrum, can be defined as shown in formula 3.1.

$$H^*(10) = \int h_{\varphi}(E) \Phi(E) dE \quad (3.1)$$

where  $E$  is the incident energy of the particle,  $h_{\varphi}(E)$  is the fluence-to-ambient-dose equivalent conversion function, and finally  $\Phi(E)$  is the neutron fluence as a function of energy for a given neutron field. The latter represents the quotient of the number of particles,  $dN$ , incident upon a small sphere of cross-sectional area  $da$  (formula 3.2).

$$\Phi = \frac{dN}{da} \quad (3.2)$$

More precisely, the fluence is a non-stochastic quantity – defined in a point by a single value without intrinsic fluctuations – used in the description of external radiation field.

$$R = \int C d_{\varphi}(E) \Phi(E) dE \quad (3.3)$$

It is independent from the angular distribution of the particles and it must be considered as an expected value – since it is not influenced by the statistic fluctuations of the number of particles crossing the considered surface. This quantity is involved also in the

definition of the rem meter response,  $R$  (formula 3.3). In this case  $C$  is a calibration constant, associated to the particular device and the peculiar neutron field, expressed in Sievert per count. The quantity  $d_\varphi(E)$ , instead, is the rem meter's response function in terms of counts per unit of fluence: it represents the fraction of incident neutrons detected by the device as a function of their energy. Considering these definitions, the rem meter measurement is as accurate as the energy response of  $d_\varphi(E)$  is similar to that characterising the fluence-to-ambient dose equivalent conversion function,  $h_\varphi(E)$ . Indeed, in case of correspondence between the trend of the two mentioned functions, the difference in the resulting value of  $H^*(10)$  and  $R$ , can be reconciled updating the value of the calibration constant  $C$ . In addition, the ratio  $d_\varphi(E)/h_\varphi(E)$  expresses traditionally the energy response of the rem meter, in terms of count per unit dose equivalent. Clearly, in the design phase, these considerations must be taken into account, influencing first of all the choice of materials on the basis of the interaction of neutrons with matter. In other words, an appropriate rem meter model has to ensure that those neutrons characterised by a larger importance in terms of dose equivalent have a higher probability to be detected by the device [Silari *et al.*, 2009].

## 3.2 HISTORY AND STATE OF THE ART

The first design of a rem counter device dates back to 1963, when the article “A neutron rem counter with uniform sensitivity from 0.025 eV to 10 MeV” by Andersson and Braun was published [Anderson and Braun, 1963]. The novelty introduced by this work consisted in providing a device capable to reproduce the dose equivalent for a neutron energy range that covers all neutrons emitted by nuclear power installations. A standard AB-rem-counter, as described in the article mentioned, consists of a proportional counter tube filled with boron-fluoride (BF<sub>3</sub>) or helium-3, both gases used in light of their high neutron reaction cross section. As shown in the first chapter (Figures 1.4 and 1.6), the cross section associated to neutron absorption in these compounds is roughly inversely proportional to neutron velocity: as a consequence, the reaction probability is highest for thermal neutrons. In order to shape adequately the response function of the device, or

more precisely to decrease the importance of low-energy neutrons in terms of detection probability, boron doped plastic attenuators are often used. The borated compound, serves the purpose of capturing the less energetic neutrons, preventing their detection. At the same time, to increase the probability of detecting more energetic neutrons, a moderator material surrounds the counter tube, decreasing the velocity of the incoming particles through scattering interactions. In some recent cases a cadmium layer replaces the mentioned borated plastic. The moderators employed in the most part of commercial devices, are cylindrical or spherical: the choice of this geometry ensures a more isotropic response of the detector. Concerning the material, polyethylene is generally used because of its effectiveness in slowing down neutrons. Whatever the shaping of the response function made through the choice of construction details, the drop in sensitivity restricts the useful upper energy limit to 10 MeV, as shown in the article by Andersson et al. This decrease of the rem counter performance brings about a drastic underestimation of the dose equivalent, due to the opposite trends of the response and fluence-to-ambient-dose equivalent function for neutron energies for above the thermal region. The result of the abrupt fall of the response in this part of the domain can be estimated to be equal to an inaccuracy of 40% above 20 MeV. To overcome this limitation and render the use of this type of counter possible also for high-energy accelerators, a new rem meter design was proposed at the end of 1980s. This instrument model, named LINUS, was obtained modifying a common A-B monitor: in particular, the novelty introduced consisted in the insertion of a layer of lead between the boron-doped plastic attenuator and the outer polyethylene moderator. In this layer of a thickness equal to 1 cm, inelastic scattering reactions occur [Birattari et al., 1998]. These latter involve incoming neutron characterised by energies higher than 10 MeV: as a result, low-energy neutrons are produced and subsequently moderated by the inner polyethylene, assuring their detection by the thermal counter. In light of this, the response of this kind of rem meter is improved, with respect to the conventional moderator instruments described before, in the energy region above 10 MeV, while below these values there are no significant differences. The incorporation of a high-Z material in the moderator, at the basis of the LINUS design, is reproduced in several instruments, having recourse to tungsten or lead generally. The Wendi-2 neutron rem counter, commercialised by Thermo Fisher Scientific, belongs to a group of a few improved models currently available on the market: since the study of the response function of this device represents the main task of

this work, the design and properties of this neutron detector are described below in greater detail.

### **3.3 WENDI-2**

The Wendi-2 neutron detector is the result of a meticulous research, carried out since 1992. The main purpose associated to the research on the Wide Energy Neutron Detector Instrument (WENDI) has been to design a universal rem meter, characterised by a good high-energy and isotropic directional response as well as by a reasonable weight and sensitivity and by an improved accuracy in the range of intermediate energies. In particular, the latter requirement is due to the necessity of reliable measurements of the dose in the range from 50 keV to 250 keV, since it is critical with respect to the personal dose at nuclear power plants.

The main idea was to develop a new design on the basis of the basic principles analysed before. The first result of this collaborative effort between Los Alamos National Laboratory, San Jose State University, and Varian Associates, was the production of a first-generation-design of WENDI neutron rem meters (United States Patent number 5,578,830 granted to the University of California on 26 November 1996). The invention involved a neutron dose equivalent detector for measuring neutron dose, capable of responding accurately to neutron energies according to published fluence to dose curves. The neutron dose equivalent meter, described in the patent, has an inner sphere of polyethylene, with a middle shell overlying the inner sphere, the middle shell comprising silicone (organosiloxane) loaded with boron. An outer shell overlies the middle shell and comprises polyethylene loaded with tungsten. The device defines a channel through the outer shell, the middle shell, and the inner sphere for accepting a neutron counter tube. The outer shell is loaded with tungsten to provide neutron generation that, as it will be explicated in detail below, increases the neutron dose equivalent meter's response sensitivity above 8 MeV. The main advantage introduced with this kind of design consisted in remedying to the lack of commercial rem meters with useful response at

energies higher than 20 MeV. Actually, before the introduction of WENDI-1 detectors on the market, the rem meters produced were seriously handicapped in accelerator environments, where neutrons may be produced having energies in the GeV range. Commercially available instruments, such as SNOOPY, manufactured by Nuclear Research Corporation, or the Eberline NRD, had a very poor response to high-energy neutrons. Moreover, because the SNOOPY rem meter used a cylindrical moderator, its directional response was unbalanced – in other words the shape of its response function was not identical for both side and frontal exposures.

In 1999, a second generation WENDI design was proposed, on the basis of the WENDI technology platform. The critical innovative step introduced by this design, was the further extension of the useful energy range detected by this rem meter. However, the improvement related to the high-energy response and the increased sensitivity is reached at the cost of some increase in weight – the device weighs 14 Kg. The response function of a rem counter is influenced by different factors: the size, shape and type of moderator, the amount and type of neutron absorbers used and the presence of neutron generating materials. While in the case of WENDI-1 a spherical moderator was chosen, aiming to assure a uniform directional response, in the WENDI-2 design a cylindrical geometry was adopted. This latter choice has the purpose of simplifying the manufacturing process; moreover, although a non-spherical moderator shape was chosen, by means of an extensive series of Monte Carlo simulations, it was possible to design the assembly so that coherence between the side and the end response function is guaranteed above neutron energy of 1 MeV. As discussed before, the shaping of the rem counter response function is obtained taking into account the characteristics, in terms of neutron interactions, of the different materials adopted in the device design. In particular, a neutron absorbing material is required to decrease the detection count associated to low-energy neutrons: the introduction of this type of material produces a good match between the response function of the device and the Ambient Dose Equivalent  $H^*(10)$  for the lower values of the energy range. At the same time, it is essential to introduce a neutron generator material that could increase the detected neutrons number for incident energy values higher than 8 MeV.

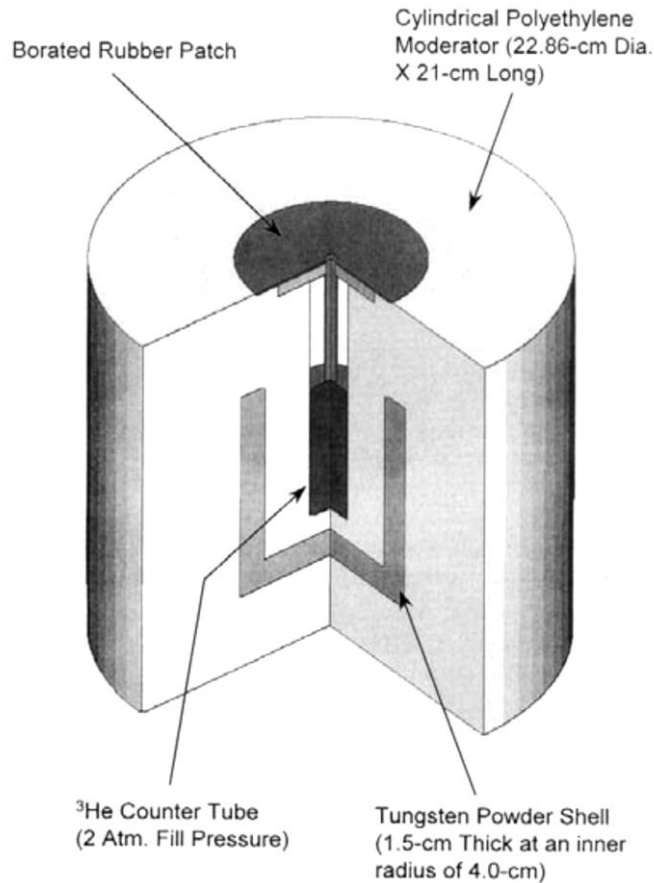


**Figure 3.1** WENDI-2 Rem Meter cutaway view [*Thermo Scientific, 2007*]

In WENDI-2 the design of these tasks are affected by the same material, i.e. the tungsten powder. The latter is allocated in the polyethylene moderator, forming a shell, as it possible to see in Figure 3.1. Therefore, the tungsten powder shell performs double duty as both a neutron generator material above 8 MeV and as an absorber below several keV, as it possible to deduce observing the trend of the capture tungsten cross section in Figure 3.2. On this basis, the high absorption resonance structure in the energy region of 0.1 keV to 1.5 keV facilitates shaping the detector response function at intermediate neutron energies.

With regards to the tungsten's proprieties, mentioned before, as neutron generator, there are different reactions of interest. First of all the (n,2n) reaction probability becomes significant above a threshold of 8 MeV in tungsten, such as in uranium, lead and, more generally, in heavy nuclei. Similarly, above an incoming energy equal to 14 MeV, the (n,3n) reaction becomes energetically possible.

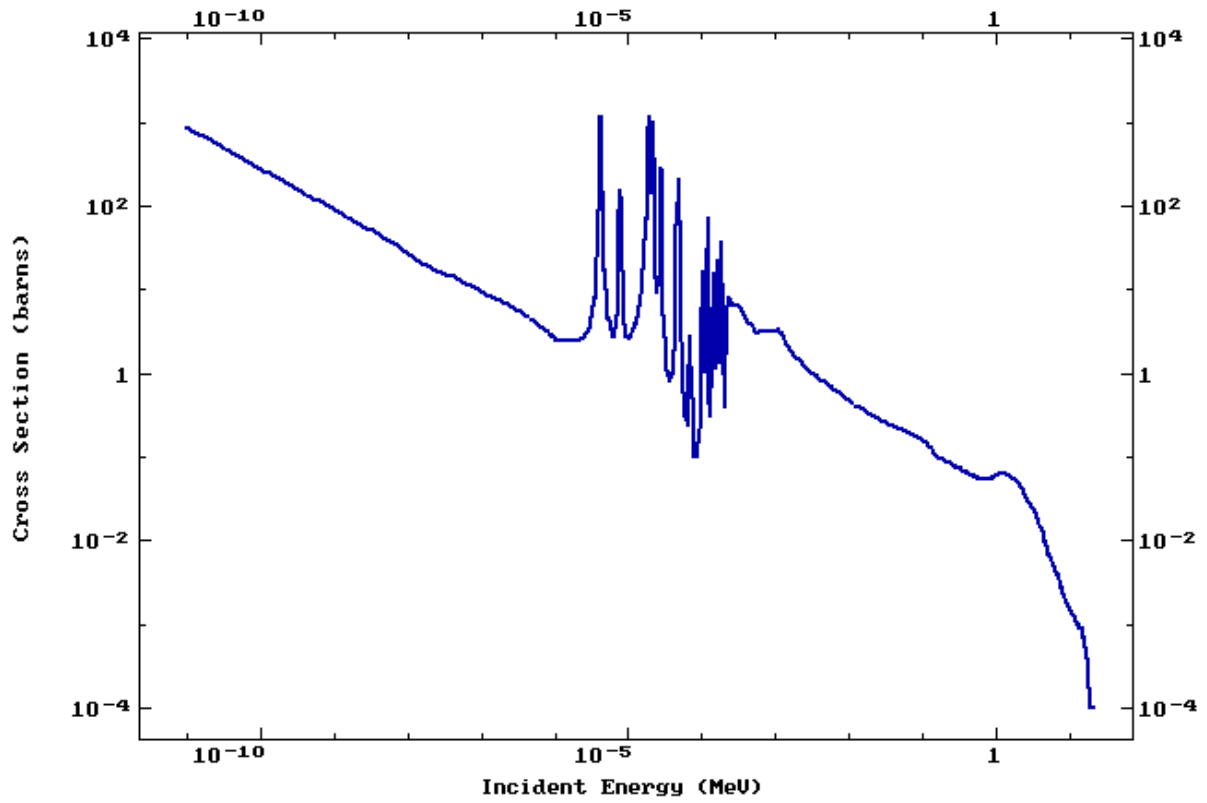


Figure 3.2 Neutron capture cross section for tungsten [ENDF, 2012]

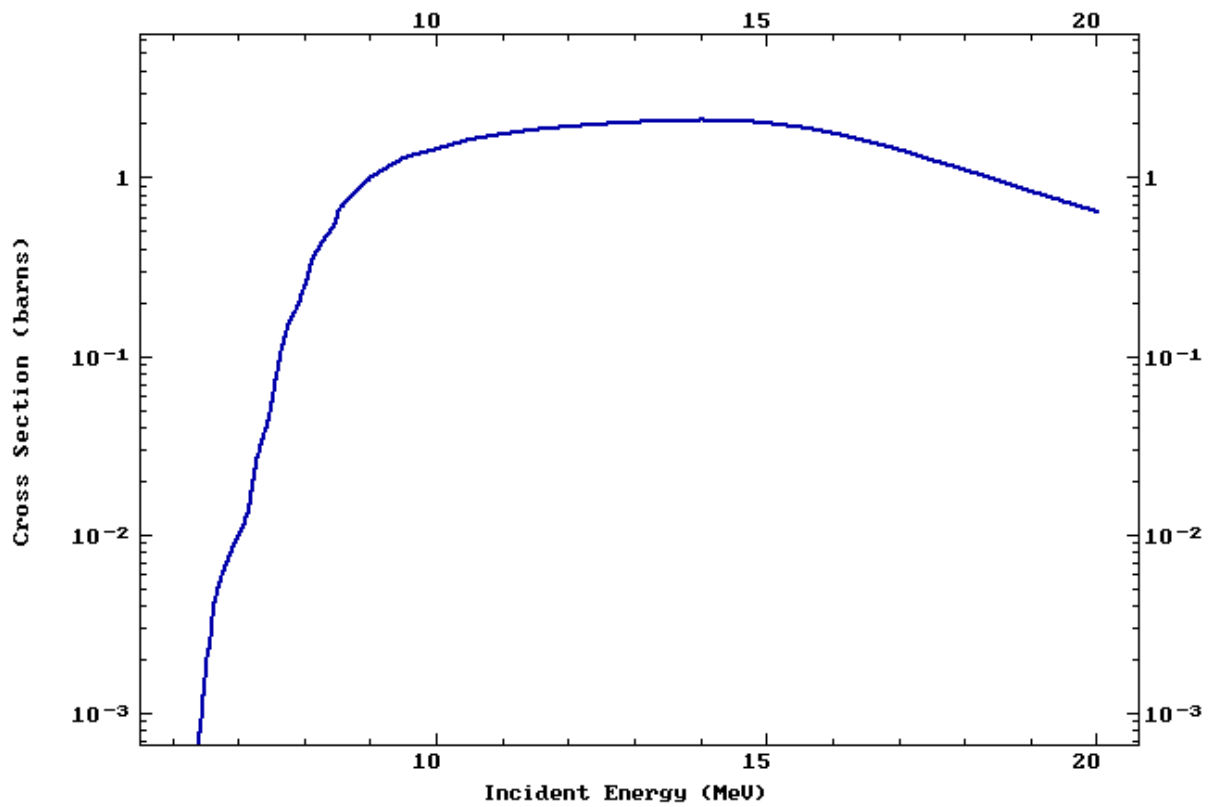
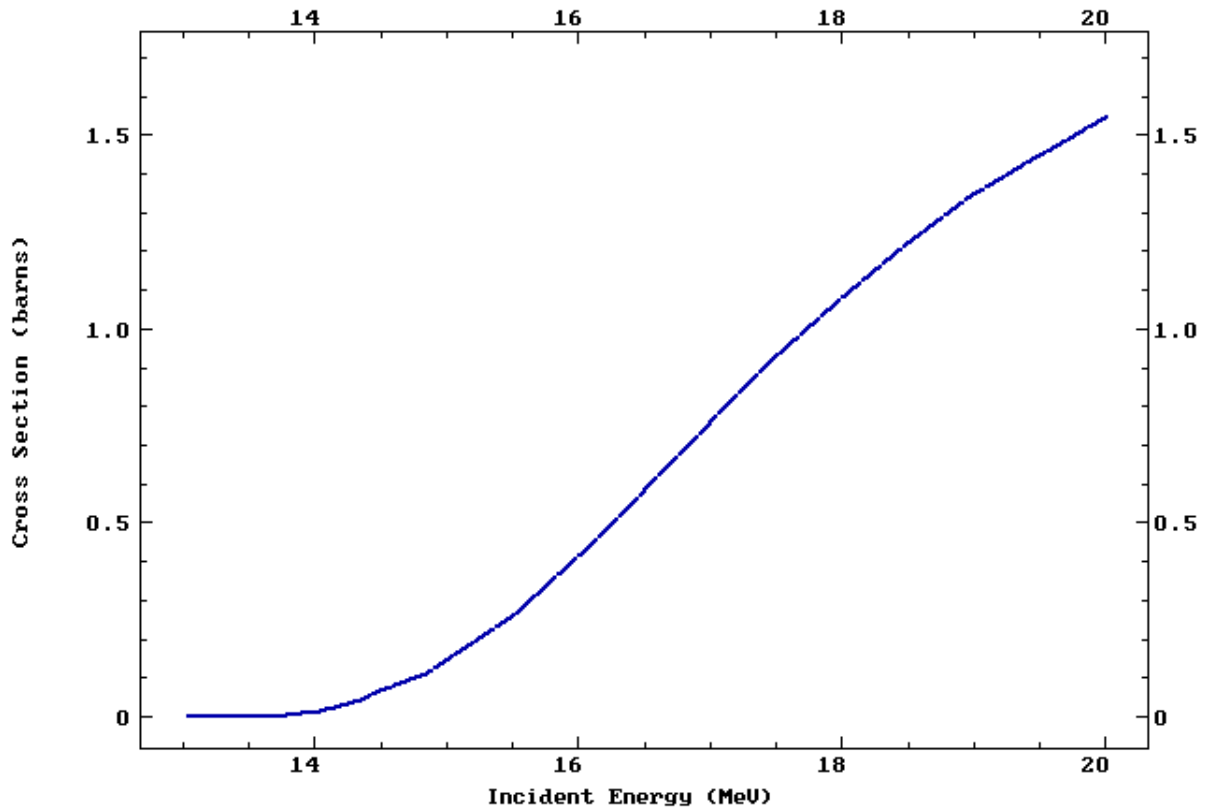


Figure 3.3  $(n, 2n)$  Tungsten cross section [ENDF, 2012]



**Figure 3.4** (n,3n) tungsten cross section [ENDF, 2012]

In addition, at higher energies a more complex process becomes relevant: the spallation process. This process involves the generation, during the intranuclear cascade, of a spectrum of additional particles, including high energy protons and pions, which are capable of producing new neutrons as well. In the centre of the detector is located the He-3 counter tube, a type of device already discussed in the former chapter. This counter tube pressurized at 2 atmospheres is typically operated at a high voltage of 1,200 V and a discriminator setting of 1 mV. The main contribution to the count rate is due to the capture reactions of thermalized neutron in the counter's active gas, however, there are two additional mechanisms that contribute to the count rate above 20 MeV: neutrons produced by photons in tungsten nuclei and charged particles tracks through the counter's tube active volume. The importance of these two minor contributions was evaluated in former scientific studies by means of MCNPX simulations. In particular, regarding the role played by the charged particles, it is estimated that at an incident neutron energy of 500 MeV the charged particle contribution is about 2.5% of the neutron-induced count rate, while at 2 GeV the percentage increases to 3%. Similarly, also the contribution due to the photoneutrons production in tungsten nuclei, due to the mentioned neutral pions

decay into highly energetic photons during the intranuclear cascade, is quite negligible: the resultant photons fluence is estimated to be much lower than the neutron fluence, contributing less than 1% of the count rate at any incident neutron energy up to 5 GeV. To analyse the main properties of the WENDI-2 detector it is essential to take into consideration directional response measurements as well as the gamma rejection capability of the device. Both these features were studied in the case of a  $^{137}\text{Cs}$  field. Regarding the directional response, results in scientific literature show that the maximum deviation – equal to 44% - occurs in the Y-Z view when the moderated neutron source is aligned with the counter tube's cable cut-out. This circumstance is common to all the commercial rem meters because of the neutron diffusion through the cable opening of the detector. Regarding the gamma discrimination, the results recorded are better than those expected for a  $^3\text{He}$  detector with a conventional moderator assembly: this improvement is due to the presence of the tungsten shell, providing effective photon shielding of the device. On the contrary, a strong decrease of the performance in this regard is observed for irradiation through the rem meter top, the only unshielded face of the detector.

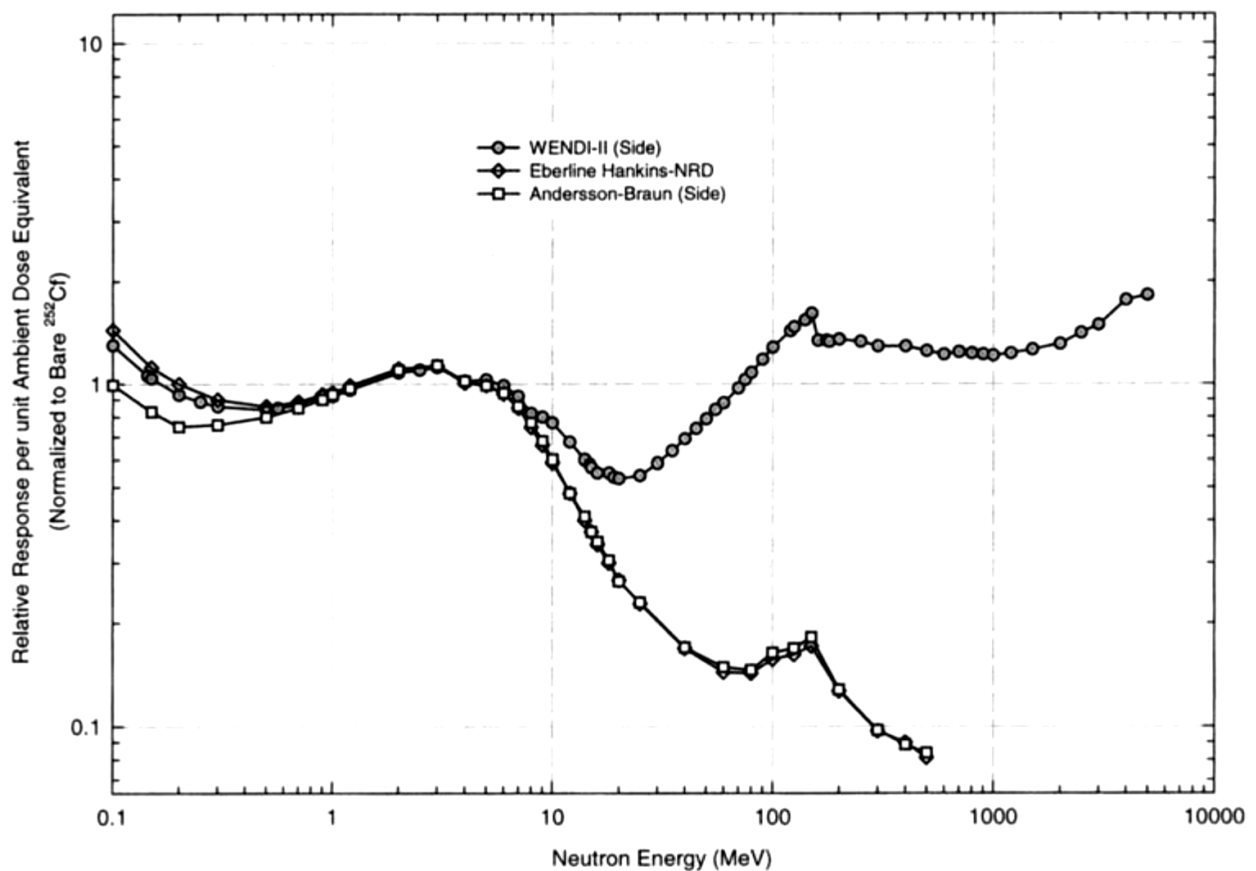


**Figure 3.5** Relative response per unit Ambient Dose Equivalent of several rem meters  
[Techno Scientific, 2007]

In conclusion, the WENDI-2 rem meter design, introducing a weight penalty of 5 kg with respect to traditional devices, as a consequence of the tungsten shell presence, ensures a more accurate dose equivalent response. This detector qualifies as a universal neutron rem meter thanks to good sensitivity and useful energy response covering a range from thermal to 5 GeV and, therefore, is particularly suitable for applications in accelerator-produced neutron fields. In the Figure 3.5, the improvement introduced by the WENDI-2 design can be appreciated comparing the relative response functions of different detectors available on the market.



# CHAPTER IV

## IBA Group

The study presented in this work was carried out in collaboration with IBA group, a medium-sized Belgian company operative in different sectors of medical and scientific technology: from cyclotrons design to sterilization and proton therapy the range of applications of company's products is wide. Born in 1986 as a spin-off of the Catholic University of Louvain (UCL), it has had a rapid and successful development during the last decades. As a result of its internal expansion and targeted acquisitions, today IBA is a dynamic and sound group and it can boast more than 47 different locations in 12 different countries around the world. It had not only reached a leader role in the emerging European market of proton therapy applications but it is also operative in North America, in Asia and Oceania. In this chapter the historical development of this company will be briefly introduced and the main applications linked to its activities will be described.

### 4.1 HISTORICAL OVERVIEW

IBA starts its history in 1986 as a spin-off of the Cyclotron Research Center of the Catholic University of Louvain-la-Neuve, which had already produced its first cyclotron in 1947. In a first moment, the idea behind the birth of this company was to exploit the developed expertise in particle accelerator technology to satisfy the needs emerging in the fields of medicine and industry. Actually, in 1984 the Isotope Production Cyclotron projects starts: the task assigned to the research center of UCL consisted in designing a cyclotron for medical isotopes production [*Jongen, 1999*]. Characterised by emitted proton energy below 15 and 30MeV, and an external ion source with axial injection to keep, the design of Cyclone 30, completed in May 1985, seemed to be extremely reliable and competitive. In spite of the patent obtained and of the innovative design, no industries

interested in this machine were found. Therefore, in order to build and sell the new cyclotron design, the Ion Beam Applications company (IBA) was officially formed on March 28<sup>th</sup> and in December 1986 the first beam of the prototype was obtained. Notwithstanding the many difficulties attendant on the scepticism about the debut on market of a small group as IBA in those days, the operation had success, leading to an explosive growth of the company.



**Figure 4.1** Cyclone 30, first machine produced by IBA

Therefore, the company took its first steps in medical imaging field but quickly recognized the necessity to diversify its own activities: staying a single product company was seen as an unacceptable risk. Soon, conscious of the revolutionary potential of radiotherapy, it started developing PET cyclotron designs. In spite of the high quality of the Cyclone 18/9 – higher energy PET cyclotron developed by the company – in PET market IBA had to deal with two giants: GE and Siemens. In order to survive the company allied to Siemens, conclude an agreement with CTI PET System in 1990. The collaboration between the two groups reached soon a crisis that led to terminate the relation. Today IBA sells its PET cyclotrons alone under its own logo, reaching 30 to 40%

world market share. According to the products differentiation strategy of the company, it broadened its area of scientific interest to proton therapy field, designing cyclotrons able to treat numerous forms of cancer with a degree of precision and efficacy never reached before. Initially, the goal should be to develop a system that could be operated by a clinical therapist and that could result cheaper and simpler than the existing ones: the IBA PT system concept was presented at PTCOG (Particle Therapy Co-Operative Group) in 1990, to obtain prospective customers feedback. Furthermore, the company opened the doors to the Asiatic market thanks to the alliance with Sumitomo Heavy Industries (SHI), former competitor in cyclotrons market and actual Japanese partner of IBA group. In 1992, the activities of IBA were expanded to the industrial sector of Sterilization and Ionization thanks to the development of an industrial, sellable machine suitable for applications in these fields, the Rhodotron (Figure 4.2). The latter, based on a patented concept of the French Atomic Energy Commission (CEA), was a new type of particle accelerator characterised by a wide range of applications. The innovation associated to the introduction of this device on the market was linked to the possibility of reaching a larger efficiency in processes of industrial interest, as sterilizing medical products, pasteurizing food and enhancing the properties of plastics. An exclusive, worldwide license for the Rhodotron technology was signed with CEA against a down-payment and royalties on each machine sold. Thanks to the establishment of an international collaboration network – that involves partner like the mentioned French Atomic Energy Commission and Sumitomo Heavy Industries in Japan – the diversification of IBA production has continued successfully. In 1997, considering the good status of the company, the shareholders decided to sell IBA. The managers looked to mount a Management Buy Out (MBO): IBA employees got together in a buy out of the shares of the company, raising their involvement in the success of the company and obtaining the opportunity to drive the future of the group. In order to find funds to accelerate the development of IBA and promote its expansion, in June 1998 the Initial Public Offering (IPO) was done on Brussels stock market. The economic operation had a large success, allowing a rapid internal growth and acquisition of other companies. In fact, IBA enters in the field of dosimetry applications thanks to the acquisition of Scanditronix in the same year and of Wellhöfer in 1999. Today, the group formed by these two excellent companies reinforces the IBA's presence in medical field, representing the most important player in worldwide dosimetry market. In March 1999, IBA acquires Radiation Dynamics Inc. (RDI), an experienced company doing DC electron accelerators; the

Belgian company has consolidated in this way its strength in irradiation technologies, especially in the field of high power low energy E-beam accelerators used for heat shrinking and polymer modification applications. This acquisition ensured to IBA the leadership in all electron beam applications, including sterilization for medical devices, food pasteurization, cross-linking and depollution, as well as in emergent technologies like oil-cracking or cargo screening. In the same year the company entered in the business of sterilization services acquiring Griffith Micro Science (GSM) and Sterigenics, the two largest companies in this market. In 2001, IBA became the majority shareholder of Eastern Isotopes, American leader of the new PET imaging products. This collaboration allowed IBA to improve its global expertise and to access to advance cyclotron technology as well as to enlarge its international distribution network. Also the presence of IBA in European radiopharmaceutical market had increased thanks to acquisitions: in 2006 the Belgian company became the leader in the European PET radio-isotopes network, creating the IBA Molecular Europe entity to integrate the Schering radiopharmaceutical business and CIS bio International. Two years later, the acquisition of CIS BIOS was completed making the company one of the world's largest player in Radiopharmaceutical business, providing the group with an extended PET isotopes network, worldwide distribution of a SPECT portfolio, and superior R&D capabilities aimed at giving Nuclear Medicine and Molecular Imaging a new invigoration.

## **4.2 IBA APPLICATIONS**

Thanks to its policy of dynamicity and to the technological expertise obtained during its activity, today IBA is a large and diversified multinational company. The activities of the group involve mainly three business units, in each of which the company can boast a position of excellence: the radiotherapy field, the production of radio isotopes and the industrial sector of sterilization and ionization.

## 4.2.1 Sterilization and Ionization

The sterilization and ionization processes covered a wide range of industrial and sanitary applications, from the disinfection of medical instrument to the food and material treatment. All the mentioned applications fall within the IBA company area of interest. As a result of the expertise matured and of the acquisitions of the major leader companies in this sector, sterilization and ionization applications have become one of IBA's principal businesses, representing nowadays 67% of the sales. The company provides all the key technologies necessary to meet the diverse applications demand in this market. Electron Beam technology, X-ray or on the use of Ethylene Oxide and Cobalt 60. This latter procedure consists of exposing products to ionizing beams emitted by  $^{60}\text{Co}$  during its disintegration. The risk of engendering radioactivity in the irradiated target is avoided thanks to the brief time of treatment: the treated products are instantly sterilized when the rays penetrate through the packaging. Similar to the described procedure, the X-rays sterilization technique allows obtaining the same penetrating properties of  $^{60}\text{Co}$  irradiation. This promising new technology offers the possibility of faster, more flexible and more environmental friendly treatment. In spite of this, the oldest and most common sterilization method is based on the use of Ethylene Oxide (Eton). The success of this technique is due to the compatibility of this compound with almost all materials, as well as to the simplicity of the procedure: absorbed by the treated product, EtO kills resident bacteria, allowing the product to meet the required sterility criteria. Finally the Electron Beam technology is entirely new and represents IBA's key technological asset. The main advantage of this method is the absence of waiting time thanks to the instantaneous sterilization realized by the beam. The latter is produced by high-energy electrons that either sterilizes or ionizes, depending on the delivered dose.

The presence on market and the success of this sterilization and ionization method is mainly due to the introduction of IBA's family of Rhodotron electron beam accelerators. These latter are radio-frequency based systems and result to be extremely reliable and compact as well as easy to maintain. Using a single accelerating cavity, resonating with a metric wave, the electrons injected recirculate through the system, gaining in energy with each passage. Eliminating the need for multiple cavities, it results in substantially smaller system, reducing investment costs. Moreover, as said before, Rhodotons offer both high ionization effectiveness and low process time. The mentioned characteristics make this

machine suitable for a wide variety of applications, all involved in IBA activities, such as sterilization of medical products, food pasteurization and enhancement of materials. The sterilization and ionization business unit of the company consists of three divisions, each focused on a distinct application: the “Medical sterilization & Analytical Labs”, “Food safety” and “Advanced Materials”.



**Figure 4.2** Example of IBA’s Rhodotron

Regarding the sterilization of medical disposables, such as syringes, surgical drapes, gloves and so forth, the company operates today the larger service network in the world. Especially the process is carried out using the described technologies that allowed treating material unable to tolerate sterilization by steam or high temperature. In parallel to its application in the world of medicine, ionization can also be used to reduce the microbial load in foods and, according to the applied dose, can achieve any desired degree of food hygiene, ranging from disinfestation to pasteurization through to sterilization. This process of pasteurization, that consists in affecting the DNA of resident microbes by depositing energy inside the food, can be carried out either with ionizing rays ( $^{60}\text{Co}$  or X-rays) or electron beams. The latter can be used only with products of limited thickness because of the restricted penetrating power of the beam, but this limitation is offset by the rapidity of the treatment. On the contrary, the great penetrating power of X-rays permits

treatment of foods in their standard packaging. Finally, the electron beam technology is wide used also to modify the characteristics of materials for the high-performance-materials market. Applications including increasing the resistance of cables to temperature, improving the properties of plastics and reticulation of composites used in the aviation industry are carried out by means of this technology: it results to be a precious instrument in a field subject to intensive research that regularly leads to important new applications.

## **4.2.2 Radioisotopes**

Although radioactive isotopes are used in a large variety of fields, such as agriculture, breeding, food, insect control, hydrology and so forth, it is in human health applications that they have led the most striking advances. Since the early years of the last century, the applications of radiations in medicine has had a large success, leading to the develop of a new and unique branch as nuclear medicine. Using small amounts of radioactive materials, it is possible to image the body, diagnose and treat diseases. In this light, radioisotopes are an ideal investigation tool, which is why their use continues to grow in all scientific and industrial sectors. In particular, the nuclear medicine industry is based on the exploitation of their traceability during biological processes. In practice, the low-level radioactivity of the incorporated radioisotopes is detected by a scanner and digitalized in order to give a live, real-time picture of how the organ under examination is functioning. In view of this consideration, radiopharmaceuticals are at the heart of progress in medical examination. They consist of compounds marked with radioisotopes and their use is continuously increasing in nuclear medicine and medical imaging fields.

IBA's primary competence resides in the production of radioisotopes for medical applications and in the design and manufacture of cyclotrons to produce them. Actually, the radioisotopes production is a critical step of the radiopharmaceuticals preparation: since such products have short life-times, their employ is limited not only in time but also geographically. Their use is limited to a single metropolitan area, or even a single hospital, especially with regard to their applications in positron emission tomography (PET). The latter consists of a technique for functional imaging: born at the beginning of

the 1980s, it rapidly became the leading-edge functional imaging technology – so that it is called “Medicine’s New Vision”. Recognizing its enormous potential, IBA imposed its presence in this market designing and producing a range of cyclotrons dedicated to the new technique.

The most popular PET radioisotopes,  $^{11}\text{C}$ ,  $^{13}\text{N}$ ,  $^{15}\text{O}$  and  $^{18}\text{F}$  can be produced by low-energy cyclotrons (<20 MeV). The company offers a range of three cyclotrons of this kind: Cyclone 18/9, Cyclone 10/5 and Cyclone 3, a high performance Oxygen generator. Among the IBA family of PET cyclotrons, the most productive machine is the Cyclone 18/9 (Figure 4.3), involved also in the present work as it will be shown in the next chapters.

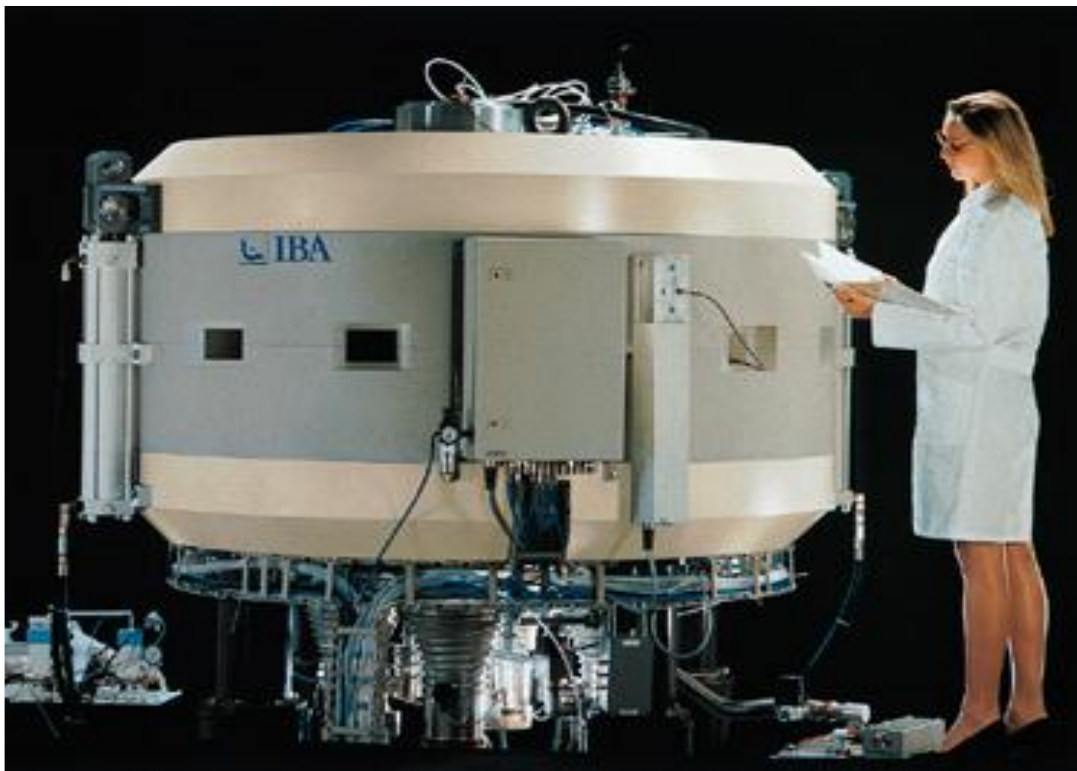


**Figure 4.3** IBA Cyclone 18/9

The company’s centers of radioisotopes production and distribution are equipped generally with this cyclotron: designed to produce PET radioisotopes in large quantities, its flexibility and high productivity make the Cyclone 18/9 an ideal solution also for large hospitals and research institution. A different role is played, in the IBA production, by the Cyclone 30 (Figure 4.1): it is essentially aimed at radio-pharmaceutical companies who produce and distribute imaging agents. The design and the production of this machine

were the key of IBA success from the moment of its foundation: it has been the first cyclotron able to produce many different types of isotopes on industrial scale. Based on innovative magnet design and acceleration of negative ions, Cyclone 30 is a 30 MeV machine designed for the industrial-scale production of radioisotopes but it can also be used in fundamental and applied research, in agriculture as well as in a growing number of new industrial techniques. It meets the criteria of efficiency and cost-effectiveness required for industrial production of radiopharmaceuticals and, for this reason, it has become the undisputed world standard, covering 90% of the market.

### **4.2.3 Advanced Radiotherapy**

In two-thirds of cancer diseases, treatment includes radiotherapy, either as principal treatment, or in combination with surgery or chemotherapy. Cancer radiotherapy is the second market which IBA developed. In particular, the company is the undisputed leader in proton therapy technology: the latter is a new and significantly more effective method of radiotherapy. The “conventional” radiotherapy methods, based on the use of electrons, X-rays or photons, have the disadvantage of not being sufficiently selective. Therefore, irradiating a tumour with this radiation species, also the healthy tissues along the beam’s trajectory to the target are damaged. This disadvantage introduces two main consequences: first of all, it obliges to reduce the ionizing doses, decreasing the effectiveness of the treatment; moreover, it precludes the “conventional” radiotherapy treatment from being used on tumours located near vital organs or radiosensitive areas of the body. In this light, the potential related to the use of proton therapy is exceptionally promising: when fired into matter, protons follow a straight-line trajectory and their stopping point is easily adjustable in function of their initial energy. This stopping point is commonly known as “Brag Peak”. The idea behind proton therapy applications is to use these favourable ballistic properties of protons to kill the tumour cells by means of ionizing energy, without involving the surrounding healthy tissues. Proton beams deliver optimal ionizing doses and permit treatment of tumours inaccessible to most other medical techniques: since this procedure is often carried out in place of the traditional surgical treatment, it is commonly referred to as “bloodless surgery”. The effectiveness

of the method had been demonstrated by different and independent studies, based on the treatment of nearly 20000 patients. Considering the medical success of the proton therapy, it is clear that the only obstacle to the large adoption and diffusion of this technology is associated to technological and economic restriction. More precisely, to be medically effective, protons must reach very high energies, which have been possible only in the powerful and expensive accelerators used in nuclear research fields. The merit of the Belgian company is to have pushed back the frontiers of proton therapy thanks to the design of a practical and affordable proton therapy system. The latter is created to operate within the hospital environment: the high-energy proton beams generated by its 230 MeV cyclotron can be instantaneously switched among four separate treatment rooms, carrying out up to 30000 annual irradiation sessions. Each treatment room is equipped with a 360° rotating beam system, allowing hitting the tumour from the most favourable direction. Every detail of the treatment session is monitored and controlled by highly advanced computer software. The energy of emitted protons can be calculated so that the particle stop only within the target volume – up to a depth of the Bragg Peak equal to 32 cm – destroying the malignancy without passing through and damaging healthy tissues. In 2001, the first patient was treated with a proton therapy system installed by IBA at Massachusetts General Hospital, Boston, now known as Francis H. Burr Proton Therapy Center. Since then, installing over half of the PT system worldwide, IBA has become the undisputed leader in that field. Although proton therapy is the main branch of the company business in the field of radiotherapy, the company boasts a significant presence also in other sector of this market. In fact, in addition to the mentioned technology, IBA offers also compact neutron therapy system, solutions for brachytherapy and dosimetry equipment. More deeply, brachytherapy is a cancer treatment technique developed to spare patients from surgery interventions. It consists of inserting radioactive implants into the tumour in order to destroy it from the inside. The main radioisotope suitable for this method is Palladium-103. This nuclide may be effective in a wide range of diseases such as breast and prostate cancers, and it could be used also in cardiology. The applications of  $^{103}\text{Pd}$  brachytherapy have shown themselves to be exceptionally effective, leading to a rapid grown of demand for treatment. To meet the request of this high-potential market, IBA developed a new cyclotron able to replace nuclear reactors for cost-effective industrial production of  $^{103}\text{Pd}$ . All the mentioned applications linked to radiotherapy necessitate the use of a large arsenal of auxiliary devices related for dosimetric measurements. The IBA group produces, thanks to the

expertise of the acquired leader company Scanditronyx, a comprehensive choice of dosimetry devices for both conventional radiotherapy and proton therapy. These products constitute a source of reliably recurring revenues for the company: unlike particle accelerators, dosimetry devices are relatively low cost and are daily used in the hospital radiotherapy department.



# CHAPTER V

## Modelling WENDI-2

Aim of this work is to study the response function of the rem meter WENDI-2 for a wide range of neutron energies, to evaluate the reliability of the equivalent dose value given by the detector. For this purpose Monte Carlo Codes, MCNP and MCNPX, have been used to calculate the response function of the detector, to compare the latter with the results reported in existing scientific literature.

This chapter describes briefly the capabilities of the software used in the computational model of the detector and the general structure of an MCNP input file. Also analysed are the geometry of the WENDI rem meter, as simplified in the simulations, and the structure of the input files associated to this work. In the final part of the chapter a comparison of the results calculated with those in the existing studies is presented.

### 5.1 MCNP AND MCNPX

Developed by Los Alamos National Laboratories, the Monte Carlo N-Particles Code (MCNP) represents a powerful instrument for scientific research in a wide range of applications. This software package, written in the ANSI-Standard Fortran90 programming language, can be used for neutron, photon, electron or coupled particles transport, treating an arbitrary three-dimensional configuration based on a structure made by cells, bounded by several kinds of surfaces. The possibility of treating more species of particles is offered by the MCNPX code (Monte Carlo N-Particle eXtended): this latter is capable of simulating interactions of 34 different types of nucleons and ions, including all those simulated by MCNP [*MCNPX User's Manual, 2005*].

Clearly, the MCNPX code has a wider field of applications, ranging from the design of accelerator spallation targets, and medical physics (especially proton and neutron therapy) to high energy dosimetry and neutron detection or nuclear safeguards, multiplying this way the potential of MCNP. The 2.5.0 version of MCNPX was used to reproduce the WENDI-2 response: the need to use MCNPX instead of MCNP was related to the need to calculate the total amount of (n,p) reactions occurring in the counter tube volume.

It is extremely important to consider that the accuracy of the calculation is linked first of all to the series of data used in the simulation, i.e., the cross section libraries associated to the different versions of the MCNP and MCNPX software packages. The main sources of nuclear data libraries used by MCNP are evaluations from the ENDF (Evaluated Nuclear Data File) system, ACTI (Advanced Computational Technology Initiative), ENDL (Evaluated Nuclear Data Library), EPDL (Evaluated Photon Data Library), ACTL (Activation Library) and from the Nuclear Physics Group (T-16) in Los Alamos. The continuous-energy nuclear and atomic data evaluated are processed by codes such as NJOY in order to convert them in a format appropriate for MCNP. The construction of processed data libraries is a delicate phase, considering that it is necessary to retain as much of the details from the original evaluations as feasible. All data tables available to MCNP, associated to neutron and photon interactions, neutron-induced photons, neutron dosimetry or activation and thermal particle scattering  $S(\alpha,\beta)$ , are listed on a directory file, XSDIR: this file gives the code all the information on where to find individual data tables. The code allows selection of specific data tables by means of an unambiguous identifier associated to each table, called ZAID: this latter consists of the atomic number Z and mass number A of the isotope of interest, in addition with a library alphanumeric specifier ID. In MCNP5 more than 836 neutrons interaction tables are available, for approximately 100 different isotopes and elements. Frequently, several tables for single isotopes are provided, not only because of different evaluations but also because of different temperatures and processing tolerances relating to the data. In addition to all standard neutron libraries available with MCNP5, MCNPX 2.5 uses additional data of different types, including cross sections for the Bertini model (BERTIN), gamma emission libraries for decaying nuclei (PHTLIB), photon and electron interaction data, special 150-MeV libraries for neutron (LA150N) proton (LA150H) or photonuclear reactions (LA150U).

The input file, created by the user, contains all the information about the problem to be run, such as:

- Geometry specification
- Description of materials and selection of cross-section evaluations
- Locations and description of the source
- Type of answer or tallies required

The file structure is exactly the same for MCNP5 and MCNPX2.5.0, excluding several new input cards only available in MCNPX. The format is based on different types of cards - where the word “card” denotes a single line of input up to 80 characters long.

As can be seen in figure 5.1, the first block of cards is related to the definition of the cells in which the geometry of the problem is subdivided. A following blank line delimiter signals the separation between series of inputs: the second block concerns the construction of the different surfaces bounding the previous cells.

Finally, the DATA CARDS section, consists of several kinds of input lines: first of all the source specifications (location, energy, direction of flight etc.) are introduced in this block; then one or more tallies of interest, that are the answers the user wants to evaluate, are inserted. The last input line is dedicated to the number of simulating particles. The user can instruct MCNP to make various tallies concerning particle current, particle flux or energy deposition; each of these tallies is normalised on starting particles production (with the exception of a few special cases related to criticality sources). The units of measure in which the main data are supplied to MCNPX are shown in Table 5.1.

The physical models used by MCNPX 2.5.0 are different, depending on the energy of the incident particle: for neutron energies lower than 20 MeV the free-gas thermal treatment is set as default, for higher energy values the Bertini model is employed. The free gas thermal treatment takes into account the thermal motion of the nearby atoms and assumes that the medium is a free gas. In addition, it is also considered that in the energy region below 4 MeV, where the thermal effects are significant, the elastic scattering cross section at zero temperature is nearly independent of the energy of the neutron and, furthermore, that the reaction cross sections are nearly independent of temperature. The MCNPX default thermal treatment of neutron collisions consists of adjusting the elastic

cross section taking into account the velocity of the target nucleus, when the kinematics of a collision are being calculated.

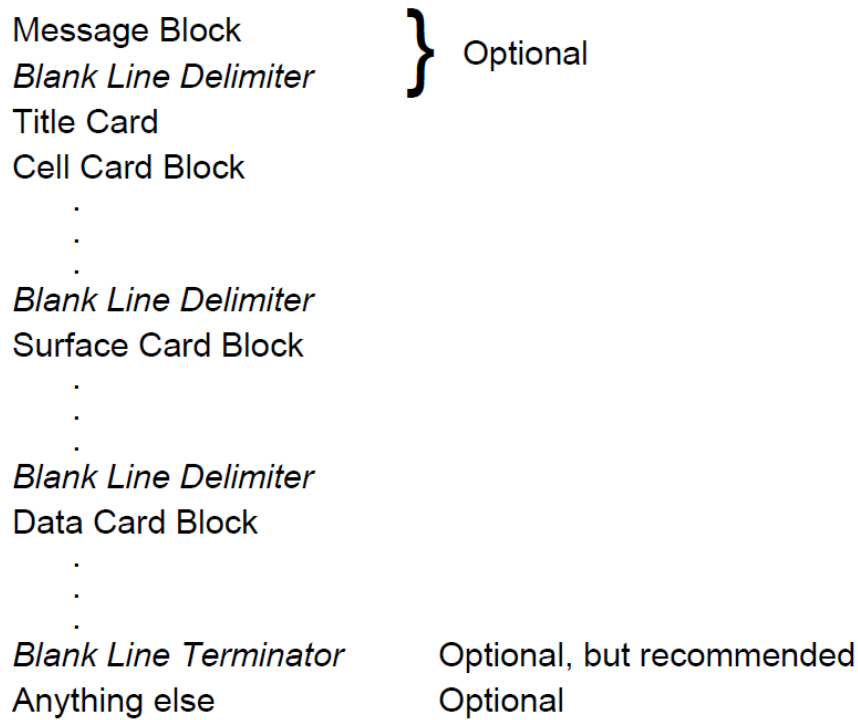


**Figure 5.1** Format of the initiate-run file [*MCNPX User's Manual, 2005*]

Although this approach is adequate for most practical problems, providing a thermal treatment of neutron collisions that runs almost as fast as a non-thermal treatment, in some applications the effects of chemical binding and crystal structure for incident neutron energies belonging to the thermal domain cannot be ignored without serious error.

<b>DIMENSION</b>	<b>UNIT OF MEASUREMENT</b>
Length	Cm
Energy	MeV
Atomic Density	atoms/barn-cm
Mass Density	g/cm <sup>3</sup>
Cross sections	Barn
Time	shakes (10 <sup>-8</sup> sec)
Temperature	MeV

**Table 5.1** Main Unit of measurement used by MCNP and MCNPX

In these cases the user can have recourse to an explicit capability, available only for a limited number of substances and temperatures and related to the incident neutron energies below about 4 eV. When this kind of card is introduced for a given material component, the free-gas treatment can be used down to the energy where  $S(\alpha,\beta)$  data are available, typically a few electron volts. At that point the thermal scattering model automatically overrides the default treatment. Data tables appropriate for use with the  $S(\alpha,\beta)$  scattering treatment include chemical (molecular) binding and crystalline effects that become important as the neutron energy becomes sufficiently low.

In the energy range above 20 MeV, the model used by MCNP is the Bertini intranuclear cascade. The application of this model is related with the primaries interactions between the incident particle and one or more nucleons of the target nucleus, according to a cascade process. In this case, the particles interaction is treated ignoring the presence of other nucleons. Each particle is considered until it remains within the system with energy higher than a cut-off value  $E_{cut}$ . When no particle satisfies these conditions, the intranuclear cascade ends, leaving the nucleus in an excited status.

## **5.2 WENDI-2 RESPONSE FUNCTION**

As it was discussed in former chapters, the detection of neutrons in the rem meter detector WENDI-2 is effected indirectly through the detection of protons produced by (n,p) reactions in the helium volume of the proportional gas. The aim of this presentation is to analyse the structure of the input files used for the simulations. According to previous studies the simulation model took into consideration only the main count rate production mechanism, which is the capture of thermalized neutrons in the proportional active gas volume. Actually, at neutron energy values higher than 20 MeV, an additional contribution on the count rate can be considered: the tracks trough the helium active volume of charged particles different from protons, such as pions, deuterons or tritons. But according to the study of Olsher, at an incident neutron energy of 500 MeV, the charged particles contribution was determined to be about 2.5% of the neutron-induced count rate, while at 2 GeV, the percentage increased slightly to 3%". Due to this analysis, it was considered appropriate to neglect this minor contribution to the total count rate that would complicate the model without a real advantage in term of calculation accuracy.

Also, the detector efficiency was assumed to be 100%: in other words, according to the present study, each non-elastic reaction gives rise to one count. The response function of the detector was built evaluating the number of counts per unit fluence in the helium active volume for different values of incident neutron energy.

According to previous studies in literature [*Osher et al, 2000* and *Vanahudenhove, 2012*], a monoenergetic point neutron source located at 50 cm from the centre of the detector was considered as neutron source. The energies considered covered a wide range: from 1 meV to 5 GeV. Within this domain a sizeable number of values, 93, was considered to provide good comparison with results reported in previous studies. Hence, the different points of the response function were calculated normalising the number of counts to the average neutron fluence in the active volume by means of two different types of simulations. First of all, an input file named WENDI was used to calculate the total amount of (n,p) reactions occurred in the active volume of the gas (that is, in light of what was said before, the number of counts). A second input file, TUBE, was used to evaluate the neutron fluence averaged on the active volume, as described in detail in paragraph 5.2.1.

### **5.2.1 Input file WENDI**

As shown previously, the first step in writing an input file is to create a computational model consistent with the geometry of the problem that needs solving. In the input file for the simulations of WENDI-2, the geometry of the detector was reproduced using seven cells (Figure 5.3). The first cell was introduced to simulate the active volume of the counter gas tube, equal to 23.95 cm<sup>3</sup>: it is filled with He-3 characterised by a mass density of 2.4E-4 g/cm<sup>3</sup>, corresponding to a gas pressure of two atmospheres [*Thermo Scientific, 2007*]. The second cell is associated with the stainless steel cathode of the counter tube. These two cells simulate the 252180 Cylindrical High Temperature He3 Neutron Detector manufactured by LND, Inc. in which thermal neutron detection is realised by means of the inelastic reaction  ${}^3\text{He}(n,p){}^3\text{H}$ .

Since the composition and density of stainless steel do not appear among the

specifications of the device distributed by the producer, the mass density was arbitrarily set equal to  $8 \text{ g/cm}^3$  while a generic composition, reported in Table 5.2, was chosen for this material.

ELEMENT	ATOMIC NUMBER	MASS FRACTION
Iron	26	0.74
Chromium	24	0.18
Nickel	28	0.08

**Table 5.2** Stainless steel composition

A third cell completes the inner part of the detector, simulating the upper part of the central hole that is left empty by the counter tube, and is filled with air.

Among the remaining four cells, only the fourth and the fifth belong to the detector body: the first of these two cells represents the tungsten shell consisting of a cylindrical layer (1.5 cm of thick, inner radius 4 cm) where the element powder is characterised by an effective density equal to  $10.624 \text{ g/cm}^3$  (corresponding to a tap density of  $9.5 \text{ g/cm}^3$ ). The cylindrical polyethylene (density  $0.94 \text{ g/cm}^3$ ) region, surrounding the counter tube and containing the tungsten shell, is simulated by the fifth cell.

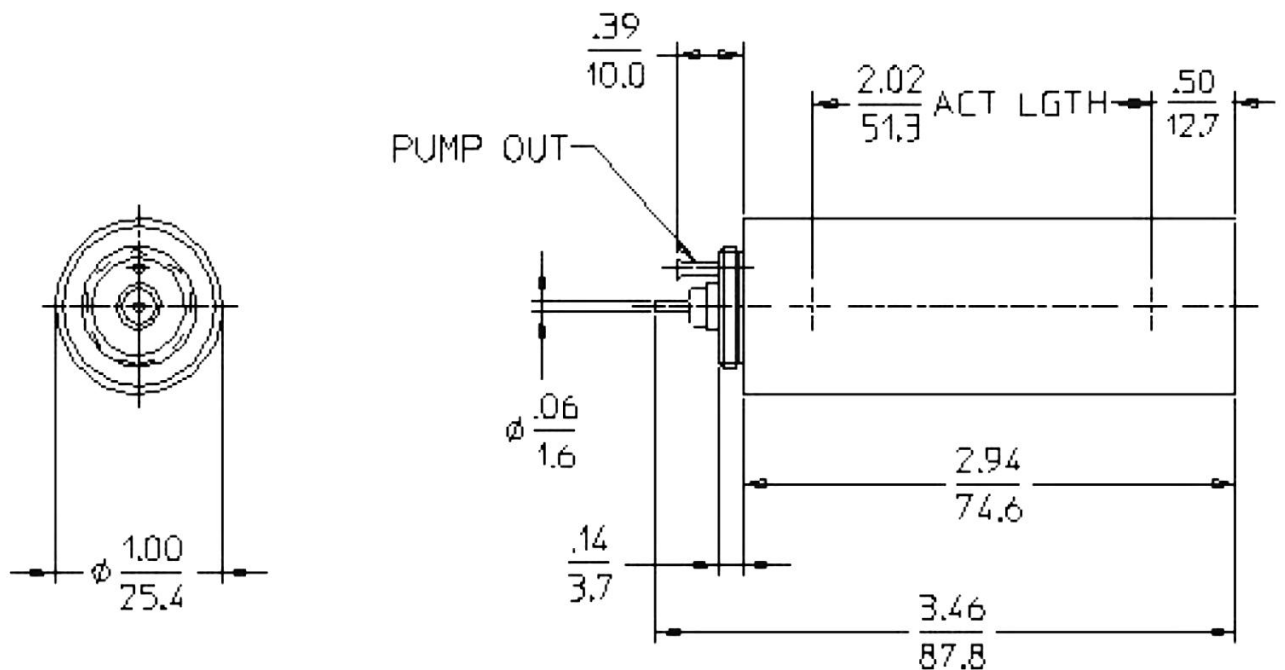


**Figure 5.2** 252180 Cylindrical High Temperature He3 Neutron Detector [LND, Inc data sheet]

The composition and the density of the cathode material do not constitute the only lack of information concerning the detector structure simulated. Actually, more details were omitted, in particular the depth of the central orifice and the distance between the bottom of the counter tube and the tungsten shell were set arbitrarily, trying to use reliable values according to the entire geometry of the rem meter.

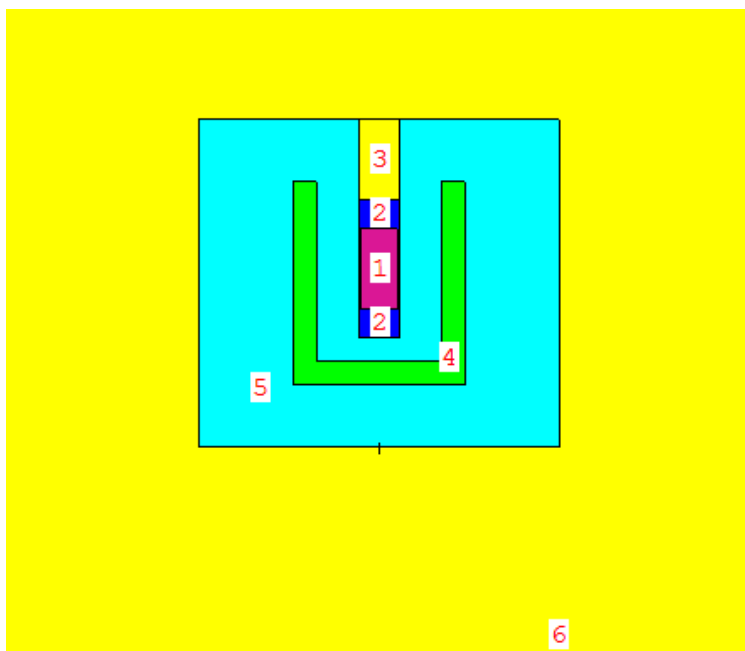


**Figure 5.3** WENDI-2 geometry in WENDI input file [VISED2, 2000]

Finally, the last two cells are assigned to reproduce the external environment filled with air at atmospheric pressure (cell 6) and the universe, that is a void cell external to the simulated system (cell 7). The presence of a borated rubber patch in the upper part of the rem meter was not considered in the simulations because of the excessive lack of information about this piece.

Figure 5.3 shows the detector structure [VISED2, 2000], associated to the input file WENDI. The surface block consists of seventeen cards: each line concerns a plane or cylindrical surface bounding the cells described before. The origin of the Cartesian coordinate system is located in the middle of the bottom surface of the detector.

Regarding the data cards, the first input line introduced in this block is that associated to the source definition (SDEF card). As mentioned before, in order to find different points of the response function, a monoenergetic point source was considered: modifying the

energy value for each simulation through the ERG command, it was possible to cover an energy range from meV to GeV. The source is positioned in correspondence of the side of the detector at 50 cm ( $y = 50$ ) from the centre of the rem meter, with a value on the z-axis equal to half height of the device ( $z = 10.5$ ). As a variation reduction technique, the direction of flight of the particles emitted was reduced to the solid angle including the entire detector: this way, particles that do not intercept the rem meter are not simulated, with a significant advantage in terms of run time. This artifice is realised using a DIR command: by means of this instruction it is possible to introduce a direction distribution with reference to the unit vector parallel to the y-axis and directed in the positive sense of the axis in this case; this axis is introduced by the VEC command. The proposed distribution was characterised by three-input values associated to the three bins in which the domain of the polar angle cosine was divided. Each bin was linked to an emission probability for those cosine values: this way, it was possible to select for the neutrons emitted only those flight directions with cosine values ranging from 0.955 to 1 - which represents the solid angle covering the whole rem meter (the azimuthal angle is sampled uniformly between 0 and 1). The following cards are allocated to the tallies definition. To calculate the total amount of (n,p) reaction occurred, an F4 tally card was introduced and was correlated with a multiplier card FM4. The first input, F4, calculates the neutron fluence averaged over the active volume of the proportional gas in terms of particles/cm<sup>2</sup> (each tally, as mentioned, is per starting particle). Multiplying the result of F4 card by the atomic density of the material and the microscopic (n,p) reaction cross section of <sup>3</sup>He gas, the total production of protons through neutron capture in the counter tube is obtained. This is possible thanks to the use of a tally multiplier card. The first of the three input introduced in the FM card is a multiplicative constant, set to -1: the negative value introduced allows to multiply  $|-1|$  times the atomic density (in atoms/barns-cm) associated to the cell to which the tally refers. The material of interest is specified by the second input of the card. Finally an (n,p) reaction cross section identifier number is introduced as third input.

Also other instructions regarding the parameters of calculation are present in the WENDI input file. In particular both neutron and photon transport are taken into account in the simulations, through the use of a MODE P, N card. Thanks to this command, it is possible to consider also the minor contribution to the count rate related to the photoneutron production in the tungsten shell. Indeed, for incident neutron energies above 20 MeV, the

interaction of highly energetic photons, produced by the decay of neutral pions during the intranuclear cascade, and tungsten nuclei, leads to the emission of neutrons that can subsequently reach the inner part of the detector. Nevertheless, the photon fluence is much lower than the neutron fluence and photoneutron production is estimated to contribute less than 1% to the total count rate for incident neutron energies up to 5 GeV.

The importance of both neutrons and photons is set equal to 1. The use of a PHYS card allows the setting of the upper energy limit for neutrons, equal to 5000 MeV instead of the 100 MeV default value. Since the simulations covered a wide range of neutron energies, it was essential to take into consideration the chemical binding and the crystalline effects of the polyethylene moderator that become important as the neutron's energy becomes lower. For this reason simulations were run considering thermal scattering, by means of the cross section data poly.01t belonging to ENDF5 evaluation, in order to allow the comparison between the two approaches. Finally, 10,000,000 particles were launched, ensuring the reliability of the simulations results and an associated error lower than 1%.

## **5.2.2 Input file TUBE**

Two different version of the input file TUBE were used. The first simulation, evaluating the neutron fluence averaged on the counter tube active volume filled with helium, served to compare the results of the present work with those in literature. The second version of the file, considering the volume of the tube filled with air, allowed studying the influence of the material of reference in the calculation of the response function. In both cases the file TUBE can be defined as a simplification of the previously described input file WENDI.

In the version with helium, the geometry of the problem is in fact restricted to the naked counter helium tube of the detector, as shown in Figure 5.4a. In order to reproduce this structure four cells are sufficient. The first two cells are allocated, as in the former case, to represent the gas active volume (cell 1) and the stainless steel counter cathode (cell 2). The features of these sections are exactly the same described before discussing the

WENDI file. The other two cells are used to simulate an external environment, that is a cylindrical region filled with air at atmospheric pressure (cell 3), and the outside universe.

Regarding the second version of the file, only two cells were used, as shown in Figure 5.4b: cell 1, represents the active volume of the counter tube, cell 2 the external environment. The only filling material considered is air.

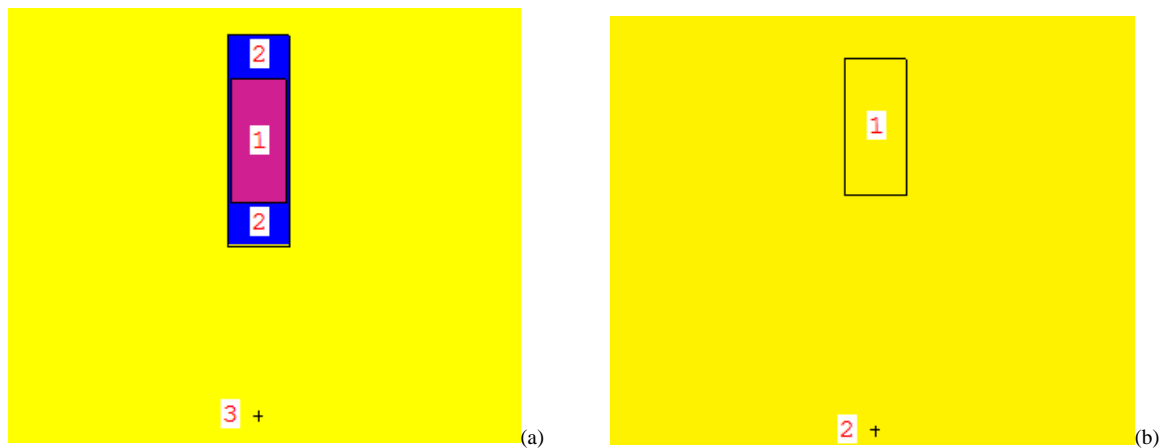


**Figure 5.4** Geometry used in TUBE input file: (a) Helium version, (b) Air version [VISED2, 2000]

In both cases, the positions of the surfaces and cells are exactly the same as those used in the WENDI file. Also, the source specifications have rigorously the same structure and values introduced before. Both photons and neutrons are considered and the upper limit for neutron energy is set equal to 5000 GeV. The main difference between the WENDI and TUBE files, besides the geometry, is the use of the tallies: in the second one the neutron fluence averaged on the gas volume is calculated, so that no multiplier cards are needed. Therefore, only a F4 card is introduced and, because of the absence of the polyethylene moderator, no thermal scattering treatment is required. The number of simulated particles, as before, is set equal to 10,000,000.

### 5.2.3 Simulations results

Before evaluating the simulated response function of the rem meter, it is appropriate to analyse more deeply the output results from the input files just described.

The difference between the average fluence calculated by the two mentioned versions of the input file Tube, appears to be significant only in the first part of the energy range considered. The average fluence in air appears to be independent of the emission energy, showing a constant behaviour through the entire domain considered, due to the absence of obstacles along the neutrons flight path. On the contrary, neutron fluence calculated in helium appears to be constant only at higher energies. This result could be explained considering that, at lower source energy values, many neutrons are stopped or scattered by the cathode material before reaching the active gas volume. However, the difference between the two curve is significant only below 0.2 eV, rising to a factor of 3.18 at 1meV.

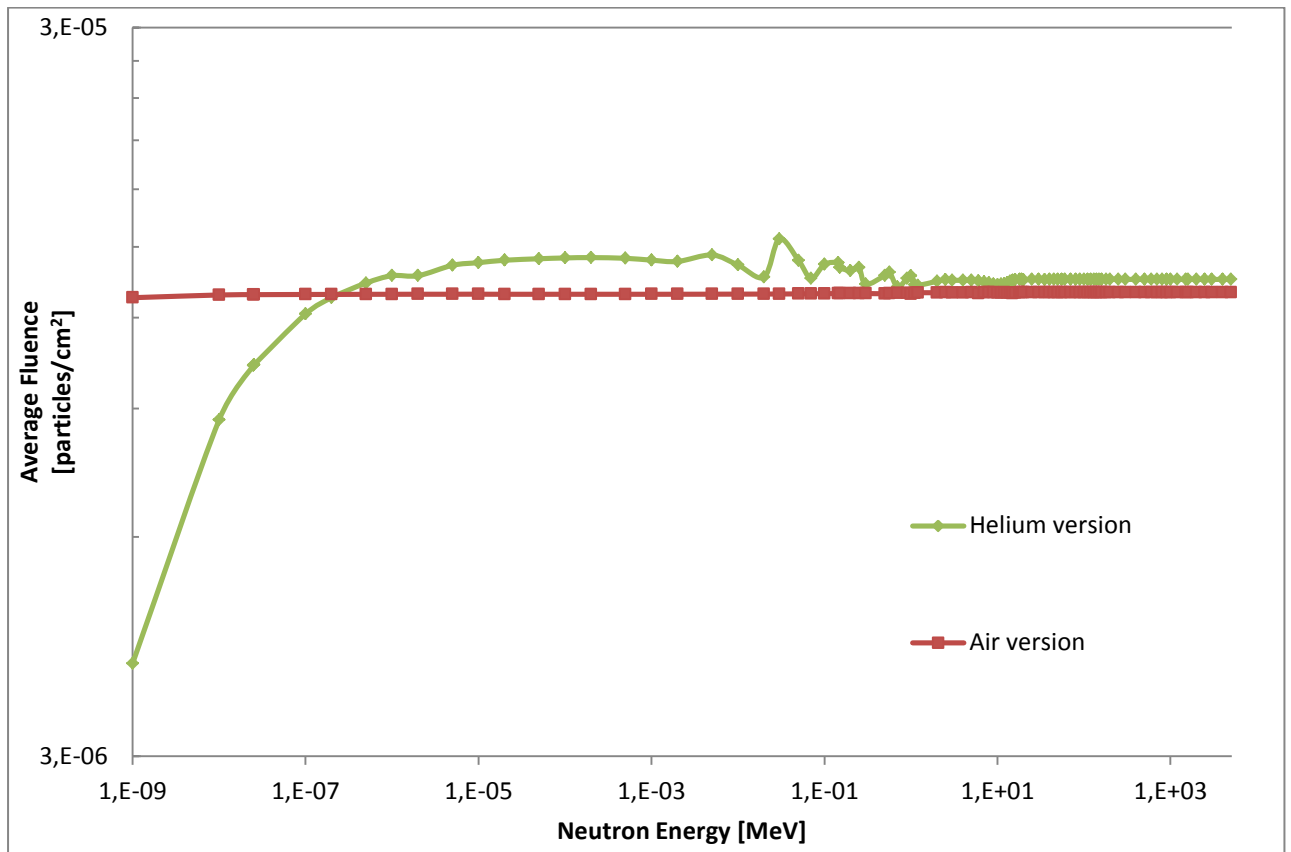


**Figure 5.5** Trend of the average fluence in the counter tube

Concerning the simulations conducted with the input file WENDI, the opportunity to take into account the thermal scattering of neutrons in polyethylene moderator was evaluated. A comparison between the output results, obtained with and without a thermal scattering treatment, was made for a few incident neutron energies.

As can be seen in Figure 5.6, the difference between the two trends is quite wide below 1 MeV, reaching a factor equal to an order of magnitude below  $10^{-7}$  MeV. On the contrary, it almost disappears at higher energies. Due to this fact, thermal scattering was considered, despite the greater computational effort and run time.

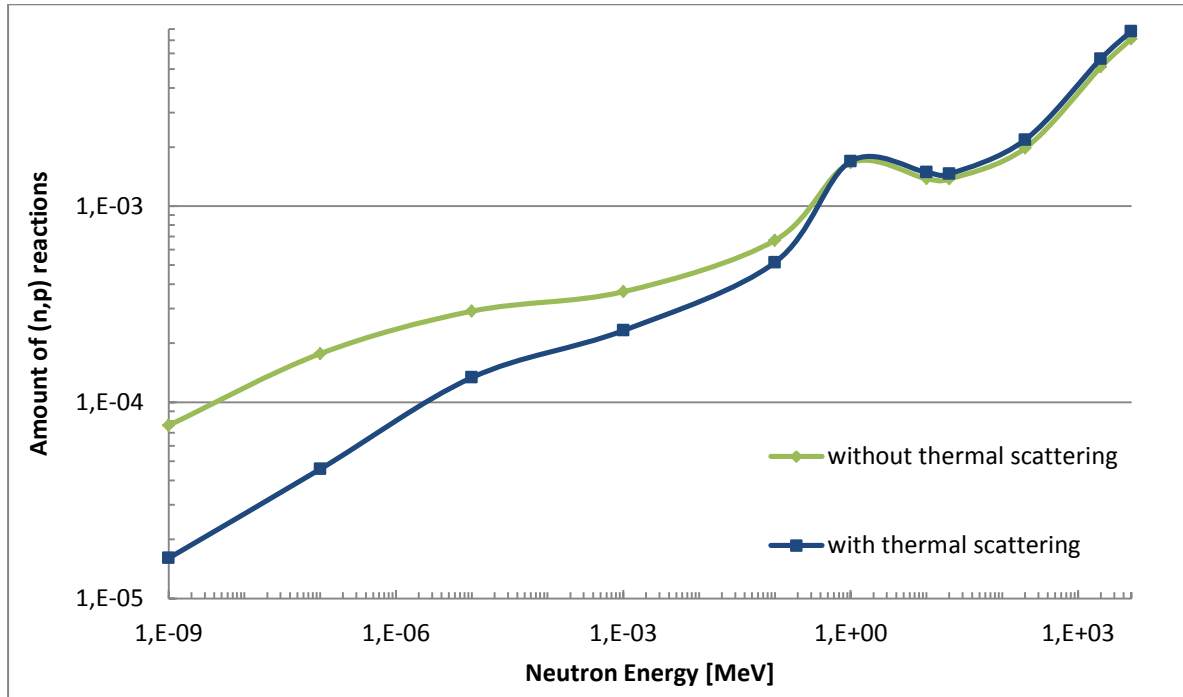


**Figure 5.6** Comparison between the output results of WENDI input file with and without thermal scattering treatment

To calculate the detector response function points, 93 energy values of the source were simulated and interpolated obtaining the curves shown in this chapter. In Figure 5.7 the trend of the simulation results, with thermal scattering treatment, is shown.

Concerning the first part of the domain (from 1 meV to 1 eV), the increasing trend of the function can be explained considering the increase of the neutron fluence as shown in Figure 5.5. In the central energy region the trend of the function is smoother because of the high absorption resonance mechanism characterising the tungsten in the energy interval between 1 eV and 1.5 KeV. Above 8 MeV and 14 MeV, instead, the (n,2n) and (n,3n) reactions respectively become energetically feasible, amplifying the amount of reactions occurring. At higher energies the number of (n,p) reactions increases further because of the more complex spallation mechanism associated to the tungsten shell above 20 MeV.

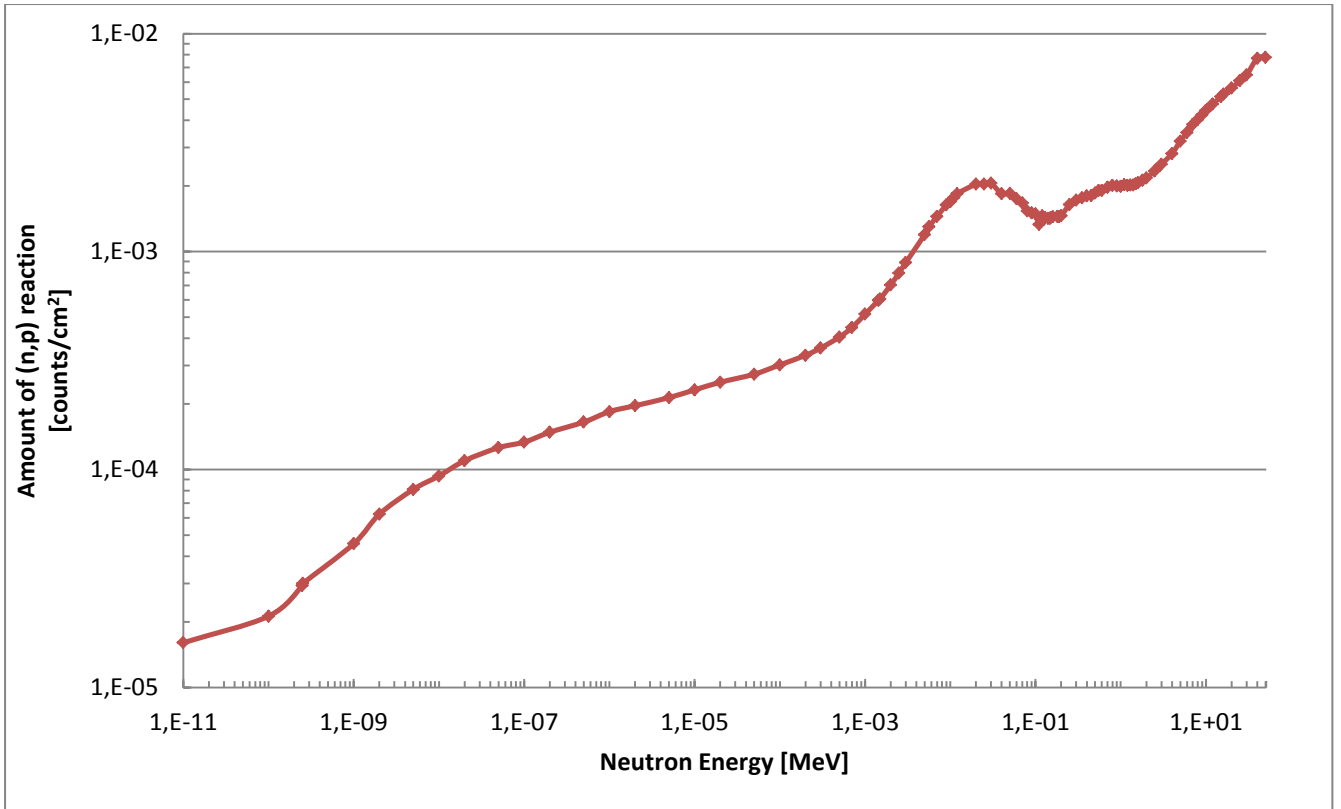


Figure 5.7 WENDI output results (with thermal scattering treatment)

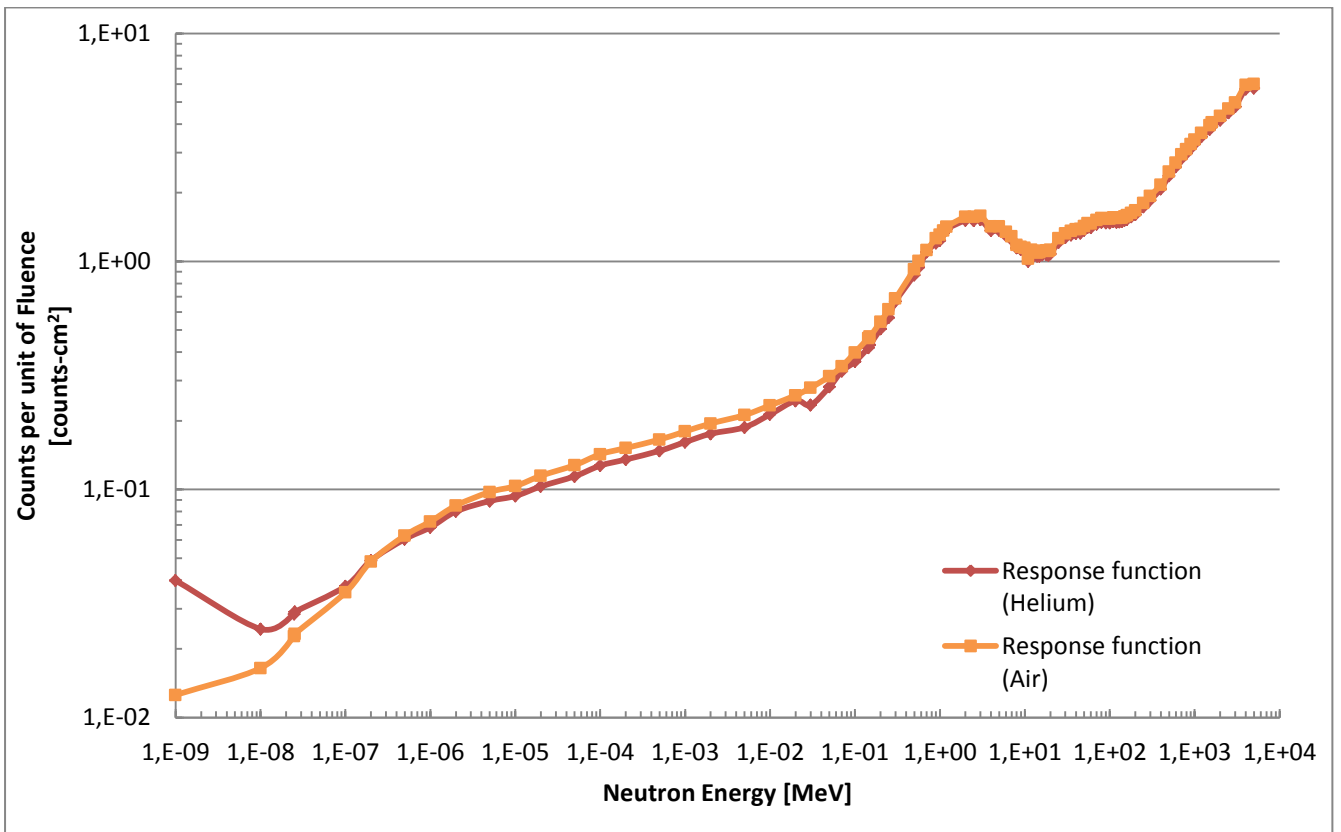
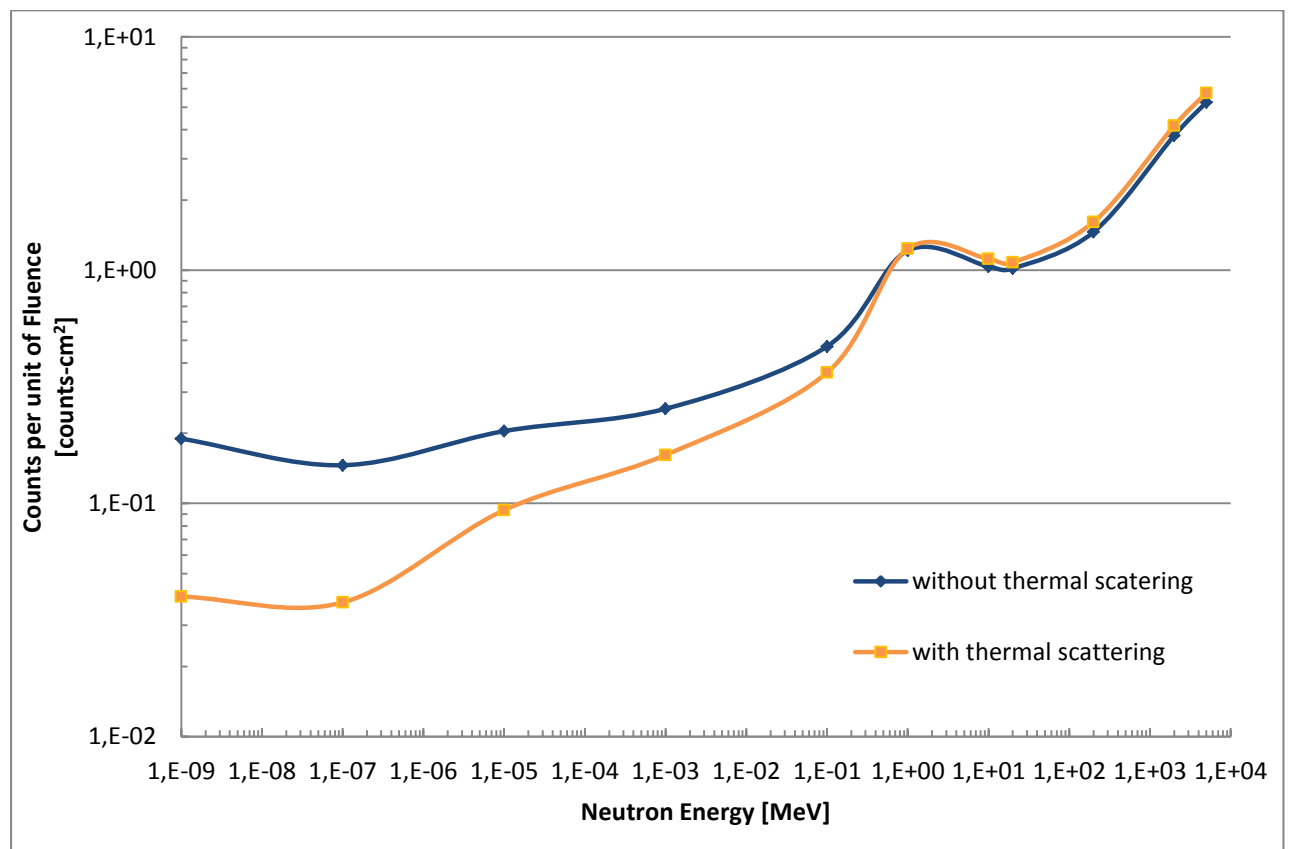


Figure 5.8 WENDI-2 detector simulated response function

The response function was built on the basis of these results normalizing the number of (n,p) reactions to the average fluence in the inner gas volume for each source energy value. In Figure 4.8 the response functions obtained considering the average fluence in helium and that in air are shown. As might be expected taking into account the trend of the neutron average fluence calculated (Figure 5.5), the difference between the two curves has a maximum equal to a factor of 3.18 at 1 eV, while it almost disappears at energies higher than 20 meV. In light of this, it can be argued that the choice of the material of reference for the calculation of the average fluence has a limited significance. According to the former studies, only the response function calculated on the basis of the average neutron fluence in helium has been taken into account for more detailed analysis. Hereafter the definition of response function will be restricted to the results calculated dividing the amount of (n,p) reactions by the neutron fluence in the helium gas volume.

A comparison between the rem meter response functions, calculated with the thermal scattering and that obtained with the use of the free-gas thermal treatment, is shown in Figure 5.9.



**Figure 5.9** Comparison between the response functions obtained with and without taking into account the thermal scattering

The curve calculated without the thermal scattering treatment shows an overestimation reaching 4.7 from the lower limit to 0.1 MeV. This behaviour can be easily explained considering that the thermal scattering cross section increases when the energy of the incident particles decreases. The analysis of the two curves showed the significant difference between the two series of data below 1 keV and consequently it corroborated the choice of taking into account the thermal scattering associated to the neutron transport in the polyethylene moderator.

### 5.3 COMPARISON WITH FORMER STUDIES

Two previous studies were taken into consideration to compare the results obtained with those in literature: Olsher's work [*Olsher's et al., 2000*] and the Vanaudenhove article [*Vanaudenhove et al., 2003*]. In the Vanaudenhove study a different MC code was used: Geant4 [*Geant4, 2009*]. In Figure 5.10 the present simulations results and those presented in the Vanaudenhove article, both obtained without a thermal scattering treatment, are presented.

As can be seen, there is a good match between the two curves: the little inconsistencies can be explained considering the use of different Monte Carlo codes (MCNPX for the present simulation and GEANT in the previous work) and of different simulation parameters. Regarding the significant error when neglecting the thermal treatment, the response function was not more deeply investigated in this sense: only the curve obtained taking into account the thermal scattering was used for the next applications and measurements.

In Figure 5.11 it is possible to compare the present simulations results with the WENDI detector response function shown in the former scientific literature. The curve reproduced in the present work is in good agreement with the response function associated to the Olsher's study, while the slight overestimation related to the GEANT model can be again related to differences in simulation conditions or physics setting. All the curves considered in Figure 5.11 have been obtained using the thermal scattering treatment.

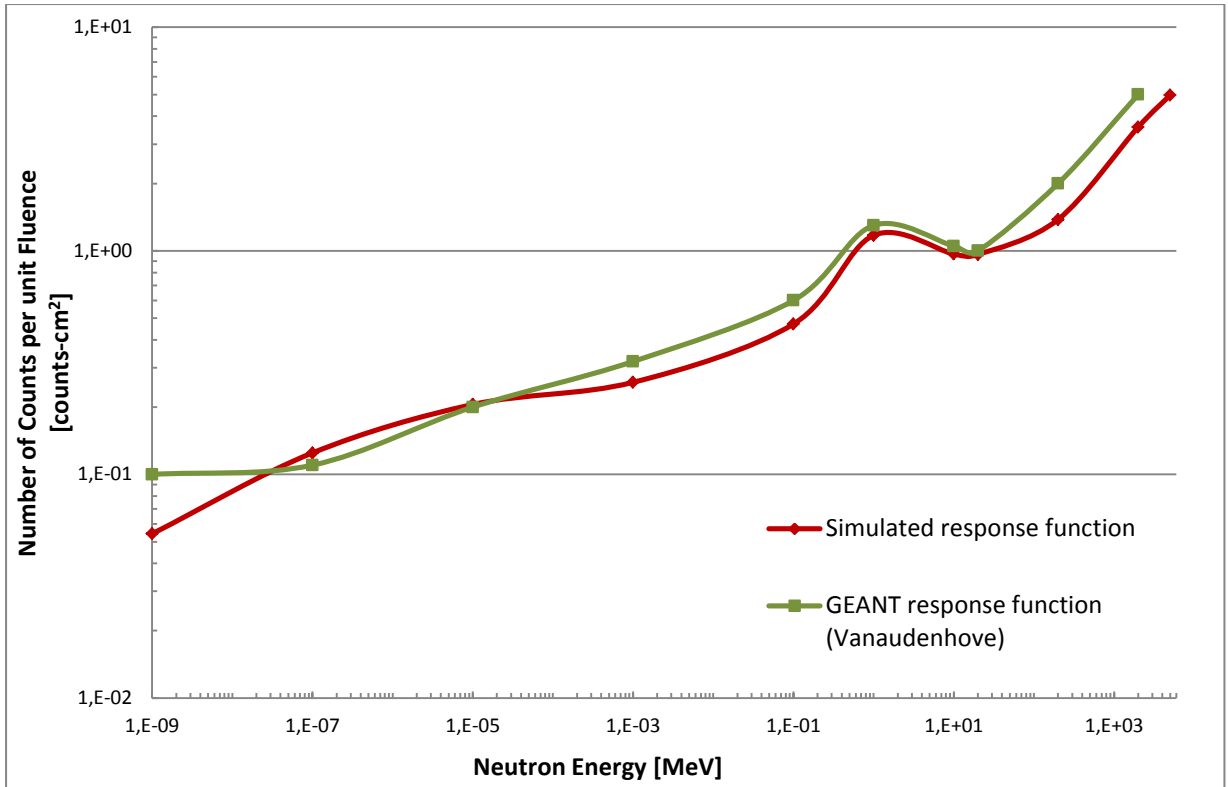


**Figure 5.10** Response function obtained in this work (MCNPX) and in Vanaudenhove et al. work, without taking into account thermal scattering in the polyethylene moderator

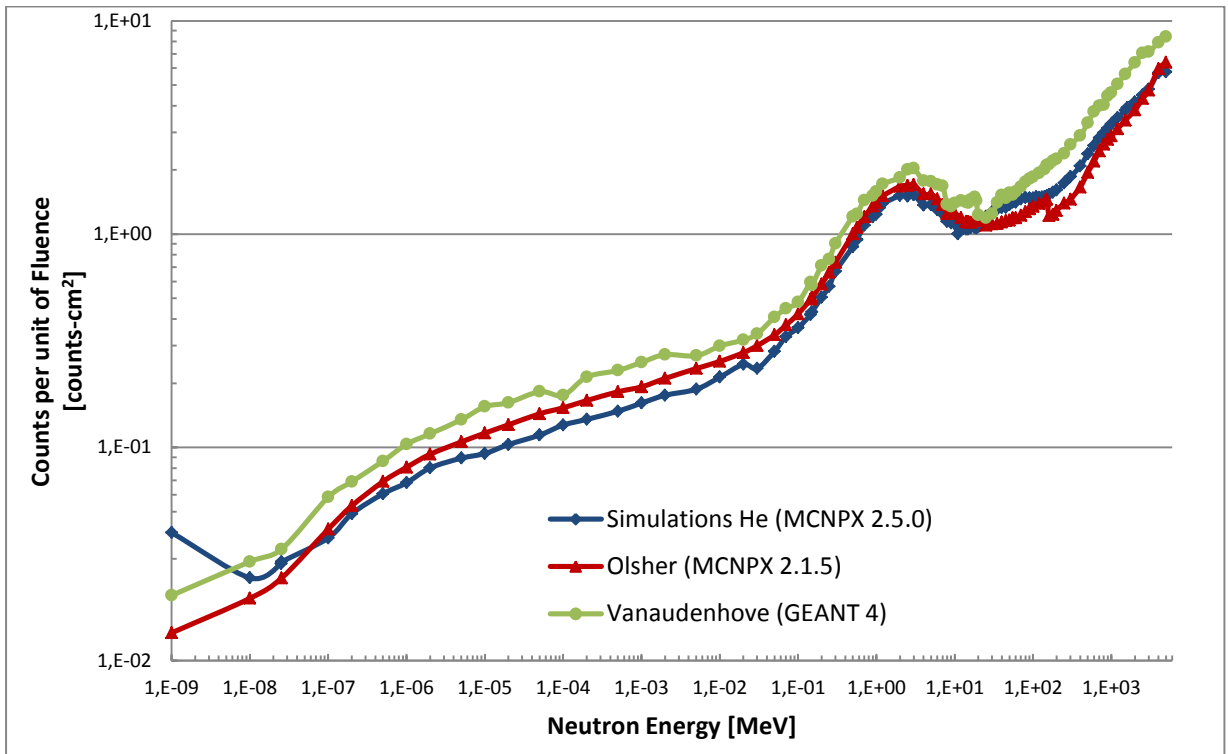


**Figure 5.11** Comparison between the calculated response function and those shown in Olsher's (2000) and Vanaudenhove's (2003) articles

In particular, the response function obtained by the present simulations underestimate the results presented by Olsher over nearly the entire domain, rising to a factor of 0.78 at 30 keV. Overestimations can be observed at the lower limit of the energy domain and above 250 MeV. In more detail, the difference between the two series of data rises to a factor of 2.95 at 1 meV. This gap is probably due to the use of different thermal scattering libraries in the two studies. In spite of this, more investigations were not made by reason of the lower importance of the radiation quality at these energies - that implies a lower interest of the results accuracy in this part of the domain. In the range from 25 MeV to 3 GeV the overestimation rises a maximum, equal to 1.28, at 300 MeV: the deviation in this part of the domain seems to be not very significant.

Considering the comparison with the GEANT model, the simulated function present an underestimation up to a factor equal to 0.63 at 200 eV and to 0.64 at 2.5 GeV. Also in this case, at the lower energy limit, the simulated response function overestimates the result by a factor of 1.97.

## **5.4 COMPARISON WITH FLUENCE-TO-DOSE CONVERSION FUNCTION**

The principle of a rem meter, as introduced in Chapter III, is that its response function matches approximately the ICRP fluence-to-ambient equivalent dose conversion function, so that its absolute response is nearly proportional to the ambient equivalent dose.

Therefore, to evaluate the reliability of the information given by the detector, the simulated response function and the data taken into account were compared to the  $H^*(10)$  fluence-to-ambient dose conversion function. To be able to compare the curves, regardless of the calibration factor, they have been normalised 2 MeV. The choice of this energy value has the purpose of reproducing approximately the calibration factor corresponding to a  $^{252}\text{Cf}$  fission source, proposed in the Olsher's study and equal to 0.743.

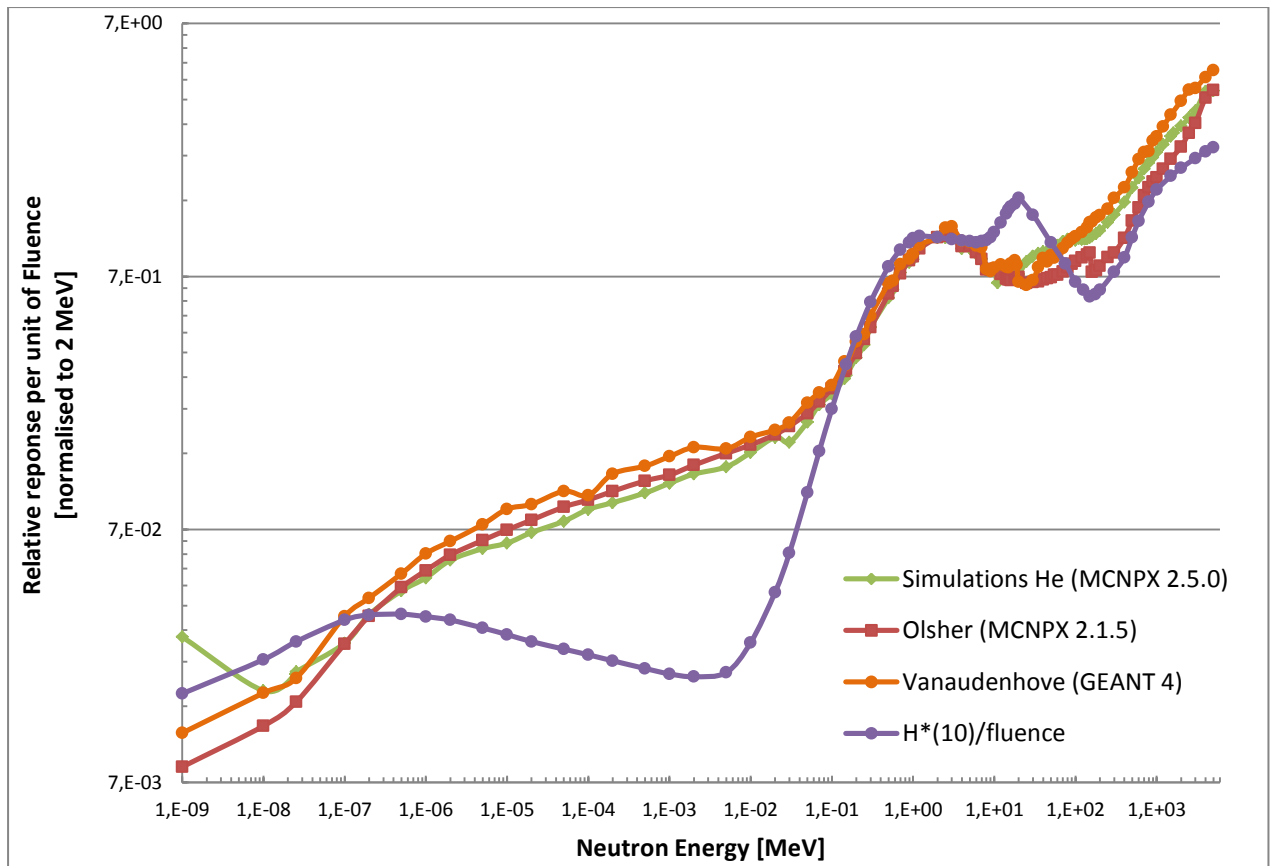


**Figure 5.12** Comparison between the response functions analysed and the ICRP fluence-to-dose conversion function

As it is possible to see in Figure 5.12, there are two main regions of incongruence. Above 75 GeV and from 0.2 eV to 0.15 MeV, the response of the detector, associated to each work considered, overestimates the fluence-to-dose conversion function. The difference between the latter and the present results rises to a factor of 1.7 at 200 MeV and 6.8 at 2 keV. The zones of underestimation are less large than the overestimation regions. They cover the energy values lower than 0.2 eV, that are of little interest to radiation protection, and a portion of the energy domain included between 4 and 75 MeV.



# CHAPTER VI

## WENDI-2 Response

The study of the WENDI-2 response function (cf. Chapter V) has shown that this detector is likely to provide relatively accurate measurements of the neutron ambient dose equivalent in fields with a wide neutron energy spectrum. However, with a fixed calibration factor, the accuracy of the response will depend on the nature of the local neutron spectrum. Therefore, the detector response might not be as accurate in all types of workplaces, neither in all considered positions inside a given workplace. Monte Carlo simulations of the neutron spectra and the neutron ambient dose equivalent in various positions inside a given workplace are thus necessary for assessing the accuracy of the measurements made with the WENDI-2 detector. In this thesis, MCNPX simulations of the WENDI-2 response around an 18 MeV  $H^-$  cyclotron have run, reproducing an existing workplace located in the IBA assembly hall in Louvain-la-Neuve (Belgium).

In this chapter, the input files of these simulations will be discussed briefly. Then, the simulation results will be presented and compared to the neutron ambient dose equivalents previously computed in separate MCNPX simulations. The latter results have been obtained by Valérie De Smet, currently working at the Research Institute of the ISIB on a project dedicated to the dosimetry of high energy neutrons for radiation protection in proton therapy centers (the FIRST-project "FREDONE", in collaboration with IBA).

### 6.1 INPUT FILE

The IBA Academy is a bunker in the IBA assembly hall dedicated to the training of IBA customers. It contains a Cyclone 18/9, a fixed-energy cyclotron that can accelerate  $H^-$  ions up to 18 MeV and deuteron ions up to 9 MeV. This type of cyclotron is typically used for the production of PET radioisotopes, as mentioned in Chapter V.

In Figure 6.1 and 6.2 the side view and median plane, respectively, of the geometry of the Cyclone 18/9 reproduced in the simulations are shown. The external part of the machine is in steel and is reproduced in blue in Figure 6.1 and 6.2, the central vacuum is drawn in orange, yellow is used for the copper cells and purple for air.

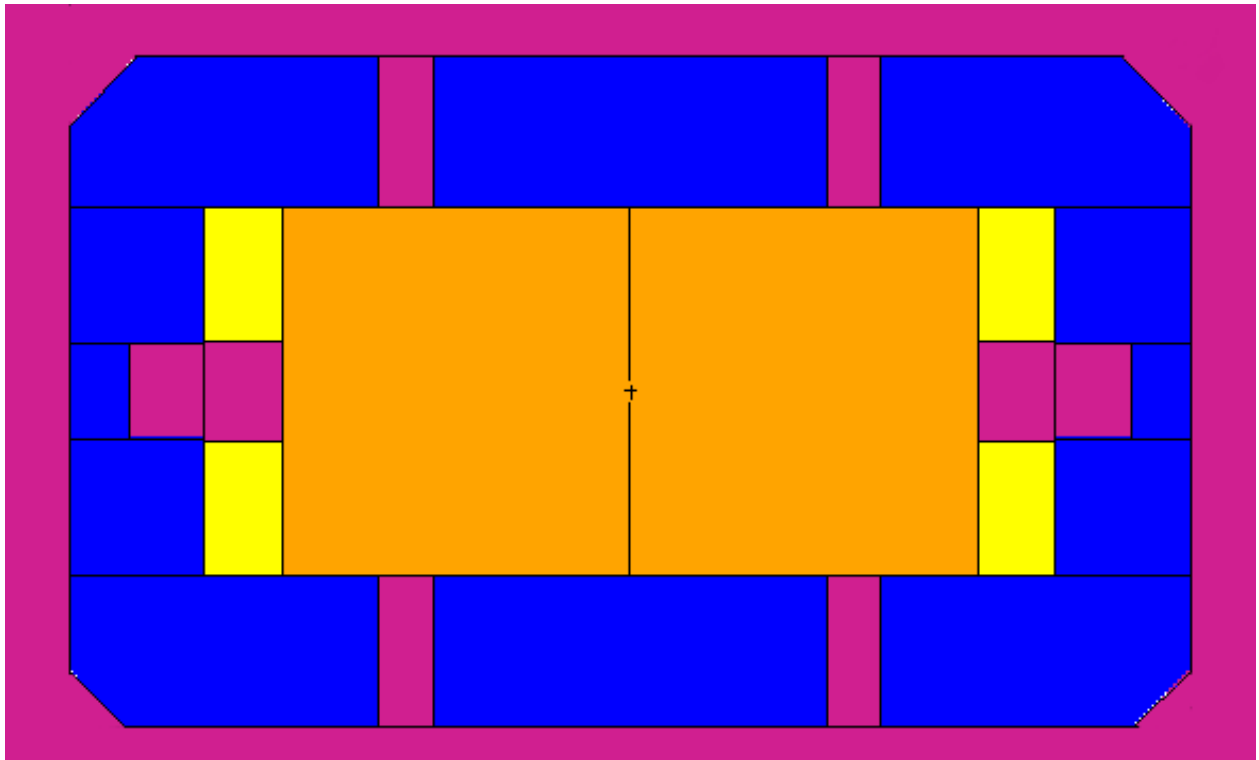


**Figure 6.1** Side view of Cyclone 18/9 reproduced in simulations [VISED2, 2000]

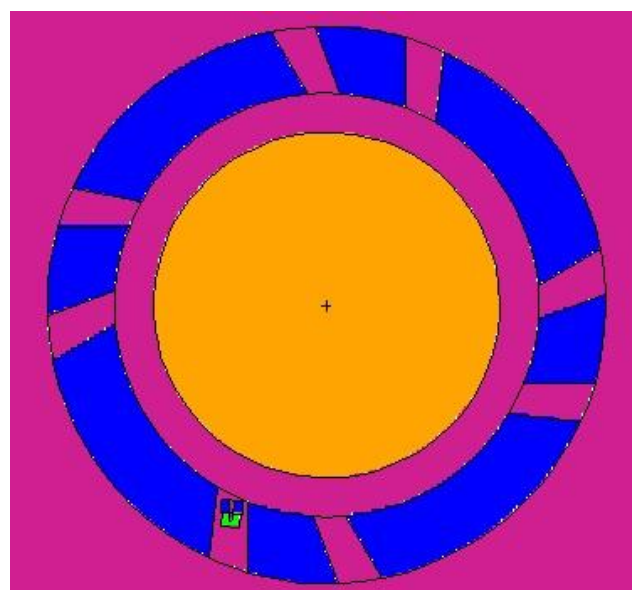


**Figure 6.2** Cyclone18/9 geometry and copper target [VISED2, 2000]

The machine has 8 different ports in which suitable targets can be inserted. During customer training, a copper target is used instead of a standard PET target and, in our case-study, this copper target is located in port 6, as shown in Figure 6.2.

In Figure 6.3 it is possible to see the structure of the target. It consists of two main parts: the steel support is represented in blue in the picture while the green cell reproduces the target material, i.e. copper.

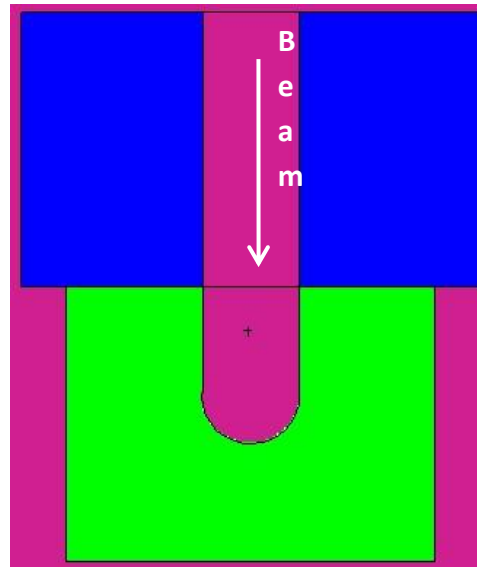


**Figure 6.3** Geometry of the copper target used in simulations [VISED2, 2000]

We considered the case in which this copper target is irradiated with an 18 MeV  $H^+$  beam of 20  $\mu A$ . The particle source in our simulations has actually been directly defined as a neutron source with 20 angular bins having each their specific energy distribution. These distributions have been previously calculated with MCNPX by Frédéric Stichelbaut (IBA), considering the irradiation of a thick cylindrical copper target by a thin beam of 18 MeV protons.

To estimate the response of the detector in this case study, the structure of the IBA bunker has been simulated and evaluations have been made for different positions in the workplace. Figures 6.4 and 6.5 show respectively the side view and the median plane of the structure of the IBA Academy bunker and its access maze as simulated. The response of the WENDI-2 detector has been simulated for 9 different positions: three around the cyclotron (in front of the "south", "east" and "west" walls) and six along the maze.

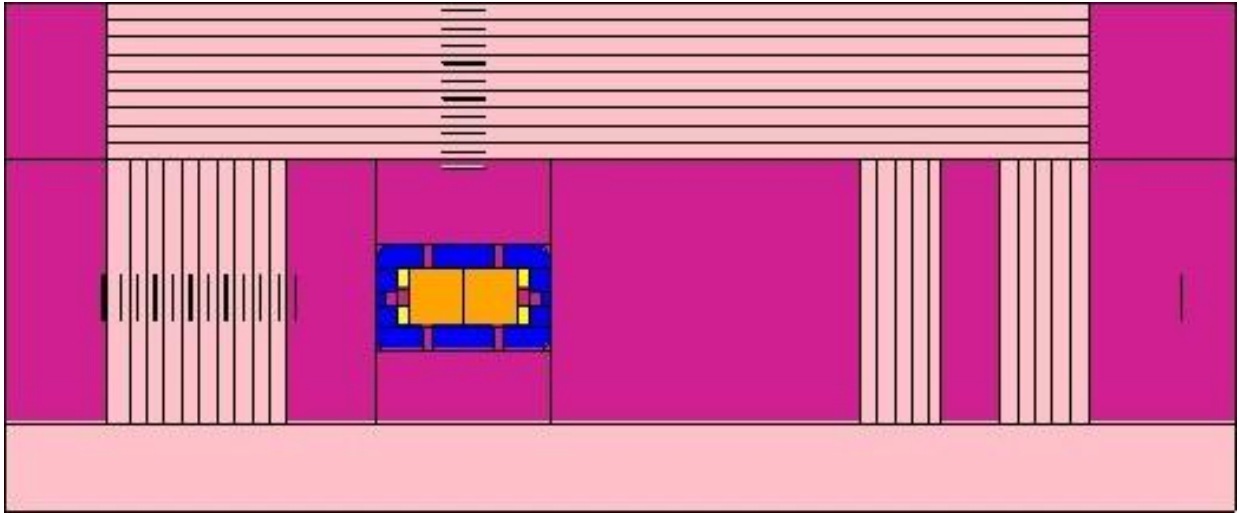


**Figure 6.4** Side view of the IBA Academy bunker reproduced in the simulations [VISED2, 2000]

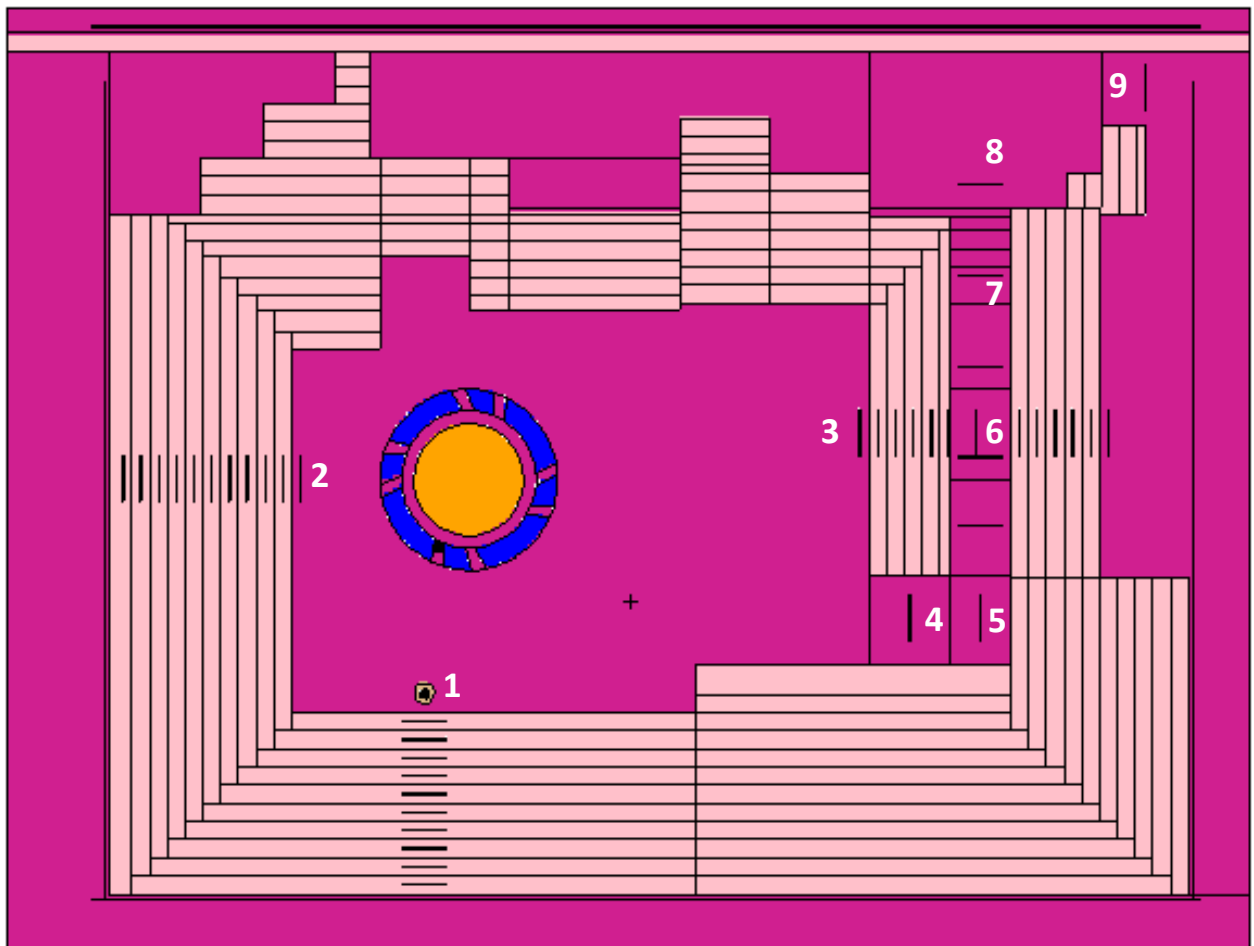


**Figure 6.5** Geometry of IBA Academy reproduced in the input file. This figure corresponds to the simulation in which the WENDI-2 detector is located in position 1, in front of the "south" wall. All other simulated positions are indicated by numbers as well [VISED2, 2000].

In each simulation only one position of the detector has been considered, so that the neutron field was not influenced by the presence of other detectors. Each position of the rem counter was chosen in a place where the value of the ambient dose equivalent  $H^*(10)$  was already known for the same irradiation conditions. These  $H^*(10)$  values have been computed with MCNPX by Valérie De Smet, considering parallelepipedic air volumes in which the average neutron fluence was tallied (using the F4 tally) and folded with the ICRP-74 fluence-to- $H^*(10)$  conversion function (using the DE card). In this way it has been possible to compare the results given by the detector simulations with the ambient dose equivalent.

The geometry of WENDI-2 introduced in the present input file was identical to that reproduced in the input file WENDI described in Chapter V. Also the tally related to the evaluations of the counts recorded by the detector is unchanged: an F4 tally modified by a FM multiplier card previously described. For the simulations of the detector positions 1.2 and 3 around the cyclotron, no variance reduction technique was used. Regarding the positions in the maze, instead, the variance reduction technique called "geometry splitting" was applied by giving neutron and photon importance values greater than one to various cells: air cells in the maze and around the bunker, as well as concrete cells in the maze walls.

## **6.2 RESULT ANALYSIS**

For each simulation a number of particle large enough to obtain an acceptable value of the MCNPX error was simulated. In Table 6.1 the results of the simulations in terms of detector counts as well as the associated error are presented. As introduced in Chapter V, the amount of counts is considered to be equal to the amount of (n,p) reactions in the active volume of the detector, neglecting minor contributions. As expected, the maximum value of the count rate is obtained in position 1 in front of the "south" wall in the cyclotron chamber: in this case the detector has been simulated in front of the irradiated target and no obstacles other than air are present between the port and the rem counter.

Regarding the positions in the maze, the number of the counts recorded decreases with the distance from the chamber access (position 4).

POSITION	COUNTS PER EMITTED SOURCE PARTICLE	MCNPX ERROR
1	$1.33505 \cdot 10^{-05}$	0.0082
2	$2.71239 \cdot 10^{-06}$	0.0151
3	$5.85846 \cdot 10^{-07}$	0.0316
4	$3.48931 \cdot 10^{-07}$	0.0416
5	$2.49958 \cdot 10^{-07}$	0.0475
6	$1.82902 \cdot 10^{-08}$	0.0628
7	$5,38306 \cdot 10^{-09}$	0.076
8	$2.46419 \cdot 10^{-09}$	0.0567
9	$1.30678 \cdot 10^{-10}$	0.0478

**Table 6.1** Results of simulations for all detector positions considered

Since the count rate is expressed in number of reactions per emitted source particle, to express the response of the detector in terms of an equivalent dose rate ( $\mu\text{Sv/h}$ ), it is necessary to evaluate the neutron production rate in the target. With the given value of the ion current ( $20 \mu\text{A}$ ) the number of protons hitting the target per second is equal to  $1.248 \cdot 10^{14}$ . In these operational conditions, the amount of secondary neutrons produced by the interaction of protons in the target material is estimated to be equal, on average, to  $6.95643 \cdot 10^{-3}$  neutrons per hitting proton [*Stichelbaut, 2010*]. In light of this, it is possible to calculate the neutron yield, in terms of neutrons produced in the target per unit time, multiplying the proton current by the average number of neutrons produced by each proton (formula 6.1).

$$1.248 \cdot 10^{14} \frac{p}{s} \times 6.95643 \cdot 10^{-3} \frac{n}{p} = 8.685 \cdot 10^{11} \frac{n}{s} \quad (6.1)$$

Knowing the yield of the neutrons produced in the target the number of (n,p) reactions per unit time, and hence the number of counts per unit time, can be calculated. The latter is in fact estimated, for the different simulated positions, multiplying the secondary neutron yield, obtained in Formula 6.1, by the result of simulations, i.e. the number of counts per emitted source particle. The last step in the calculation of the WENDI-2 dose response consists in dividing the number of counts per unit time by the calibration factor expressed in  $\frac{\text{counts/s}}{\mu\text{Sv/h}}$ . This proportionality factor, provided by Thermo Scientific, is calculated with regards to a  $^{252}\text{Cf}$  source and it is equal to 0.84 [*Thermo Scientific, 2007*]. The results of the calculations described are shown in Table 6.2. Since the difference between the present results and those presented in Table 6.1 consists of multiplicative factors, the trend of the response considering all the detector positions simulated is the same as that previously described: the highest value of equivalent dose is registered in front of the irradiated target (position 1), the lowest at the exit of the maze.

POSITION	WENDI RESPONSE	WENDI RESPONSE
	[counts/s]	[ $\mu\text{Sv/h}$ ]
<b>1</b>	$1,15904 \cdot 10^{07}$	$1.37981 \cdot 10^{07}$
<b>2</b>	$2,35480 \cdot 10^{06}$	$2.80333 \cdot 10^{06}$
<b>3</b>	$5.08610 \cdot 10^{05}$	$6.05488 \cdot 10^{05}$
<b>4</b>	$3,02929 \cdot 10^{05}$	$3.60630 \cdot 10^{05}$
<b>5</b>	$2,17004 \cdot 10^{05}$	$2.58338 \cdot 10^{05}$
<b>6</b>	$1,58789 \cdot 10^{04}$	$1,89034 \cdot 10^{04}$
<b>7</b>	$4,67337 \cdot 10^{03}$	$5.56354 \cdot 10^{03}$
<b>8</b>	$2,13932 \cdot 10^{03}$	$2.54681 \cdot 10^{03}$
<b>9</b>	$1,13450 \cdot 10^{02}$	$1,35059 \cdot 10^{02}$

**Table 6.2** Response of WENDI-2 rem counter expressed in counts/s and  $\mu\text{Sv/h}$ .

## 6.3 COMPARISON WITH H\*(10) CALCULATION

As previously mentioned, the calculation of the ambient dose equivalent H\*(10) has involved MCNPX simulations of the average fluence in parallelepipedic air volumes folded with the ICRP 74 conversion function (cf. Chapter II). A multiplier card has been used to obtain the result in terms of  $\mu\text{Sv}/(\mu\text{A}\cdot\text{h})$  by means of the proportionality factor  $1.56307\cdot 10^{-20}$ . The latter is obtained from the multiplication of the average number of neutrons produced per hitting proton per unit time ( $6.95643\cdot 10^{-3}\text{s}\cdot\text{neutrons/proton}$ ) by the number of protons per unit of current and time ( $2.24694\cdot 10^{16}\text{ protons}/\mu\text{A}\cdot\text{h}$ ), by the conversion factor equal to  $106\ \mu\text{Sv}/\text{Sv}$ . Then the MCNPX results have been multiplied by  $20\ \mu\text{A}$  to obtain the value of H\*(10) expressed in  $\mu\text{Sv}/\text{h}$ . As it possible to see comparing the values presented in Table 6.3, the evaluation of the ambient dose equivalent given by the WENDI-2 detector is more precise for position 1, with an overestimation by a factor of 1.065. Regarding the location of the detector on the other wall of the chamber, the overestimation rises to a factor of 1.409 in position 2 and 1.674 in position 3.

<b>Position</b>	<b>H*(10)</b> [ $\mu\text{Sv}/\text{h}$ ]	<b>Relative error</b> H*(10)	<b>R<sub>WENDI-2</sub></b> [ $\mu\text{Sv}/\text{h}$ ]	<b>Relative error</b> R <sub>WENDI-2</sub>	<b>R<sub>WENDI-2</sub>/H*(10)</b>
<b>1</b>	$1.296\cdot 10^{07}$	0.0016	$1.38\cdot 10^{07}$	0.0082	<b>1.065</b>
<b>2</b>	$1.990\cdot 10^{06}$	0.0045	$2.80\cdot 10^{06}$	0.0151	1.409
<b>3</b>	$3.617\cdot 10^{05}$	0.0085	$6.05\cdot 10^{05}$	0.0316	1.674
<b>4</b>	$2.034\cdot 10^{05}$	0.0088	$3.61\cdot 10^{05}$	0.0416	1.773
<b>5</b>	$1.472\cdot 10^{05}$	0.0118	$2.58\cdot 10^{05}$	0.0475	1.755
<b>6</b>	$9.889\cdot 10^{03}$	0.0223	$1.89\cdot 10^{04}$	0.0628	1.912
<b>7</b>	$1.935\cdot 10^{03}$	0.0408	$5.56\cdot 10^{03}$	0.0760	2.875
<b>8</b>	$9.219\cdot 10^{02}$	0.0579	$2.55\cdot 10^{03}$	0.0567	2.763
<b>9</b>	$4.601\cdot 10^{01}$	0.0575	$1.35\cdot 10^{02}$	0.0478	<b>2.935</b>

**Table 6.3** Comparison between H\*(10) values (calculated by Valérie De Smet) and the response of the WENDI-2 detector simulated in this work

Also the evaluations of the dose given by the detector for the positions along the maze are characterized by an overestimation of the  $H^*(10)$  value: the response overestimation increases up to a factor of 2.935, registered for the ninth position simulated. This trend in the detector response is due to the differences between the energy spectra of the neutron fields in the several positions considered and that of the  $^{252}\text{Cf}$  fission source used for the evaluation of the fixed calibration factor.

Comparing the  $^{252}\text{Cf}$  spectrum, in Figure 6.6, with those shown in Figure 6.7 and 6.8, it can be deduced that the response function in each position is as similar to the corresponding  $H^*(10)$  value as the related spectrum is similar to that of the calibration source.

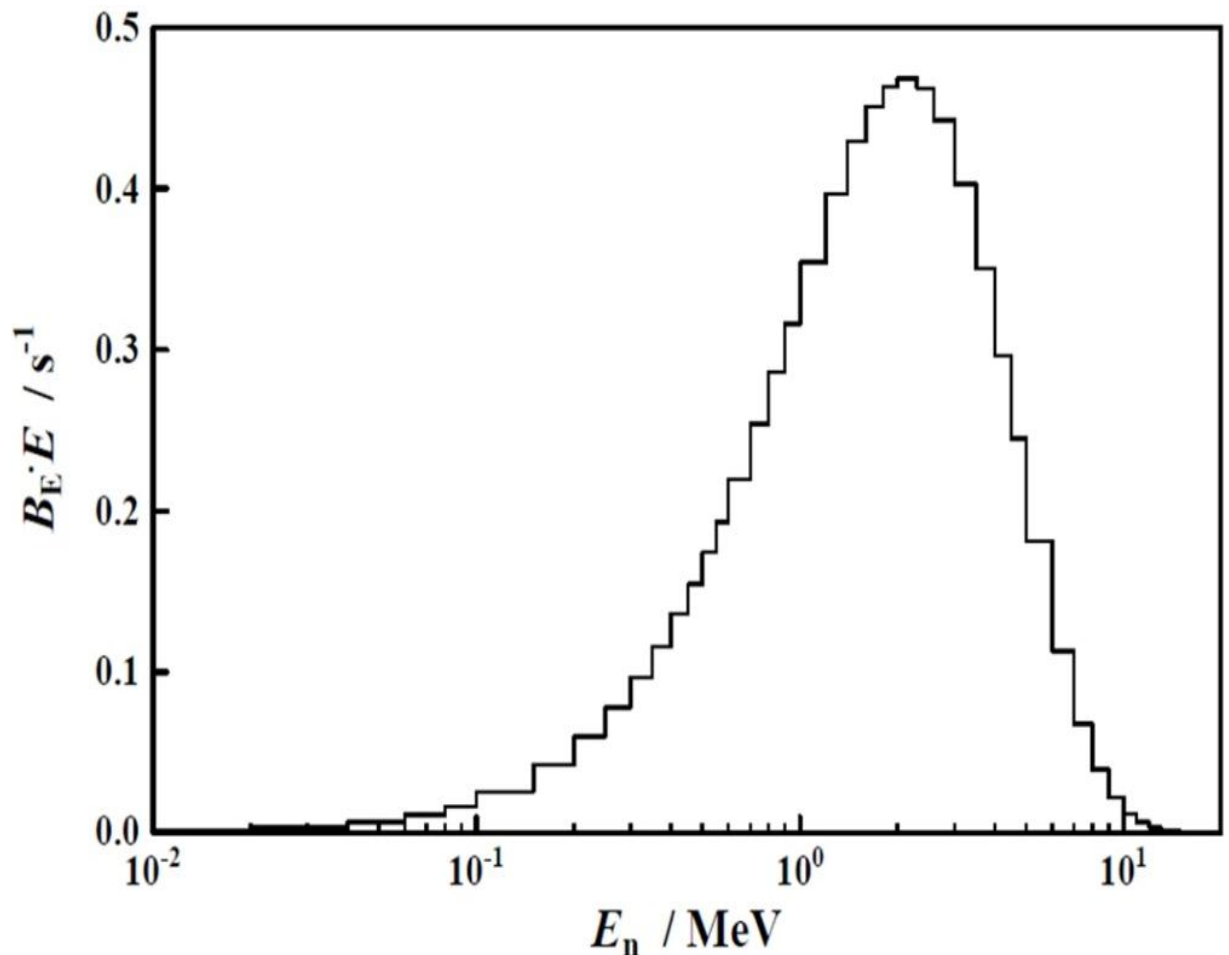


**Figure 6.6** Neutron energy spectrum of a  $^{252}\text{Cf}$  fission source [ISO, 2000]

In position 1, where the best detector evaluation of the  $H^*(10)$  has been found, the neutron spectrum is the most similar to that of the calibration source: it reaching the maximum values between 10 keV and 1 MeV – i.e., the maximum involves the same

energy region where the maximum of the  $^{252}\text{Cf}$  spectrum is located. This latter, as can be seen in Figure 6.6, shows an average energy of 2.1 MeV and a most probable energy of 0.7 MeV [Martin et al., 2000]. On the contrary, the spectrum relating to position 9 (Figure 6.8(f)), appears as the most different from that shown in Figure 6.6, being characterised by a series of picks all distant from the energy region of the  $^{252}\text{Cf}$  maximum. In agreement with what was said before, the result of the detector response in this position differs more from H\*(10) than in the other positions, being characterised by an overestimation factor equal to 2.935.

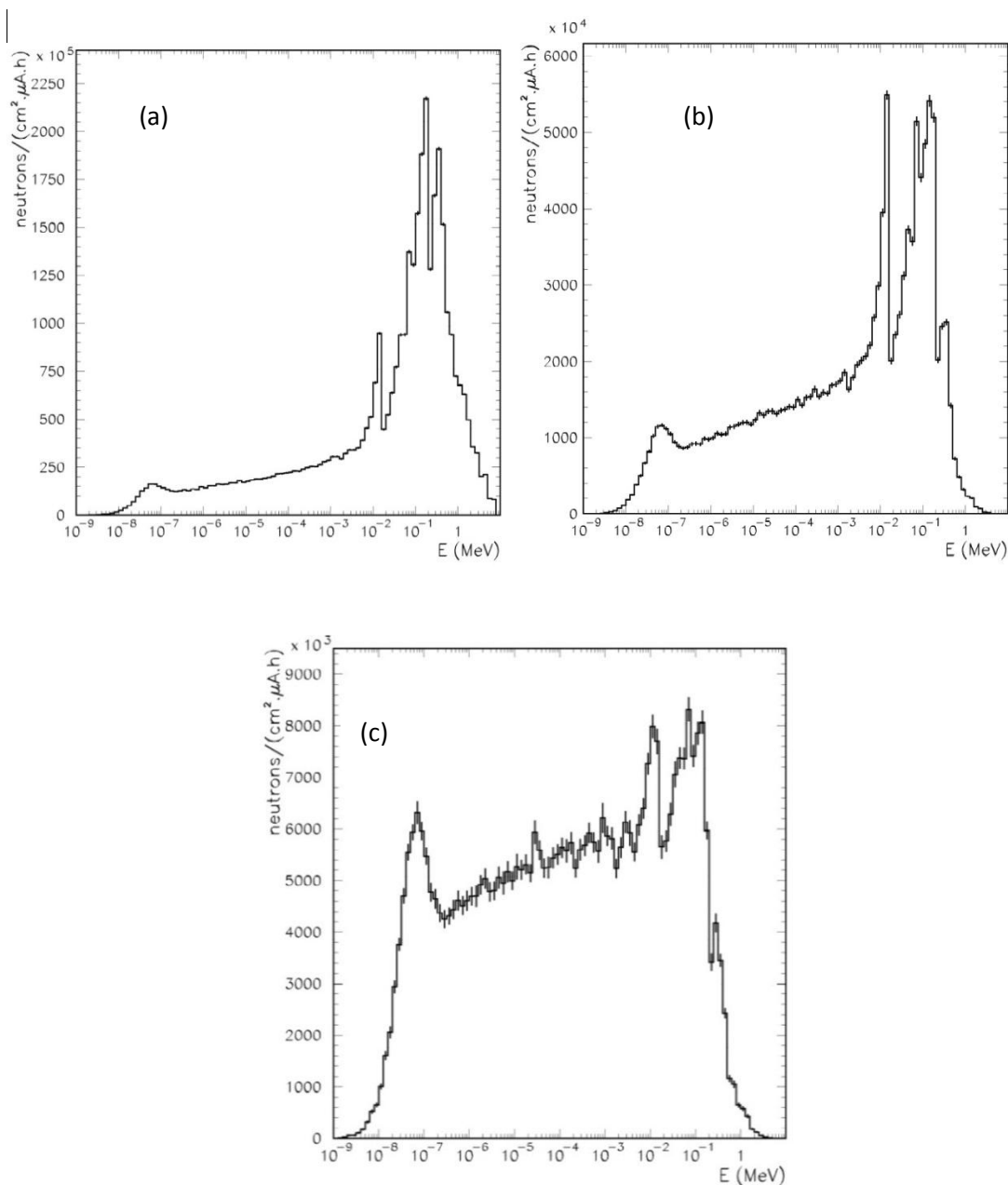


**Figure 6.7** Neutron energy spectra in the cyclotron chamber: (a) position 1 in front of the “south” wall, (b) position 2 in front of the “west” wall, (c) position 3 in front of the “east” wall

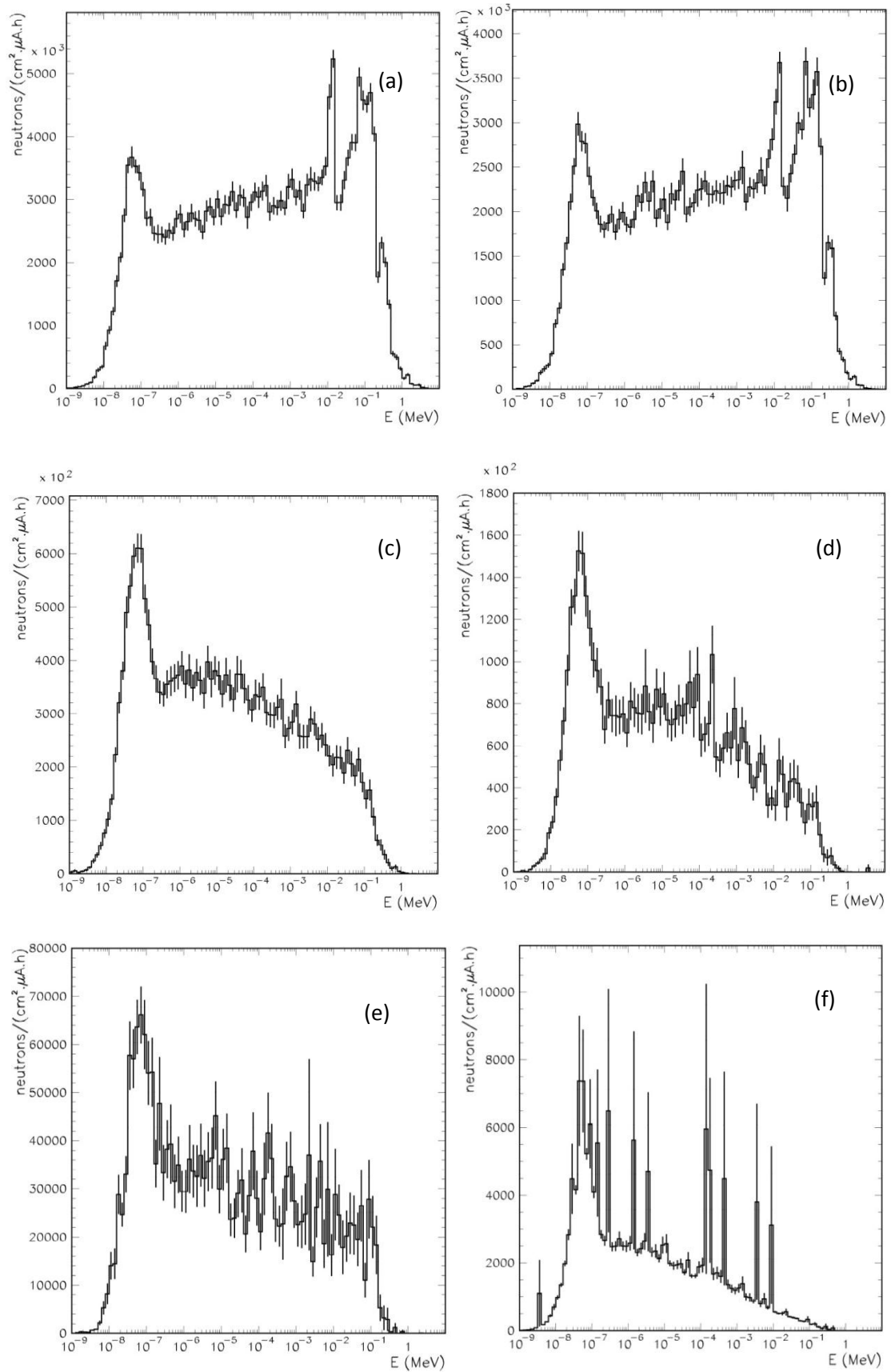


**Figure 6.8** Neutron energy spectra in maze positions: (a) position 4, (b) position 5, (c) position 6, (d) position 7, (e) position 8, (f) position 9

In light of these considerations, the calibration factor provided by Thermo Scientific and evaluated with respect to a  $^{252}\text{Cf}$  source, can be considered valid only in the evaluations of the ambient dose equivalent that involve a similar neutron field. On the other hand, the large difference in the detector response shows the need of suitable calibrations for different points of the facility.

# CONCLUSIONS

In this work a study of the extended range rem meter WENDI-2 response is presented. The result obtained by a general measurement process is influenced by the characteristics of the measuring device used. In the case of radiation detection, the contribution given to the resulting value by the detector is generally not negligible, especially considering a range of energies different from that of maximum effectiveness of the device. In light of what has been discussed in the foregoing pages, knowing the response function of the rem meter means having a precise idea of the reliability of the measurement provided by the detector in different neutron radiation fields, to be able to adjust the measurement process as needed.

The first step of this investigation has consisted of modelling the WENDI-2 detector, reproducing the structure of this device in an MCNPX input file. In this phase, in keeping with existing scientific literature, only the significant aspects of the detector geometry as well as the count rate contributions have been taken into account. For 93 energy values the response function has been estimated in terms of counts per unit fluence and interpolated in a continuous curve. Each point has been evaluated by simulations with respect to a single value of a point monoenergetic neutron source, and the value has been obtained dividing the total amount of the count rate by the fluence averaged on the active volume of the proportional counter gas. The count rate and the averaged fluence have been obtained by two different simulations. Afterward, the MCNPX detector model has been introduced in a more comprehensive simulation of a workplace existing at IBA and characterised by the presence of a PET cyclotron. The object of simulation has been to evaluate the response of the detector to continuous neutron radiation fields, like those present in cyclotron facilities. The reliability of the response in terms of neutron equivalent dose has been evaluated comparing the results obtained with the corresponding values of  $H^*(10)$  equivalent ambient dose, calculated in the same irradiation condition.

The study of the WENDI-2 rem meter response function and its comparison with the fluence-to-dose conversion function has shown that this device is likely to provide relatively accurate measurements of the neutron ambient dose equivalent on a wide neutron energy range. The energy domain considered is in fact included between 1 meV

and 5 GeV, an interval of great interest in a large number of applications. On the other hand, the evaluation of the detector response in the IBA Academy bunker – i.e. the second series of simulations run – has shed light on the limitations of the use of a fixed calibration factor. In fact, to obtain the response of the detector in terms of  $\mu\text{Sv/h}$  instead of counts/s, a proportional factor (equal to 0.84 according to the rem meter producer) is used. This multiplier constant has been evaluated with respect to a  $^{252}\text{Cf}$  fission source: the simulations carried out in this work have shown that the use of a fixed calibration factor makes the reliability of the measurements subject to the influence of the nature of the local neutron spectra. In other words, for neutron spectra very different from that of the  $^{252}\text{Cf}$  source used for the calibration, accepting a constant value of the calibration factor can lead to a significant error in the measurements.

In light of this, more work should be done to determine the suitable values of the calibration factor for each measurement and to evaluate the dependence of the absolute response function on the type of calibration performed. It would also be useful to carry out experimental measurements and to compare the results given by the detector with those simulated with MCNPX. Such an investigation would allow estimating the influence of the wall effects in the counter tube as well as the counter electronics on the absolute response function of the detector.

# REFERENCES

[*Andersson and Braun, 1963*] ANDERSSON, I.O., BRAUN, J., 1963. *A neutron rem counter with uniform sensitivity from 0.025 eV to 10 MeV*. In: Proceedings of the IAEA Symposium on Neutron dosimetry, IAEA, Vienna, vol. 2, pp. 87-95.

[*Berkovski et al., 2003*] BERKOVSKI, V., BONCHUK, Y., RATIA, G., 2003. *Dose per unit content functions: a robust tool for the interpretation of bioassay data*. In: Proceedings of Workshop on Internal Dosimetry of Radionuclides. Radiation Protection Dosimetry, vol. 105, No 1-4, pp. 399–402.

[*Birattari et al., 1998*] BIRATTARI, C., ESPOSITO, A., FERRARI, A., PELLICIONI, M., RANCATI, T., SILARI, M., 1998. *The extended range neutron rem counter 'LINUS': overview and latest developments*. Radiation Protection Dosimetry, vol. 76, No 3, pp. 135-148.

[*ENDF, 2012*] ENDF: Evaluated Nuclear Data File, database version of June 15, 2012. Data available at <http://www-nds.iaea.org/exfor/endl.htm>

[*Geant4, 2009*] Geant4, 2009, version 9.3, <http://geant4.web.cern.ch>

[*ICRP, 1991*] ICRP, 1991. *The 1990 Recommendations of the International Commission on Radiological Protection*. ICRP Publication 60. Ann. ICRP 21 (1–3)

[*ICRP, 2008*] ICRP, 2008. *The 2007 Recommendations of the International Commission on Radiological Protection*. ICRP Publication 103. Ann. ICRP 37 (2–4).

[*ISO, 2000*] INTERNATIONAL ORGANISATION FOR STANDARDIZATION (ISO), March 27, 2000. *Neutron Reference Radiation – ISO 8529*, EDMS 812014, available at <http://dpnc.unige.ch/~rapin/AmBe/Neutron-ISO-DIS-8529-1.pdf>

[Jongen, 1999] JONGEN, Y., 1999. *IBA: a short, biased story of a university spin-off in the field of particle accelerators*, IBA Group presentation.

[Knoll, 2000] KNOLL, G. F., 2000. *Radiation Detection and Measurement*, 3rd ed., John Wiley and Sons, Inc., Hoboken, New Jersey.

[LND, Inc data sheet] LND, INC. 252180 *Cylindrical High Temperature He3 Neutron Detector*, product specifications available at <http://www.lndinc.com/products/552/>

[Martin et al., 2000] MARTIN, R. C., KNAUER, J. B., BALO, P. A., 2000. *Production, Distribution, and Applications of Californium-252 Neutron Sources*, Applied Radiation and Isotopes, vol. 53, pp. 785-792.

[MCNPX User's Manual, 2005] PELOWITZ, D. , 2005, Ed., *MCNPX User's Manual, Version 2.5.0, LA-CP-05-0369*, Los Alamos National Laboratory Document.

[OECD, 1996] OECD NUCLEAR ENERGY AGENCY, EUROPEAN COMMISSION, 1996. *Considerations on the concept of dose constraint*. The Agency, Paris.

[Olsher et al. 2000] OLSHER, R.H., HSU, H.-H., BEVERDING, A., KLECK, J.H., CASSON, W.H., VASILIK, D.G., DEVINE, R.T., 2000. *Wendi: an improved neutron rem meter*. Health Physics, vol. 79, pp. 170–181.

[Silari et al., 2009] SILARI M., AGOSTEO, S., BECK, P., BEDOGNI, R., CALE, E., CARESANA, M., DOMINGO, C., DONADILLE, L., DUBOURG, N., ESPOSITO, A., FEHRENBACHER, G., FERNÁNDEZ, F., FERRARINI, M., FIECHTNER, A., FUCHS, A., GARCÍA, M.J., GOLNIK, N., GUTERMUTH, F., KHURANA, S., KLAGES, TH., LATOCHA, M., MARES, V, MAYER, S., RADON, T., REITHMEIER, H., ROLLET, S., ROOS, H., RÜHM, W., SANDRI, S., SCHARDT, D., SIMMER, G., SPURNÝ, F., TROMPIER, F., VILLA-GRASA, C., WEITZENEGGER, E., WIEGEL, B., WIELUNSKI, M., WISSMANN, F., ZECHNER, A., ZIELCZYŃSKI, M., 2009. *Intercomparison of radiation protection devices in a high-energy stray neutron field. Part III: Instrument response*. Radiation Measurements, vol.44, pp. 673–691.

[Stichelbaut, 2010] STICHELBAUT, F., December 8<sup>th</sup>, 2010. *Shielding Validation for Cyclone 18 Installation at CHU Montréal*, IBA Group presentation.

[Thermo Scientific, 2007] THERMO FISHER SCIENTIFIC INC., 2007. *FHT 762 Wendi-2 Wide Energy Neutron Detector*, data available online at <https://static.thermoscientific.com/images/D10459~.pdf>

[UNSCEAR, 2000] UNSCEAR, 2000. *Sources and Effects of Ionising Radiation*. United Nations Scientific Committee on the Effects of Atomic Radiation Report to the General Assembly with Scientific Annexes, United Nations, New York, NY.

[Vanaudenhove et al., 2003] VANAUDENHOVE, T., DUBUS, A., PAULY, N., 2003. *Comparison of GEANT4 hadronic models for the WENDI-II rem meter response function*. Radiation Protection Dosimetry, Vol. 0, No. 0, pp. 1–6.

[VISED2, 2000] SCHWARZ, R. A., *MCNP Visual Editor*, version 1.0.0.1, 2000, <http://mcnpvised.com>



## Ringraziamenti

Giunta al termine di questo lavoro colgo l'occasione per ringraziare il professor Mostacci, relatore di questa tesi, per non essersi mai ridotto a svolgere il suo dovere, mostrando al contrario un grado di disponibilità e di attenzione raro quanto prezioso. Desidero ringraziare la professoressa Gerardy e il dottor Stichelbaut per avermi dato l'opportunità di collaborare con loro e di vivere un'esperienza che non dubito abbia influenzato e influenzerà significativamente il mio percorso personale. Ringrazio inoltre Valérie e Jonathan per la loro pazienza e per avermi soccorso prontamente quando necessario: senza di loro probabilmente non sarei arrivata a scrivere quest'ultima pagina (e forse neanche la prima). Un grazie infine va a Thibault Vanaudenhove per aver messo a mia disposizione i risultati delle sue ricerche.

